RAY : PHOTOPRODUCTION OF PSEUDOSCALAR MESONS AT HIGH ENERGY

Thesis Title: Photoproduction of Pseudoscalar Mesons at High Energy

Siddhartha Ray Ph.D. Thesis

Department of Physics McGill University

ABSTRACT

Firstly, forward photoproduction of neutral pi and eta mesons is simultaneously described in terms of models involving Regge poles and Regge cuts. Two distinct models are used to produce good fits to the existing data - the Dual Absorptive Model (DAM) and the Weak Cut Model (WCM). This analysis is extended to certain quantities of the processes $\pi N \to \omega N$ and $\pi N \to \rho N$ through the use of vector dominance relations. The suitability of using the absorption prescription to calculate the Regge cut contributions corresponding to Reggeized vector exchanges for the imposition of the DAM requirements is discussed. The DAM results are compared to those of the WCM and some tests for experimentally distinguishing between these two models are suggested.

Secondly, photoproduction of charged pions in both forward and backward directions is discussed in detail in terms of the Veneziano model, a crossing symmetric dual model. A simple model with a small number of beta functions (and essentially without any free parameters) is seen to explain the forward structure of different experimental quantities and also to correctly predict the residues of some higher baryon resonances. In the backward direction, the introduction of some satellite terms is seen to be neccessary to account for the differential cross-sections.

PHOTOPRODUCTION OF PSEUDOSCALAR MESONS

AT HIGH ENERGY

A thesis submitted to the Faculty of Graduate Studies and Research in partial fulfilment of the requirements for the degree of Doctor of Philosophy.

by

Siddhartha Ray

Department of Physics
McGill University

July,1972

Author's statement

The original work contained in the thesis is in two parts:-

1) Forward photoproduction of neutral pi and eta mesons has been studied for the first time in terms of the Dual Absorptive Model (DAM). Also, the requirements of the DAM have been imposed for the first time through the introduction of suitable combinations of Regge poles and Regge cuts generated by the absorption prescription. This analysis has been extended through vector dominance to certain quantities of the processes $\pi N \to \rho N$ and $\pi N \to \omega N$. A parallel study of the above reactions has also been carried out in terms of the Weak Cut Model (WCM) and some tests for experimentally distinguishing between the DAM and the WCM have been suggested. (Part B).

2) Photoproduction of charged pions in both forward and backward directions has been studied for the first time in terms of the Veneziano Model, with a small number of beta functions and essentially without any free parameters. (Part C).

ABSTRACT

Firstly, forward photoproduction of neutral pi and eta mesons is simultaneously described in terms of models involving Regge poles and Regge cuts. Two distinct models are used to produce good fits to the existing data - the Dual Absorptive Model (DAM) and the Weak Cut Model (WCM). This analysis is extended to certain quantities of the processes $\pi N \to \omega N$ and $\pi N \to \rho N$ through the use of vector dominance relations. The suitability of using the absorption prescription to calculate the Regge cut contributions corresponding to Reggeized vector exchanges for the imposition of the DAM requirements is discussed. The DAM results are compared to those of the WCM and some tests for experimentally distinguishing between these two models are suggested.

Secondly, photoproduction of charged pions in both forward and backward directions is discussed in detail in terms of the Veneziano model, a crossing symmetric dual model. A simple model with a small number of beta functions (and essentially without any free parameters) is seen to explain the forward structure of different experimental quantities and also to correctly predict the residues of some higher baryon resonances. In the backward direction, the introduction of some satellite terms is seen to be neccessary to account for the differential cross-sections.

ACKNOWLEDGEMENTS

I am extremely grateful to Professor A.P.Contogouris , who suggested and directed this work, for his constant help, advice and guidance. I am specially indebted to Professor C.S.Lam, Dr. E.N.Argyres and my colleague Milo Svec, all of whom collaborated in some part of the work reported here and helped greatly in my understanding of the subject. I am also very grateful to my fellow students Earl Gordon and Bob Gaskell for many hours of invigorating and fruitful discussions and their help in the actual typing of this thesis.

I would also like to thank the McGill Physics Department and the National Research Council of Canada for financial support.

TABLE OF CONTENTS

PART A : GENERAL DISCUSSIONS

CHAPTER 1

INTRODUCTION

Photoproduction has always been a useful tool for the study of the interactions and structure of hadrons. Strong similarities exist between certain purely hadronic processes and photoproduction of certain particles on hadrons. For example, photoproduction of neutral ρ mesons closely resembles elastic hadronic reactions, while photoproduction of pions and kaons has many similarities with certain inelastic hadronic reactions. At high energies, the phenomenological approaches to these two types of reactions are also quite similar.

In testing high energy models, photoproduction of pseudoscalar mesons has often been superior to most hadronic reactions. One reason for this is the superior quality of the photoproduction data, which are more precise and reliable compared to the data for most hadronic reactions. Another reason is the amount of the existing data; details are known not only of the angular distribution and the energy dependence of the differential cross-sections, but also of polarised photon asymmetries, polarised target asymmetries etc.

During the past few years, most of the high energy phenomenology has been based on models involving Regge poles and Regge cuts. Photoproduction of psedoscalar mesons has offered some of the most important phenomenological arguments in support of the existence of Regge cuts. These are the forward peak in $\gamma N \rightarrow \pi^{\pm} N$ (to be discussed in§ 7.2), the large positive values for polarised photon asymmetry for $\gamma p \rightarrow \pi^{0} p$ and the absence of dips in the differential cross-sections for $\gamma p \rightarrow \eta p$ (to be discussed in Chapter 5).

Regge phenomenologists have mostly used either the Weak Cut Model (WCM)[1-4] or the Strong Cut Reggeized Absorption Model (SCRAM)[5-7]. It is now accepted that each of these models is only partly successful, facing serious difficulties in a number of two-body processes. In an effort to combine the successes of these models, Harari has proposed the Dual Absorption Model (DAM)[8]. On the basis of this model, Harari offers explanations for a number of experimental facts on hadronic and photoproduction reactions. However most of these explanations are strictly on a qualitative basis; no quantitative comparison with the data has been presented so far.

A main purpose of this thesis is to study the photoproduction of neutral pseudoscalar mesons in the framework of the Regge theory. Our models involve the exchange of Regge poles and cuts; however we incorporate in them, at least approximately, the basic requirements of the DAM.Vector dominance relates $\gamma N \rightarrow \pi^{0} N$ (and $\gamma N \rightarrow \eta N$) to certain quantities for the processes $\pi N \to \omega N$ and $\pi N \to \rho N$; our analysis has been extended to these quantities as well. Our motivation for this analysis is to determine whether the DAM, formulated in terms of Regge poles and cuts, accounts for the basic features of the experimental data. In addition, the results we obtain in the framework of the DAM are compared with fits of the same processes in the framework of the WCM. Means of experimentally distinguishing between these two models are discussed.

In the last part of this thesis, we study the photoproduction of charged pions in the framework of the Veneziano representation. Since for charged pion photoproduction, measurements have been made in both forward and backward directions, our basic objective is to test the ability of this crossing-symmetric dual model (with a small number of satellite terms) to correctly account for the experimental situation in the two separate regions of interest.

This thesis is divided into four parts. Part A (Chapters 1-4) contains, in addition to this introduction, the notation and symbols used throughout this thesis, formulae for the important physical quntities (Chapter 2), a brief review of the WCM and the SCRAM (Chapter 3) and a discussion of the physical principles and of the most important qualitative predictions of the DAM (Chapter 4). In part B (Chapters 5 and 6), we present our analysis of $\gamma N \to \pi^0 N$,

$\gamma N \to \eta N$ and related vector meson production processes. Part C (Chapters 7,8 and 9) contains our study of the photoproduction of charged pions in the Veneziano model. Part D is a collection of three appendices, where we have presented detailed derivations of some of the most important formulae used in this thesis.(*)

(*) This thesis is based to a great extent on two publications: Part B on Ref (9) and Part C on Ref (10).

CHAPTER 2

DEFINITIONS, NOTATION and *FORMULAE*

In this chapter, we shall define the symbols and notation that will be used throughout the rest of the thesis. We shall also define the invariant amplitudes used in photoproduction, give their relations with the corresponding helicity amplitudes in different frames of reference and express the experimentally measured quantities (differential cross-section, polarisation etc.) in terms of these invariant amplitudes. Algebraic details will be kept to a minimum in this chapter. Whenever more details are required for our discussions, we shall consider these in Appendix II. We shall discuss here only the formulae for the pion photoproduction. The corresponding relations for the photoproduction of eta mesons will be introduced later in Chapter 5 as modifications of pion production formulae. We shall also discuss the different Regge exchanges, both poles and cuts, that are allowed in the various processes under consideration.

2.1 CGLN Amplitudes

Chew, Goldberger, Low and Nambu[11] (henceforth referred as CGLN) have defined a particular set of invariant amplitudes and have also given their isospin and angular momentum decompositions. In this section, we shall summarise the CGLN relations.

Pion photoproduction is described by (Fig. 1)

$$\gamma(k) + N(p_1) \rightarrow \pi(q) + N(p_2) \tag{2.1}$$

where the quantities inside the brackets denote the corresponding four-momenta of the particles taking part in the reaction. The four-momenta have the following components:

$$k=(\vec{K},k);\ q=(\vec{q},\omega);\ p_1=(\vec{p}_1,E_1);\ p_2=(\vec{p}_2,E_2) \tag{2.2}$$

After satisfying energy momentum conservation and mass-shell restrictions, only two independent scalars can be formed out of the four four-momenta. CGLN take them as

$$\nu = -\frac{P.k}{M} = -\frac{P.q}{M} \quad ; \qquad \nu_1 = -\frac{q.k}{2\ M} \tag{2.3}$$

where M= mass of nucleon and $P= \frac{1}{2}(p_1+p_2)$. ν and ν_1 can of course be replaced by any two of the Mandelstam variables s,t and u, which are defined as follows:

$$s=(p_1+k)^2=W^2 \ ; \quad t= (k-q)^2=\mu^2 -2k\omega+2kq\ \mathrm{Cos}\,\theta_s$$
$$u=(k-p_2)^2= M^2-2kE_2-2kq\ \mathrm{Cos}\,\theta_s \tag{2.4}$$

Here μ = mass of the pion, θ_s= scattering angle in the C.M. system of the s-channel and W= total energy in C.M. system.

The complete invariant photo-meson transition element is given by

$$H = M_A A+ M_B B+ M_C C+ M_D\ D \tag{2.5}$$

where A,B,C,D are functions of ν and ν_1 (or say s and t) as well as nucleon isotopic spin τ. The gauge invariant scalar coefficients are

$$
\begin{aligned}
M_A &= i\gamma_5\ \gamma.\varepsilon\ \ \gamma.k \\
M_B &= 2i\gamma_5(P.\varepsilon\ q.k - P.k\ q.\varepsilon) \\
M_C &= \gamma_5(\gamma.\varepsilon\ q.k - \gamma.k\ q.\varepsilon) \\
M_D &= 2\gamma_5(\gamma.\varepsilon\ P.k - \gamma.k\ P.\varepsilon - iM\ \gamma.\varepsilon\ \gamma.k)
\end{aligned}
\qquad (2.6)
$$

where ε is the photon polarisation vector, and the γ's are the usual Dirac matrices.

Let A_i denote any of the four invariant amplitudes A,B,C and D . In the isotopic spin space A_i can be decomposed as follows:

$$A_i(s,t,\tau) = \delta_{\alpha 3}\ A_i^{(+)}(s,t) + \tfrac{1}{2}[\tau_\alpha,\tau_3]A_i^{(-)}(s,t) + \tau_\alpha\ A_i^{(0)}(s,t) \qquad (2.7)$$

where α denotes the isotopic spin index of the outgoing pion. The cross-sections for the four possible charge combinations are obtained by setting:

$$
\begin{aligned}
&\text{i)}\ A_i = \sqrt{2}\ (A_i^{(-)} + A_i^{(0)}) && \text{for}\quad \gamma p \to \pi^+ n \\
&\text{ii)}\ A_i = \sqrt{2}\ (A_i^{(-)} - A_i^{(0)}) && \text{for}\quad \gamma n \to \pi^- p \\
&\text{iii)}\ A_i = (A_i^{(+)} + A_i^{(0)}) && \text{for}\quad \gamma p \to \pi^0 p \\
&\text{iv)}\ A_i = (A_i^{(+)} - A_i^{(0)}) && \text{for}\quad \gamma n \to \pi^0 n
\end{aligned}
\qquad (2.8)
$$

In the C.M. system, the differential cross-section can be written as

$$\frac{d\sigma}{d\Omega} = \frac{q}{k}\ |\langle 2|F|1\rangle|^2 \qquad (2.9)$$

where $|1\rangle$, $|2\rangle$ denote the initial and final Pauli spinor states. For a given isotopic spin combination, F can be written as

$$F = i\vec{\sigma}\cdot\vec{\varepsilon}F_1 + \frac{\vec{\sigma}\cdot\vec{q}\,\vec{\sigma}\cdot(\vec{k}\times\vec{\varepsilon})}{qk}F_2 + \frac{i\vec{\sigma}\cdot\vec{k}\;\vec{q}\cdot\vec{\varepsilon}}{qk}F_3 + \frac{i\vec{\sigma}\cdot\vec{q}\;\vec{q}\cdot\vec{\varepsilon}}{q^2}F_4 \qquad (2.10)$$

where $\vec{\sigma}$ is the Pauli spin matrix.

The F_i's are related to the A_i's in the following fashion:

$$4\pi\frac{2W}{W-M}\,\frac{F_1}{[(M+E_1)(M+E_2)]^{\frac{1}{2}}} = A+(W-M)D+\frac{2M\nu_1}{W-M}(C-D)$$

$$4\pi\,\frac{2W}{W-M}\,\left[\frac{M+E_2}{M+E_1}\right]^{\frac{1}{2}}\,\frac{F_2}{q} = -A+(W+M)D+\frac{2M\nu_1}{W\ M}(C-D) \qquad (2.11)$$

$$4\pi\,\frac{2W}{W-M}\,\frac{1}{[(M+E_2)(M+E_1)]^{\frac{1}{2}}}\,\frac{F_3}{q} = (W-M)B+(C-D)$$

$$4\pi\,\frac{2W}{W-M}\,\left[\frac{M+E_2}{M+E_1}\right]^{\frac{1}{2}}\,\frac{F_4}{q^2} = -(W+M)B+(C-D)$$

The angular dependence of the F_i's is also given by CGLN in terms of expansions involving derivatives of Legendre Polynomials as follows:

$$F_1 = \sum_{\ell=0}^{\infty}\{[\ell M_{\ell+} + E_{\ell+}]P'_{\ell+1}(x) + [(\ell+1)M_{\ell-} + E_{\ell-}]P'_{\ell-1}(x)\}$$

$$F_2 = \sum_{\ell=1}^{\infty}[(\ell+1)M_{\ell+} + M_{\ell-}]P'_{\ell}(x) \qquad (2.12)$$

$$F_3 = \sum_{\ell=1}^{\infty}\{[E_{\ell+} - M_{\ell+}]P''_{\ell+1}(x) + [E_{\ell-} + M_{\ell-}]P''_{\ell-1}(x)\}$$

$$F_4 = \sum_{\ell=1}^{\infty}[M_{\ell+} - E_{\ell+} - M_{\ell-} - E_{\ell-}]P''_{\ell}(x)$$

where $x = \cos\theta_s$

The energy dependent amplitudes $M_{\ell\pm}$ and $E_{\ell\pm}$ refer to transitions initiated by magnetic and electric radiations respectively, leading to final states of orbital angular momentum ℓ and total angular momentum $\ell \pm \frac{1}{2}$.

2.2 Basic Formulae for Pion Photoproduction

Let λ_{N_1}, λ_{N_2}, λ_π and λ_γ denote the helicities of the incident nucleon, the outgoing nucleon, the produced pion and the incident photon respectively. We shall denote the s-channel helicity amplitudes by $f_{\mu\lambda}$ where $\mu = \lambda_{N_2} - \lambda_\pi$ and $\lambda = \lambda_{N_1} - \lambda_\gamma$.

The relations between the $f_{\mu\lambda}$'s and the amplitudes F_i's introduced in eqn.(2.10) are[12] :

$$
\begin{aligned}
f_{\frac{1}{2},\frac{3}{2}} &= -\frac{1}{\sqrt{2}} \operatorname{Sin}\theta_s \operatorname{Cos}\frac{\theta_s}{2} (F_3 + F_4) \\
f_{\frac{1}{2},\frac{1}{2}} &= \sqrt{2} \operatorname{Cos}\frac{\theta_s}{2} \{F_2 - F_1 + \tfrac{1}{2}(1 - \operatorname{Cos}\theta_s)(F_3 - F_4)\} \\
f_{-\frac{1}{2},\frac{3}{2}} &= \frac{1}{\sqrt{2}} \operatorname{Sin}\theta_s \operatorname{Sin}\frac{\theta_s}{2} (F_3 - F_4) \\
f_{-\frac{1}{2},\frac{1}{2}} &= \sqrt{2} \operatorname{Sin}\frac{\theta_s}{2} \{F_1 + F_2 + (1 - \operatorname{Cos}\theta_s)(F_3 + F_4)\}
\end{aligned}
\qquad (2.13)
$$

In terms of the $f_{\mu\lambda}$'s, the differential cross-sections for pion production by photons polarised perpendicular and parallel to the plane of production are (see Appendix II for more details) :

$$\frac{d\sigma_\perp}{d\Omega} = \frac{1}{2}\,\frac{q}{k}\,\left[\,\left|f_{\frac{1}{2},\frac{3}{2}} + f_{-\frac{1}{2},\frac{1}{2}}\right|^2 + \left|f_{\frac{1}{2},\frac{1}{2}} - f_{-\frac{1}{2},\frac{3}{2}}\right|^2\right] \tag{2.14}$$

$$\frac{d\sigma_\parallel}{d\Omega} = \frac{1}{2}\,\frac{q}{k}\,\left[\,\left|f_{\frac{1}{2},\frac{3}{2}} - f_{-\frac{1}{2},\frac{1}{2}}\right|^2 + \left|f_{\frac{1}{2},\frac{1}{2}} + f_{-\frac{1}{2},\frac{3}{2}}\right|^2\right]$$

so that

$$\frac{d\sigma}{d\Omega} = \frac{1}{2}\left(\frac{d\sigma_\perp}{d\Omega} + \frac{d\sigma_\parallel}{d\Omega}\right) = \frac{1}{2}\,\frac{q}{k}\,\left[\,\left|f_{\frac{1}{2},\frac{3}{2}}\right|^2 + \left|f_{-\frac{1}{2},\frac{1}{2}}\right|^2 + \left|f_{\frac{1}{2},\frac{1}{2}}\right|^2 + \left|f_{-\frac{1}{2},\frac{3}{2}}\right|^2\right] \tag{2.15}$$

The recoil nucleon polarisation (in the direction $\hat{k}\times\hat{q}$) is

$$P(\theta) = -\,\frac{q}{k}\,\frac{1}{\frac{d\sigma}{d\Omega}}\;\mathrm{Im}\left(f_{\frac{1}{2},\frac{3}{2}}\,f^*_{-\frac{1}{2},\frac{3}{2}} + f_{\frac{1}{2},\frac{1}{2}}\,f^*_{-\frac{1}{2},\frac{1}{2}}\right) \tag{2.16}$$

The polarised photon asymmetry is defined as

$$\Sigma(\theta) = \frac{\frac{d\sigma_\perp}{d\Omega} - \frac{d\sigma_\parallel}{d\Omega}}{\frac{d\sigma_\perp}{d\Omega} + \frac{d\sigma_\parallel}{d\Omega}}$$

and is given by

$$\Sigma(\theta) = -\,\frac{q}{k}\,\frac{1}{\frac{d\sigma}{d\Omega}}\;\mathrm{Re}\left(f_{\frac{1}{2},\frac{3}{2}}\,f^*_{-\frac{1}{2},\frac{1}{2}} - f_{\frac{1}{2},\frac{1}{2}}\,f^*_{-\frac{1}{2},\frac{3}{2}}\right) \tag{2.17}$$

And finally, if we denote by $\frac{d\sigma_+}{d\Omega}$ and $\frac{d\sigma_-}{d\Omega}$,the differential cross-sections for target nucleons polarised 'up' and 'down' in the direction $\hat{k}\times\hat{q}$, then the polarised target asymmetry is defined as

$$T(\theta) = \frac{\frac{d\sigma_+}{d\Omega} - \frac{d\sigma_-}{d\Omega}}{\frac{d\sigma_+}{d\Omega} + \frac{d\sigma_-}{d\Omega}}$$

and is expressed as

$$T(\theta) = \frac{q}{k} \frac{1}{\frac{d\sigma}{d\Omega}} \quad \mathrm{Im}\,(f_{\frac{1}{2},\frac{3}{2}} f^*_{\frac{1}{2},\frac{1}{2}} + f_{-\frac{1}{2},\frac{3}{2}} f^*_{-\frac{1}{2},\frac{1}{2}}) \tag{2.18}$$

We shall now give the expressions for the asymptotic forward and backward cross-sections and other relevant quantities in terms of the CGLN invariants. Here we shall only outline the method of obtaining these expressions, leaving the algebraic details for Appendix II. For this purpose, we remember that to the leading order in s, for $s\to\infty$, t fixed (small angles, forward direction)

$$\mathrm{Cos}\ \theta_s \to 1 + \frac{2t}{s} \tag{2.19a}$$

and for $s\to\infty$, u fixed (large angles, backward direction)

$$\mathrm{Cos}\ \theta_s \to -1 - \frac{2u}{s} \tag{2.19b}$$

Imposing these limits in Eqn. (2.11), the asymptotic relationships between the F_i's and the A_i's can be obtained. These, in turn, relate the CGLN invariants to the s-channel helicity amplitudes $f_{\mu\lambda}$'s (SHA) through eqn. (2.13). From these, using eqn. (2.14), we immediately obtain

$$\frac{d\sigma_\perp}{dt} = \frac{1}{16\pi}\left[|A|^2 - t|D|^2\right]$$

$$s\to\infty,\ t \text{ fixed} \qquad (2.20)$$

$$\frac{d\sigma_\parallel}{dt} = \frac{1}{16\pi}\left[|A+tB|^2 - t|C|^2\right]$$

and

$$\frac{d\sigma_\perp}{du} = \frac{1}{64\ \pi s}\left[|2MA+s(C+D)+(M^2+u)(C-D)|^2 - 4u|A+M(C-D)|^2\right]$$

$$s\to\infty,\ u \text{ fixed} \qquad (2.21)$$

$$\frac{d\sigma_\parallel}{du} = \frac{1}{64\ \pi s}\left[|2MA+s(C+D)+(M^2-u)(C-D)|^2 - 4u|A-sB|^2\right]$$

It should be noted here that the asymptotic forward cross-section is dominated by exchanges in the t-channel, while the backward cross-section is dominated by exchanges in the u-channel.

In terms of the A_i's, we have in the forward direction

$$P(\theta) = -\frac{\sqrt{-t}}{16\pi\,\frac{d\sigma}{dt}}\ \operatorname{Im}\ \left[A^*(C+D)+tB^*C\right] \qquad (2.22)$$

and

$$T(\theta) = -\frac{\sqrt{-t}}{16\pi\,\frac{d\sigma}{dt}}\ \operatorname{Im}\ \left[A^*(C-D)+tB^*C\right] \qquad (2.23)$$

2.3 Parity Conserving t-channel Helicity Amplitudes and Analyticity Constraints

The singularity free parity conserving t-channel helicity amplitudes (PCTHA) would be denoted by $\tilde{f}^{\sigma,\sigma_c}_{\lambda_N-\lambda_{\bar{N}},\lambda_\gamma}(s,t)$, where $\sigma=P(-)^J$ is the normality of the exchanged system and $\sigma_c=C(-)^J$. The reason for considering σ and σ_c in the PCTHA is that in any reaction with an initial or final t-channel state of equal mass particles, say $m_1=m_2$, and with $\lambda_1=\pm\lambda_2$, both σ and σ_c of the asymptotically dominant exchanges are well specified.

The method of constructing parity conserving helicity amplitudes has been described by Gell-Mann et al[13] and the relations between the singularity free PCTHA for photoproduction and the CGLN amplitudes have been derived by Diu and Le-Bellac[14]. These are:

$$A = -\frac{4}{t-4M^2}\left[M\tilde{f}^{++}_{11} + \frac{t}{4}\tilde{f}^{++}_{01}\right]$$

$$B = \frac{1}{t}\left[\tilde{f}^{-+}_{01} + \frac{4}{t-4M^2}\left(M\tilde{f}^{++}_{11} + \frac{t}{4}\tilde{f}^{++}_{01}\right)\right] \tag{2.24}$$

$$C = \tfrac{1}{2}\tilde{f}^{--}_{11}$$

$$D = -\frac{2}{t-4M^2}\left[\tilde{f}^{++}_{11} + M\tilde{f}^{++}_{01}\right]$$

The inverse relations are

$$\tilde{f}^{-+}_{01} = A+tB \quad ; \quad \tilde{f}^{++}_{01} = -A+2MD$$
$$\tilde{f}^{--}_{11} = 2C \quad ; \quad \tilde{f}^{++}_{11} = MA-\frac{t}{2}D \tag{2.25}$$

Since the invariant amplitudes are analytic at t=0, we immediately see from the expression of B in (2.24), that B would have a pole at t=0 , unless

$$\tilde{f}^{-+}_{01} + \frac{4}{t-4M^2}[M\tilde{f}^{++}_{11} + \frac{t}{4}\tilde{f}^{++}_{01}] = 0 \qquad \text{at } t=0$$

or

$$\tilde{f}^{++}_{11}(s,0) = M\tilde{f}^{-+}_{01}(s,0) \tag{2.26}$$

This is also evident from the expressions for $\tilde{f}^{-+}_{01}$ and $\tilde{f}^{++}_{11}$ in eqn. (2.25). When in later chapters we shall write down explicit expressions for the invariant amplitudes, we shall have to satisfy this kinematic (or analyticity) constraint.

2.4 Regge Exchanges in the t-channel (Fig. 2)

With the isospin decomposition of CGLN, it follows that $A_i^{(+)}$, which does not contribute to charged pion production, corresponds to I=0; $A_i^{(-)}$ and $A_i^{(0)}$, which do contribute, have I=1. If we consider neutral pion production, we see that the isovector part of the photon has positive G parity, while the outgoing neutral pion has negative G parity. This means that the isoscalar exchange $A_i^{(+)}$ has negative G parity and hence negative C. Similarly, $A_i^{(0)}$ has G=+ and C=-.

If we now consider the two charged pion photoproduction processes, we also see that $A_i^{(-)}$ and $A_i^{(0)}$ have opposite charge conjugation. So $A_i^{(+)}$ receives contributions from ω (and ϕ) exchange, $A_i^{(0)}$ from ρ and B, and $A_i^{(-)}$ from π, A_1 and A_2 exchanges.

In view of the fact that in these reactions, σ and σ_c of the asymptotically dominant exchanges are well specified, it is clear that $\tilde{f}^{-+}_{01}$ will be dominated by the exchange of trajectories π and B, $\tilde{f}^{++}_{01}$ and $\tilde{f}^{++}_{11}$ by ρ, ω (and ϕ) and A_2 and $\tilde{f}^{--}_{11}$ by A_1. On the basis of these observations we have constructed Table 2.1.

There is a well known theorem due to Stichel[15] which states that for pseudoscalar mesons, the differential cross-section with photons polarised perpendicular to the plane of production is dominated by natural parity exchanges, while the differential cross-section with photons polarised parallel to the plane of production is dominated by unnatural parity exchanges. This implies that, for example in eqn. (2.20), $\frac{d\sigma_\perp}{dt}$ essentially receives contributions from ω (and ϕ), ρ and A_2, while $\frac{d\sigma_\parallel}{dt}$ receives contributions from π, B and A_1.

So far, we have only considered the exchange of Regge poles. In addition to these poles in the complex angular momentum plane, branch cuts may also exist. The theoretical basis of Regge cuts is already well known[16,17].

In this work we consider cuts generated by the simultaneous exchange of a Regge pole (R) and n Pomerons(P). Since the Pomeron has vacuum quantum numbers, cuts corresponding to R will contribute to exactly the same amplitudes. Moreover, the cut contribution will also have to obey the analyticity constraint (2.26). There is however one important difference. Unlike a Regge pole, a Regge cut has no definite normality. Hence at t=0, a certain cut may give non-zero contributions to both $\tilde{f}^{++}_{11}$ and $\tilde{f}^{-+}_{01}$ of (2.26), implying non-zero contributions (and of comparable magnitude) to both $\frac{d\sigma_{\perp}}{dt}$ and $\frac{d\sigma_{\parallel}}{dt}$. This is the case with the ρ-Pomeron and the ω-Pomeron cuts of this work.

Table 2.1 t-channel Exchanges, Quantum Numbers and PCTHA's

Regge trajectory	Spin of lowest particle J	Parity P	Charge conjugation C	I-spin I	$\sigma = P(-)^J$	$\sigma_C = C(-)^J$	I-spin index	PCTHA receiving leading contribution
$\omega(\phi)$	1	−	−	0	+	+	(+)	$\tilde{f}_{01}^{++}$, $\tilde{f}_{11}^{++}$
ρ	1	−	−	1	+	+	(0)	$\tilde{f}_{01}^{++}$, $\tilde{f}_{11}^{++}$
A_2	2	+	+	1	+	+	(−)	$\tilde{f}_{01}^{++}$, $\tilde{f}_{11}^{++}$
π	0	−	+	1	−	+	(−)	$\tilde{f}_{01}^{-+}$
B	1	+	−	1	−	+	(0)	$\tilde{f}_{01}^{-+}$
A_1	1	+	+	1	−	−	(−)	$\tilde{f}_{11}^{--}$

CHAPTER 3

A BRIEF REVIEW OF EXISTING REGGE CUT MODELS

In this chapter, we shall briefly review the basic principles of the two principal Regge cut models - the Weak Cut Model (WCM)[1-4] and the Strong Cut Reggeized Absorption Model (SCRAM)[5-7]. The guiding philosophy behind the calculation of Regge cut contributions will also be discussed. Detailed mathematical derivations for Regge cut contributions, as calculated in this thesis, will be given in Appendix I. The predictions of both the WCM and the SCRAM with respect to some specific reactions and their agreements and disagreements with experimentally observed characteristics will be pointed out. We shall also discuss very briefly a third model, the Peripheral Model (PM)[18,19], and point out its similarities and dissimilarities to the WCM and the SCRAM.

3.1 Some commonly used Methods for the Calculation of Regge Cuts

As in § 2.1, for the two-body reaction $1+2\to3+4$ (Fig. 3) we denote by $f_{\mu\lambda}(s,t)$ the s-channel helicity amplitudes, where $\mu=\lambda_4-\lambda_3$, $\lambda=\lambda_2-\lambda_1$ and $\lambda_1,\lambda_2,\lambda_3$ and λ_4 are the helicities of the particles 1,2,3 and 4 respectively. In the impact parameter representation, we can write

$$f_{\mu\lambda}(s,t)= 2k^2 \int_0^\infty b \quad db \quad J_n(bq) \quad f_{\mu\lambda}(s,b) \tag{3.1}$$

where $n=|\lambda-\mu|$ = total helicity change, b= impact parameter, k= C.M. momentum and $q=\sqrt{-t}$ = momentum transfer. The inverse transformation is given by

$$f_{\mu\lambda}(s,b)= \frac{1}{2k^2} \int_0^\infty q\, dq \;\; J_n(bq) \;\; f_{\mu\lambda}(s,t) \tag{3.2}$$

We shall be concerned with Regge cuts generated by the simultaneous non-planar exchange of a Reggeon (R) and n Pomerons (P) and shall calculate the corresponding contributions through the absorption prescription.

This prescription is motivated by the well known peripheral model with absorption[20], in which

$$f_{\mu\lambda}(s,b) \;\; = \;\; f_{\mu\lambda}^{(B)}(s,b) \;\; \eta(s,b) \tag{3.3}$$

$f_{\mu\lambda}^{(B)}(s,b)$ is the transform of a proper elementary particle exchange (≡ Born term) and $\eta(s,b)$ (the so-called 'absorption function') has the form shown in Fig.4. Then the contribution to $f_{\mu\lambda}(s,t)$ from the part $b \geqslant b_0$ of the integral in (3.1) is essentially the same as the contribution of the Born term, but the contribution for $b < b_0$ will be effectively depleted, in particular at b= 0.

In the Regge phenomenology, $f_{\mu\lambda}^{(B)}(s,b)$ is replaced by the transform $f_{\mu\lambda}^{(R)}(s,b)$ of the corresponding Regge pole exchange:

$$f_{\mu\lambda}^{(R)}(s,b)= \frac{1}{2k^2} \int_0^\infty q \;\; dq \;\; J_n(bq) \;\; f_{\mu\lambda}^{(R)}(s,t) \tag{3.4}$$

Thus

$$f_{\mu\lambda}(s,t) = 2k^2 \int_0^\infty b \quad db \quad J_n(bq)\ \eta\ (s,b) \quad f_{\mu\lambda}^{(R)}(s,b) \qquad (3.5)$$

With appropriate choice of the absorption function η (s,b), it follows that the asymptotic behaviour of the difference $f_{\mu\lambda}(s,t)-f_{\mu\lambda}^{(R)}(s,t)$ has a number of properties[4] in common with multi-Regge exchange models leading to moving branch points in the complex angular momentum plane. Thus we can write

$$f_{\mu\lambda}(s,t) = f_{\mu\lambda}^{(R)}(s,t) + f_{\mu\lambda}^{(cut)}(s,t) \qquad (3.6)$$

We shall now describe very briefly the two most commonly used methods of calculating the absorption function η (s,b). Henyey et al[5] (Michigan prescription) have used the Sopkovich approach[21], which can be seen to introduce a Regge cut corresponding to Reggeon-single Pomeron exchange. In the impact parameter representation this method gives

$$f_{\mu\lambda}(s,t) = 2k^2 \int_0^\infty b\ db \quad J_n(bq) \quad e^{i\chi(b)}\ f_{\mu\lambda}^{(R)}(s,b) \qquad (3.7)$$

where χ (b) is the phase shift due to elastic scattering (ie Pomeron exchange part), and is given by

$$e^{i\chi(b)} = 1+ \frac{i}{k^2} \int_0^\infty q\ dq \quad J_0(bq) \quad f^{(P)}(s,t) \qquad (3.8)$$

$f^{(P)}(s,t)$ is the elastic scattering amplitude, which is empirically fitted in the forward direction by

$$f^{(P)}(s,t) = i\,\frac{\sigma_t k^2}{4\pi}\, e^{-\frac{A}{2}q^2} \tag{3.9}$$

σ_t is the total elastic cross-section of the relevant process and A is determined by fitting the corresponding diffraction peak. From (3.8) and (3.9),

$$e^{i\chi(b)} = 1 - \frac{\sigma_t}{4\pi A}\, e^{-\frac{b^2}{2A}} = 1 - C\, e^{-\frac{b^2}{2A}} \tag{3.10}$$

where

$$C = \frac{\sigma_t}{4\pi A} \tag{3.11}$$

So the Michigan prescription corresponds to the absorption function

$$\eta\,(s,b) = 1 - C\, e^{-\frac{b^2}{2A}} \tag{3.12}$$

This is easily seen to be of the form of Fig.4.

Another commonly used prescription is due to Arnold[1]. This prescription uses the full eikonal representation and obtains

$$f_{\mu\lambda}(s,t) = 2k^2 \int_0^\infty b\, db\;\; J_n(bq)\; [\,1 - e^{i\chi(s,b^2)}\,] \tag{3.13}$$

where

$$\chi(s,b^2) = \frac{i}{2k^2}\int_0^\infty q\, dq\;\; J_n(bq)\;\; f^{(R)}_{\mu\lambda}(s,t) \tag{3.14}$$

Eqn. (3.13) gives

$$f_{\mu\lambda}(s,t) = 2k^2 \int_0^\infty b\;\; db\;\; J_n(bq)\; (-i\chi)\; [1 + \frac{i\chi}{2!} - \frac{\chi^2}{3!}\; \ldots] \tag{3.15}$$

The first term inside the parenthesis can be taken to represent single scattering and corresponds to the Regge pole exchange part. Then the second and higher order terms represent second and higher order (iė multiple) scattering and correspond to the absorption correction. If we only consider the first order cuts, then

$$f_{\mu\lambda}(s,t) \simeq 2k^2 \int_0^\infty b \quad db \quad J_n(bq) \; (-i\chi)[1 \;\; + \frac{i\chi}{2}] \qquad (3.16)$$

If, as in the usual absorption prescription, the first order cut is generated by the simultaneous exchange of a Reggeon and a Pomeron, then the term $\sim \chi^2$ in (3.16) is to be replaced by $\chi_R \; \chi_P$ where χ_R corresponds to Reggeon exchange and χ_P to Pomeron exchange. So, the Michigan prescription is equivalent to the first terms of the Arnold prescription.

In this thesis, all cut contributions will be calculated through the Michigan prescription. From (3.6) and (3.12), we have

$$f_{\mu\lambda}^{(RP)}(s,t) \equiv f_{\mu\lambda}^{(cut)}(s,t) = -2k^2 \int_0^\infty b \; db \; C \; e^{-\frac{b^2}{2A}} \; J_n(bq) \; f_{\mu\lambda}^{(R)}(s,b)$$

which after some algebra gives

$$f_{\mu\lambda}^{(RP)}(s,t) \quad = \quad \int_0^{-\infty} d\tau \quad f_{\mu\lambda}^{(R)}(s,\tau)\tfrac{1}{2}C \; e^{\frac{1}{2}A(t+\tau)} \; I_n(A\sqrt{t\tau}\;) \qquad (3.17)$$

where $I_n(x)$ is the modified Bessel function defined as $I_n(x) = (-i)^n \; J_n(ix)$

The integral on the right hand side of eqn. (3.17) is multiplied by a phenomenological factor

$\tilde{\lambda}^{(R)}_{\mu\lambda}$, the so called ' coherent inelastic factor'[5]. We shall discuss in more detail the reasons for introducing this factor (§3.3). So the final formula used for calculating the cut contribution is

$$f^{(RP)}_{\mu\lambda}(s,t) = \tilde{\lambda}^{(R)}_{\mu\lambda} \int_0^{-\infty} d\tau \; f^{(R)}_{\mu\lambda}(s,\tau) \; \tfrac{1}{2}C \; e^{\frac{1}{2}A(t+\tau)} \; I_n(A\sqrt{t\tau}\,) \tag{3.18}$$

The actual calculation will be shown in Appendix I.

Notice that the particular form of η (s,b), as shown in eqn. (3.12), implies that the attenuation in the helicity amplitudes due to absorption is negligible for $b \gtrsim \sqrt{2A}$. Clearly, $R \simeq \sqrt{2A}$ is the so called 'absorption radius' (of typical value 1 fermi). In most parametrizations of elastic scattering, A is taken to be energy independent or has a weak dependence on s (iė logarithmic).

If the hadronic interaction under consideration has a range R', then clearly in eqn.(3.1), all the contribution to $f_{\mu\lambda}(s,t)$ will come from the part of the integral corresponding to $0 \leq b \lesssim R'$. In the partial wave decomposition of $f_{\mu\lambda}(s,t)$, the highest partial waves will have $\ell \sim kR'$. The peripherality of the amplitude $f_{\mu\lambda}(s,t)$ means that $f_{\mu\lambda}(s,t)$ is essentially dominated by $\ell \sim kR'$ partial waves. The contributions from the lower partial waves are substantially absorbed. In terms of the absorption prescription this implies that $R' \simeq R$. Also, the t-structure of $f_{\mu\lambda}(s,t)$ is similar to that of the Bessel function $J_n(R\sqrt{-t})$ (see eqn. (3.1)).

3.2 The Weak Cut Model (WCM)

There are different methods of calculating the cut contribution[1-4] in the Weak Cut Model, but the general principles involved and their implications are similar. In this section, we shall discuss these common characteristics of the different versions of the WCM.

For our discussion, we shall use eqn. (3.18). Notice that in the integral in this equation, at fixed s, both $f^{(R)}_{\mu\lambda}(s,\tau)$ and $e^{\frac{1}{2}A\tau}$ decrease exponentially as τ becomes more and more negative, so that the integral receives most of its contributions from the interval $0\leq-\tau\leq1$ GeV^2 .

The major differences between the WCM and the SCRAM (to be discussed in the next section) are in the t-structure of the amplitude $f^{(R)}_{\mu\lambda}(s,t)$ and in the magnitude of the factor $\tilde{\lambda}^{(R)}_{\mu\lambda}$. These differences lead to different relative magnitudes of $f^{(R)}_{\mu\lambda}(s,t)$ and $f^{(RP)}_{\mu\lambda}(s,t)$, and thus in general,to different structures of the overall amplitude $f_{\mu\lambda}(s,t)$.

In the Weak Cut Model, the Regge pole amplitude $f^{(R)}_{\mu\lambda}(s,t)$ contains the well known non-sense wrong signature zeroes [22] (NWSZ). So, if we are considering an amplitude which is dominated by vector meson exchange (e.g. ρ and ω exchanges), then the corresponding Regge pole contribution $f^{(R)}_{\mu\lambda}(s,t)$ has a zero at $t \simeq -.55$ GeV^2. More precisely, at this value of t, Im $f^{(R)}_{\mu\lambda}(s,t)$ changes sign and Re $f^{(R)}_{\mu\lambda}(s,t)$ has a double zero. Therefore the integral in (3.18) receives, in general, two significant contributions with opposite sign and the resulting cut contribution is relatively weak. Moreover, in the WCM, the factor $\tilde{\lambda}^{(R)}_{\mu\lambda}$ is taken to be unity. Therefore, the cut contribution is not enhanced in any other way. Thus for ρ and ω exchange $f_{\mu\lambda}(s,t)$ is expected to show a dip at $t \simeq -.55$ GeV^2.

The cut contribution produced by the convolution of eqn. (3.18) has its shape dependent on n, the total helicity change in the amplitude. However, since the total amplitude, in general, is dominated by the pole contribution, the location of a given zero is, roughly, the same in all helicity amplitudes, and is determined by the trajectory function and the signature of the exchanged particle. Also, the real and the imaginary parts of the total amplitude $f_{\mu\lambda}$ have, roughly, the same structure as the corresponding quantities for $f^{(R)}_{\mu\lambda}$. For $f^{(R)}_{\mu\lambda}$, the real part has double zeroes at $1 \pm \mathrm{Cos}\ \pi\alpha(t) = 0$, and the imaginary part has single zeroes at $\mathrm{Sin}\ \pi\alpha(t) = 0$

We discuss the experimental situation with regards to the presence or absence of dips in the differential cross-sections for some of the most important two-body reactions. The assumption involved in all these cases is that vector meson exchanges dominate. The experimental situation regarding the corresponding differential cross-sections is indicated in the third column of Table 3.1. In the table, n denotes the total helicity change of the <u>dominant</u> amplitude. $(\gamma p\to\pi^+ n)-(\gamma n\to\pi^- p)$ is the difference of the corresponding differential cross-sections. $X_\omega(s,t)$ is the isolated ω-exchange contribution to the process $\pi N\to\rho N$ (see eqn. (5.15)) and is defined as

$$X_\omega(s,t)=\frac{d\sigma}{dt}(\pi^+ p\to\rho^+ p)+\frac{d\sigma}{dt}(\pi^- p\to\rho^- p)-\frac{d\sigma}{dt}(\pi^- p\to\rho^0 n)$$

It is quite clear from the table that the WCM has only limited sucess in explaining the dip structure of the different reactions(*). Notice that the WCM seems to succeed usually in reactions dominated by the single flip amplitudes. This is an important observation and we shall elaborate further in the next chapter.

Another important failure of the WCM is in connection with the cross-over phenomena of the different elastic scattering cross-sections (e.g. $K^\pm p\to K^\pm p$,

---

(*) The absence of dips in the differential cross-sections for $\gamma p\to\eta p$, $\pi^+ n\to\omega p$ and in $\frac{d\sigma}{dt}(\gamma p\to\pi^+ n)-\frac{d\sigma}{dt}(\gamma n\to\pi^- p)$ has been explained by adherents to the WCM in terms of a strong B-meson exchange. There are however important difficulties in this explanation (see §6.1 and also Ref. (6))

$\pi^{\pm}p\to\pi^{\pm}p$[23]). Finally the WCM is unable to explain the polarisation data in $\pi^{-}p\to\pi^{0}n$[24]; however this last failure (even more prominent in SCRAM) is typical of all Regge cut models defined in terms of absorption prescription (3.18).

3.3 The Strong Cut Reggeized Absorption Model (SCRAM)[5-7]

In this model, the cut contribution is again generated through eqn. (3.18). However, $f_{\mu\lambda}^{(R)}$ does not have any NWSZ, and does not vanish in the region $0<-t\leq 1\ GeV^2$. Therefore, the resulting cut is stronger than that of the WCM. This cut contribution is further enhanced by choosing a value of $\tilde{\lambda}_{\mu\lambda}^{(R)}>1$. It has been argued[5] that the factor $\tilde{\lambda}_{\mu\lambda}^{(R)}$ represents the effects of diffractive dissociation of the initial (or final) particles. The choice of $\tilde{\lambda}_{\mu\lambda}^{(R)}>1$ is equivalent to the assumption that the contributions from the Regge recurrences of the intermediate states in the diagrams generating the cuts add up coherently, at least to some extent.

The cuts in this model are at least as important as the pole contributions. The value of $\tilde{\lambda}_{\mu\lambda}^{(R)}$ is adjusted so that the imaginary (and the real) part of a particular amplitude $f_{\mu\lambda}(s,t)$ has a t-structure similar to that of the Bessel function $J_n(R\sqrt{-t})$ where $R\simeq 1$ fermi. In other words, both the real and the imaginary parts of the amplitudes are peripheral. The zeroes in the amplitude are not correlated at all to the dominant exchanged trajectory or its signature; rather they are produced by the destructive interference between the pole and the cut terms, and they appear at about the same values of t as the zeroes of the corresponding Bessel functions $J_n(R\sqrt{-t})$. In general, both the real and the imaginary parts of the helicity non-flip amplitude (n= 0) have zeroes at $t \simeq -.2$ GeV^2, while those of the single-flip amplitude (n= 1) exhibit zeroes at $t \simeq -.55$ GeV^2 .

The SCRAM is quite successful in explaining the features of the reactions listed in Table 3.1 as well as in explaining the cross-over phenomena. However it fails in $\pi^- p \to \eta n$, $\pi^+ p \to \eta \Delta^{++}$, $K^- p \to \bar{K}^0 n$ and $K^+ n \to K^0 p$[23]. In all these reactions, the SCRAM predicts dips at $t \simeq -.55$ GeV^2 ; experimentally, no such dips are observed.

Another serious failure of the SCRAM is in explaining the polarisation data in $\pi^+ p$ and $\pi^- p$ elastic scattering[23]. It fares even worse in the case of $\pi^- p \to \pi^0 n$ polarisation, where it predicts large negative values around $t \simeq -.55$ GeV^2[5]; experimentally, the polarisation is large and positive in this region[24].

3.4 The Peripheral Model[18,19]

We shall use eqn. (3.5) in discussing the Peripheral Model. The fundamental differences between the PM on one hand and the WCM and the SCRAM on the other are :

a) In both the WCM and the SCRAM, the input $f^{(R)}_{\mu\lambda}(s,b)$ in (3.5) represents the corresponding Regge pole amplitude. In the PM, this input is replaced by the corresponding Born term $f^{(B)}_{\mu\lambda}(s,b)$. This is the same input as used by Gottfried and Jackson[20] in their peripheral model (see eqn. (3.3)). The Born term gives incorrect energy dependence, except for pion exchange near the forward direction. This leads directly to the other fundamental difference between the standard absorption prescriptions and this model.

b) As we have remarked in § 3.1, in the standard absorption prescriptions, the absorption radius R is either energy independent or has a weak dependence on s (logarithmic). In the PM, the absorption radius R is considered to be strongly energy dependent. The lack of variation with s in $f^{(B)}_{\mu\lambda}(s,b)$ is compensated by the strong energy dependence of the absorption function $\eta\ (s,b)$. The most commonly used $\eta\ (s,b)$ is of the Wood-Saxon form:

$$\eta\ (s,b) = \frac{1}{1 + \exp[(R-b)/d]} \qquad (3.19)$$

where d is the so called width of interaction (Fig. 5). The energy dependence of R and d are obtained in practice by fitting the differential cross-section in the charge exchange reaction $\pi^- p \to \pi^0 n$ at different energies.

In spite of the above differences between the PM and the SCRAM, there are many similarities between these two models. The objective in each case is to make both the real and the imaginary parts of the total amplitude peripheral (see for example eqn. (D.10) in Ref. (19)). So, in the PM, both the real and the imaginary parts of $f_{\mu\lambda}(s,t)$ again behave like $J_n(R\sqrt{-t})$. As such, this model enjoys basically the same successes and has the same failures as the SCRAM.

Table 3.1 The Dip Structure in some Important Reactions

Reaction	Allowed Vector Exchange	Dip Present at $t \simeq -.55$ GeV^2	Dominant Helicity Amplitude n
$\gamma N \to \pi^0 N$	$\omega(\rho)$	yes	1
$\pi^- p \to \pi^0 n$	ρ	yes	1
$\gamma p \to \eta^0 p$	$\rho(\omega)$	no	0,2
$(\gamma p \to \pi^+ n)$ $-(\gamma n \to \pi^- p)$	ρ	no	0,2
$\pi^+ n \to \omega p$	ρ	no	0,2
$X_\omega(s,t)$ for $\pi N \to \rho N$	ω	yes	1

CHAPTER 4

PHYSICAL PRINCIPLES OF THE DUAL ABSORPTIVE MODEL

In the first part of this chapter, we shall discuss the physical principles behind the Dual Absorptive Model (DAM) and point out its similarities and differences with the WCM and the SCRAM. In the second part, we shall examine some of the qualitative predictions of the DAM and compare them with experiment. Since all the reactions to be considered in this thesis are non-diffractive, the principles of the DAM shall be explained only for non-diffractive processes.

4.1 The Physical Principles of the Dual Absorptive Model[8] (DAM)

Harari made the following observations and assumptions about non-diffractive two-body hadronic interactions:

a) The general s-channel helicity amplitude $f_{\mu\lambda}(s,t)$ for any such process can be described in two different ways. The first is the t-channel description, when the features of $f_{\mu\lambda}(s,t)$ are usually explained on the basis of a few Regge poles and cuts. The second is the s-channel description, mainly in terms of resonances. Duality states that these two descriptions are essentially equivalent.

b) From the s-channel point of view, Im $f_{\mu\lambda}(s,t)$ is considered to be locally dominated by resonances of mass $m \sim s^{\frac{1}{2}}$. Re $f_{\mu\lambda}(s,t)$

on the other hand, is not determined by nearby resonances alone. It receives substantial contributions from distant resonances, including those with $s< 0$ (u-channel resonances). So one should apply the concept of duality as stated in part (a) only to Im $f_{\mu\lambda}(s,t)$.

c) The t-channel description gives the angular structure of the amplitude. In most t-channel models, any such structure occurs at approximately fixed t-values at all energies. Thus, duality demands that the s-channel description in terms of resonances should also reproduce the same t-structure. One possibility is that every single resonance exhibits these structures, so that their sum also exhibits the same characteristics. This is a strong assumption, but such a possibility cannot be ruled out. As a matter of fact, it is well known that[25] in πN scattering, the imaginary part of the single-flip amplitude has a zero at $t \simeq -.55$ GeV^2, while that of the non-flip amplitude has a zero at $t \simeq -.2$ GeV^2. As shown by Dolen, Horn and Schmidt[26], each of the prominent N^* resonances contributing to this reaction shows zeros at approximately the same fixed t-values for the corresponding helicity amplitudes. Another possibility is, of course, that the resonances do not exhibit individually the required t-structure, but only the sum of the prominent resonances at any particular energy does so. However, Harari assumes that the first alternative is more likely to occur in nature.

This assumption has an important consequence. The angle in which a given resonance produces a zero is dependent on the spin of the resonance. Also, this angle is connected to the t-value through the resonance mass (iė $\sqrt{s}$). So the assumption of zeroes of resonances at fixed t-values leads to a relation between the spin of the resonance and the resonance mass. This is

$$\ell \propto \sqrt{s} \tag{4.1}$$

where ℓ is the corresponding partial wave. Again, an examination of the prominent resonances contributing to πN scattering shows that they indeed lie on the curve $\ell \propto \sqrt{s}$ (8). Now, if k is the C.M. momentum, then $k \propto \sqrt{s}$. So the condition is that Im $f_{\mu\lambda}(s,t)$ is dominated by s-channel partial waves with $\ell \sim k$.

We can now state the basic postulates of the DAM:

a) Im $f_{\mu\lambda}(s,t)$ is dominated by the most peripheral s-channel partial waves. For total s-channel helicity flip n $(=|\lambda-\mu|)$

$$\text{Im } f_{\mu\lambda}(s,t) \sim J_n(R\sqrt{-t}) \tag{4.2}$$

where R is the radius of hadronic interaction (~ 1 fermi, defined in § 3.1). For exotic s-channel processes, Im $f_{\mu\lambda}(s,t) \sim 0$.

b) Since the real part of $f_{\mu\lambda}(s,t)$ is not locally dominated by resonances, it need not be peripheral. At asymptotic energies a definite phase relationship exists between the real and the imaginary parts [27-29], so that Re $f_{\mu\lambda}(s,t)$ is determined uniquely from Im $f_{\mu\lambda}(s,t)$. However at non-asymptotic energies, no definite statements can be made about Re $f_{\mu\lambda}(s,t)$.

We can now examine the similarities and the differences between the DAM and the older models (WCM and SCRAM). For the WCM, let us again consider amplitudes dominated by vector (e.g. ρ and ω) exchanges. In § 3.2, we saw that the WCM predicts that for the single-flip amplitude ($n=1$), Im $f_{\mu\lambda}(s,t)$ has a zero at $t\simeq -.55$ GeV^2 . It also has a kinematic zero at $t=0$. So, Im $f_{\mu\lambda}(s,t)$ has approximately the t-structure of $J_1(R\sqrt{-t})$ with $R\simeq 1$ fermi, and hence is peripheral. This is in agreement with the DAM requirements. Hence for the single-flip amplitude, the DAM is very similar to the WCM, and the corresponding cut contribution is weak. For the non-flip and the double-flip amplitudes, the DAM requires that Im $f_{\mu\lambda}(s,t)$ behave like $J_0(R\sqrt{-t})$ and $J_2(R\sqrt{-t})$ respectively. The WCM does not exhibit these characteristics and the corresponding Im $f_{\mu\lambda}(s,t)$'s are not peripheral. So, if the DAM requirements are to be satisfied through the introduction of Regge cuts, these cut contributions cannot be small for these amplitudes.

The difference between the DAM and the SCRAM lies in the fact that the latter demands that both the real and the imaginary parts of $f_{\mu\lambda}(s,t)$ be peripheral while the former only requires the imaginary part to be so. In particular, as stated for the single-flip (n=1) amplitude, the DAM is very similar to the WCM. This means that the amplitude is dominated by the corresponding pole(s) contribution. Now the real part of the pole contribution is related to the imaginary part through the signature of the pole even at comparatively low energies (~ few GeVs). Thus for n=1, if Im $f_{\mu\lambda}(s,t) \sim J_1(R\sqrt{-t})$, then

$$\mathrm{Re}\ f_{\mu\lambda}(s,t) \sim \begin{cases} J_1(R\sqrt{-t})\ \tan\frac{\pi\alpha(t)}{2} & \text{(odd signature)} \\ J_1(R\sqrt{-t})\ \cot\frac{\pi\alpha(t)}{2} & \text{(even signature)} \end{cases} \tag{4.3}$$

The SCRAM demands that both Im $f_{\mu\lambda}(s,t)$ and Re $f_{\mu\lambda}(s,t)$ behave like $J_1(R\sqrt{-t})$ at all energies, so that it definitely violates the simple phase relationship of (4.3). On the other hand, for the n=0 (and the n=2) amplitude, the DAM requires the cut contributions to be quite important, and in this respect it can be considered in agreement with the SCRAM.

4.2 Some Qualitative Predictions

In this section, we shall enumerate the qualitative predictions of the DAM with respect to some important reactions. More detailed discussions on these and other reactions can be found in Refs. (8) and (23).

Let us first consider the differential cross-sections for the reactions $\pi^- p \to \pi^0 n$, $\gamma N \to \pi^0 N$ and the combinations of differential cross-sections $X_\omega(s,t)$ for the process $\pi N \to \rho N$ (see Table 3.1). All these reactions are dominated by the single-flip (n=1) helicity amplitude, and the dominant t-channel exchanges are ρ or ω . So from (4.3) we obtain

$$\frac{d\sigma}{dt} \propto |f_{\mu\lambda}|^2 \propto \frac{|J_1(R\sqrt{-t})|^2}{\cos^2 \frac{\pi\alpha(t)}{2}} \tag{4.4}$$

where $\alpha(t)$ is the ρ or the ω trajectory. With $R \simeq 1$ fermi, $J_1(R\sqrt{-t})$ has a zero at $t \simeq -.55$ GeV^2. Since $\cos^2 \frac{\pi\alpha(t)}{2}$ is regular and non-zero at this point, all the above mentioned reactions show a dip in the differential cross-section around $t \simeq -.55$ GeV^2. As we mentioned before, the WCM and the DAM are very similar for the n=1 amplitudes. This explains why the WCM is usually successful for reactions dominated by single-flip amplitudes.

The reaction $\pi^- p \to \eta n$ is again dominated by the n=1amplitude. The dominant t-channel exchange is A_2. So again from (4.3)

$$\frac{d\sigma}{dt} \propto \frac{|J_1(R\sqrt{-t})|^2}{\sin^2 \frac{\pi\alpha(t)}{2}} \tag{4.5}$$

Here the zero of $J_1(R\sqrt{-t})$ at $t \simeq -.55$GeV^2 is cancelled by the zero of the denominator at the same point. So the cross-section should not show a dip at this point; indeed, no dip is observed experimentally.

We now consider those reactions of Table 3.1, which are dominated by $n=0$ and $n=2$ amplitudes. The DAM requires the imaginary parts of the corresponding helicity amplitudes to behave like $J_0(R\sqrt{-t})$ and $J_2(R\sqrt{-t})$ respectively. These do not have any zeroes at $t \simeq -.55$ GeV^2 . So we do not expect (and we do not observe) dips in the cross-sections for these processes in this t-region.

PART B : $\gamma N \to \pi^0 N$, $\gamma N \to \eta N$ AND RELATED PROCESSES ($\pi^+ N \to \omega p$ AND $\pi N \to \rho N$)

CHAPTER 5

CALCULATIONS WITH THE DUAL ABSORPTIVE MODEL (DAM)

In this part of the thesis, we shall try to account for the experimental features of the photoproduction of neutral pseudoscalar mesons. We shall also extend our analysis to certain quantities in the processes $\pi N \to \omega N$ and $\pi N \to \rho N$ through the use of vector dominance relations.

In the photoproduction of π^0 and η mesons, the following characteristics are to be noted:

a) The π^0 differential cross-section shows a dip in the forward direction at $t \simeq -.55\ \mathrm{GeV}^2$. The η cross-section on the other hand, does not show this dip. Remembering that a basic test of any model is its ability to predict the presence or the absence of dips in the cross-section, it is immediately seen that a simultaneous study of these reactions with any model will be useful.

b) If s is the total energy squared, M the mass of the nucleon and $\frac{d\sigma}{dt}$ the forward differential cross-section, then the quantity $(s-M^2)^2 \frac{d\sigma}{dt}$ is approximately constant for all s in these two processes.

c) The ratio $R = \frac{d\sigma}{dt}(\gamma n \to \pi^0 n) / \frac{d\sigma}{dt}(\gamma p \to \pi^0 p)$ has been measured in the forward direction. The error bars are comparatively large and it is very difficult to make any definite statements about its t-structure. However one thing to note is that this ratio is always less than unity (see Fig. 8)

d) The polarised photon asymmetry $\Sigma(\theta) = (\frac{d\sigma_\perp}{dt} - \frac{d\sigma_\parallel}{dt}) / (\frac{d\sigma_\perp}{dt} + \frac{d\sigma_\parallel}{dt})$ (see eqn. (2.17)) for the process $\gamma p \to \pi^0 p$ has also been measured (Fig. 7). This shows a small dip at $t \simeq -.55$ GeV^2. In the absence of Regge cuts, $\frac{d\sigma_\perp}{dt}$ receives leading contributions from ρ and ω exchanges, while $\frac{d\sigma_\parallel}{dt}$ is dominated by B exchange. At $t \simeq -.55$ GeV^2, the ρ and the ω contributions vanish due to the presence of the non-sense wrong signature zeroes in the amplitudes. So, if cuts are absent, $\Sigma \simeq -1$ around this point. Since the experimental value is $\simeq .5$, we have some evidence for the existence of Regge cuts.

e) The polarised target asymmetry T (defined in eqn. (2.18)) has also been measured for $\gamma p \to \pi^0 p$ (Fig. 9) at 4 GeV. The data show that T is negative in the interval $0 \leq |t| \leq 1$ GeV^2, with a maximum $|T|(\sim .6)$ at $t \simeq -.55$ GeV^2.

In this chapter, we shall present the DAM calculations. We shall try to obtain the peripherality of the imaginary parts of the different s-channel helicity amplitudes as required by the DAM through the introduction of suitable amounts of Regge cut contributions (in addition to the Regge poles), calculated through the absorption prescription (eqn. (3.18)).

5.1 General Procedure

From our discussions in chapter 2 (see Table 2.1 and eqn. (2.8)), we know that for π^0

photoproduction, the important t-channel Regge exchanges are ω, ρ and B. For all these exchanges, we consider linear trajectory functions of the form

$$\alpha_R(t) = \alpha_R(0) + \lambda_R t \tag{5.1}$$

where R denotes any of the ω, ρ and B Regge poles.

Most of the present phenomenological analyses of two-body reactions proceed through the Reggeization of the s-channel helicity amplitudes of definite parity. Here we shall proceed through the Reggeization of the invariant amplitudes A_i. The main reason for our approach is the special form of vector meson dominance relations we adopt, and this will become clear in §5.3. Another important reason is that we shall be studying charged pion photoproduction in the framework of the Veneziano model, which neccessarily involves the Reggeization of the invariant amplitudes. Certain expressions as well as some important quantities in both parts B and C are thus related in a straightforward manner (see §8.3). The relations between our Regge pole and cut contributions to the CGLN invariants and the corresponding contributions to SHA of definite parity will be discussed in §5.4 and are summarised in Table 5.1.

The contribution in the forward direction to the CGLN invariant A_i from the Regge pole trajectory $\alpha_R(t)$ is taken as

$$A_i^{(R)}(s,t) = \beta_i^{(R)}(t)\ \pi \quad \frac{1 - e^{-i\pi\alpha_R(t)}}{\Gamma[\alpha_R(t)]\ \mathrm{Sin}[\pi\alpha_R(t)]} \quad \left(\frac{s}{s_R}\right)^{\alpha_R(t)-1} \tag{5.2}$$

s_R is a constant with dimensions of GeV^2 ($\equiv$ energy scale); the residues $\beta_i^{(R)}(t)$ are smooth functions of t to be discussed below. It is evident from (5.2) that our Regge pole exchanges contain NWSZ's.

Since we proceed through the Reggeization of the invariant amplitudes, we must take special care to satisfy the analyticity constraint (eqn. (2.26)):

$$\tilde{f}_{11}^{++}(s,0) = M\ \tilde{f}_{01}^{-+}(s,0) \tag{5.3}$$

In the case of π^0 photoproduction, the leading contribution to $\tilde{f}_{11}^{++}$ comes from the ω and the ρ exchanges, while $\tilde{f}_{01}^{-+}$ receives only non-leading contributions from these exchanges. One way of satisfying (5.3) would be to make the ω and the ρ contributions to $\tilde{f}_{11}^{++}$ proportional to t (so that they vanish at t= 0), and set the corresponding contributions to $\tilde{f}_{01}^{-+}$ (= A + tB) identically equal to zero at all t. Since $\tilde{f}_{11}^{++} = MA - \frac{t}{2} D$, this means that the explicit representation for the CGLN invariant A must be proportional to t (iė $\beta_1^{(R)}(t) \sim t$). The contribution from the CGLN invariant D to $\tilde{f}_{11}^{++}$ is explicitly multiplied by t. So we have

$$A^{(\rho)} \sim t\ ;\ A^{(\omega)} \sim t;\quad B^{(\rho)} = -\frac{1}{t} A^{(\rho)}\ ;\ B^{(\omega)} = -\frac{1}{t} A^{(\omega)} \tag{5.4}$$

Here $A^{(\rho)}$ stands for the contribution to A from ρ exchange etc. These observations completely determine the residue functions $\beta_i^{(\rho)}(t)$ and $\beta_i^{(\omega)}(t)$. The forms we adopt in our calculations are shown in Table 5.2.

This method of satisfying the analyticity constraint is known as the evasive solution. For the B exchange contribution, we shall also proceed with an evasive solution. As we discuss in Appendix II (eqns. (A.II.3) and (A.II.4)), the combination of SHA

$$f_{\frac{1}{2},\frac{1}{2}} + f_{-\frac{1}{2},\frac{3}{2}} \sim A + tB$$

is dominated by t-channel exchanges of σ=−, whereas the combination

$$f_{\frac{1}{2},\frac{1}{2}} - f_{-\frac{1}{2},\frac{3}{2}} \sim A$$

is dominated by σ=+. Since the B meson has σ=−, in the asymptotic limit it only contributes to the CGLN invariant B. In terms of PCTHA, B exchange dominates only the amplitude $\bar{f}^{-+}_{01}$ (=A+tB). So if only the invariant B receives a contribution from the B exchange, the analyticity constraint (5.3) is again satisfied by evasion. The form of our B exchange contribution is also presented in Table 5.2.

In addition to the ρ, ω and B Regge poles, we consider ρ-Pomeron and ω-Pomeron Regge cuts. Their contributions to the SHA $f_{\frac{1}{2},\frac{1}{2}}$, $f_{-\frac{1}{2},\frac{1}{2}}$ and $f_{\frac{1}{2},\frac{3}{2}}$ are calculated in detail in Appendix I. The cut contributions to the double-flip (n=2) amplitude $f_{-\frac{1}{2},\frac{3}{2}}$ are very small (unless multiplied by an unusually large $\tilde{\lambda}_{\mu\lambda}$) and will be neglected.

Appendix I also contains the explicit representations of our ρ-P and ω-P contributions to the invariants A and D (denoted by $A^{(\rho P)}$, $D^{(\rho P)}$, $A^{(\omega P)}$ and $D^{(\omega P)}$). These are related to the corresponding cut contributions to SHA via eqns. (A.II.2) (see also Tables 5.1 and 5.2)

In our calculations, we use two different models of Regge cuts: Model C_1 and Model C_2 (both defined in Appendix $I^{(*)}$). We do not consider Regge cuts associated with B-meson exchange.

5.2 Formulae for the Photoproduction of π^0 and η

The photoproduction of neutral pions involve the isotopic spin combination $A_i^{(+)} \pm A_i^{(0)}$. From Table 2.1, we see that there are no known t-channel exchanges corresponding to the amplitudes $C^{(+)}$ and $C^{(0)}$. Accordingly we take

---

(*) Model C_2 is identical to Model A of Ref.(9). This ref. also presents a Regge cut model B (not presented in this thesis). As we discuss in Appendix I, these cut models differ between them with respect to non-leading (in ln s) terms; these non-leading terms are important at the energies of interest.

$$C^{(+)}(s,t) = 0 \quad ; \quad C^{(0)}(s,t) = 0 \tag{5.5}$$

Then our discussions in the previous section together with eqn. (2.20) lead to the following expressions for the differential cross-section in the forward direction for π^0 photoproduction:

$$\frac{d\sigma_{\perp}}{dt} = \frac{1}{16\pi}[|A^{(+)} \pm A^{(0)}|^2 - t|D^{(+)} \pm D^{(0)}|^2]$$

$$\frac{d\sigma_{\parallel}}{dt} = \frac{1}{16\pi}[|A^{(\omega P)} \pm (A^{(\rho P)} + tB^{(B)}|^2] \tag{5.6}$$

where $A_i^{(+)} = A_i^{(\omega)} + A_i^{(\omega P)}$; $A_i^{(0)} = A_i^{(\rho)} + A_i^{(\rho P)}$ $(i=1,4)$. The upper (lower) sign refers to the photoproduction on protons (neutrons). The differential cross-section and the polarised photon asymmetry are

$$\frac{d\sigma}{dt} = \frac{1}{2}\left(\frac{d\sigma_{\perp}}{dt} + \frac{d\sigma_{\parallel}}{dt}\right) \quad ; \quad \Sigma(\theta) = \frac{\frac{d\sigma_{\perp}}{dt} - \frac{d\sigma_{\parallel}}{dt}}{\frac{d\sigma_{\perp}}{dt} + \frac{d\sigma_{\parallel}}{dt}}$$

Also from eqn. (2.23) (using eqn. (5.5)), the polarised target asymmetry for $\gamma p \to \pi^0 p$ is given by

$$T(\theta) = -\frac{\sqrt{-t}}{16\pi\frac{d\sigma}{dt}} \,\mathrm{Im}\, [\{A^{(+)} + A^{(0)}\}^* \{D^{(+)} + D^{(0)}\}] \tag{5.7}$$

For the photoproduction of η mesons, eqns. (5.6) are to be modified in the following fashion. In our notation, $A_i^{(R)}$ denotes the contributions to the π^0 amplitude A_i from the Regge trajectory R. If $A_i^{(R)}(\eta)$

denotes the corresponding contribution to η production, then

$$A_i^{(R)}(\eta) = \frac{g_{\gamma\eta R}}{g_{\gamma\pi R}} \; A_i^{(R)} \tag{5.8}$$

where $g_{\gamma\pi R}$ denotes the coupling of R to the $\gamma-\pi$ vertex, while $g_{\gamma\eta R}$ is the corresponding coupling to the $\gamma-\eta$ vertex. Now SU(6) symmetry gives

$$g_{\gamma\eta\omega}=g_{\gamma\pi\rho} \quad ; \quad g_{\gamma\eta\rho} = -g_{\gamma\pi\omega} \quad ; \quad g_{\gamma\pi\omega} = 3g_{\gamma\pi\rho} \tag{5.9}$$

where the $\omega-\phi$ and the $\eta-\chi$ mixing has been neglected [30]. So for η photoproduction we have

$$\begin{aligned} \frac{d\sigma_{\perp}}{dt} &= \frac{H}{16\pi} \; [|A^{(+)}\pm hA^{(0)}|^2 - t|D^{(+)}\pm hD^{(0)}|^2] \\ \frac{d\sigma_{\parallel}}{dt} &= \frac{H}{16\pi} \; |A^{(\omega P)}\pm h(A^{(\rho P)}+tB^{(B)})|^2 \end{aligned} \tag{5.10}$$

where

$$H = \left(\frac{g_{\gamma\eta\omega}}{g_{\gamma\pi\omega}} \right)^2 \qquad \text{and} \quad h = \frac{g_{\gamma\pi\omega}\; g_{\gamma\eta\rho}}{g_{\gamma\eta\omega}\; g_{\gamma\pi\rho}} \tag{5.11}$$

5.3 Connection with $\pi N\to\omega N$ and $\pi N\to\rho N$

Starting with the reaction $\pi N\to\omega N$, we assume that it is dominated by the same t-channel exchanges, which in § 5.1 determines $\gamma_{isoscalar}+N \to \pi^0+N$, iė the ρ and B Regge poles and the ρP cut. We are interested in the part of $\pi N\to\omega N$ which corresponds to helicity $\lambda_\omega = \pm1$ in the t-frame (or Gottfried-Jackson frame). It will become clear that the use of certain t-frame quantities allows a direct determination of the magnitude of the B- exchange at a physical value of t ($t< 0$) and independent of the magnitude and the structure of the ρP cut.

We shall use the six invariant amplitudes $B_i(s,t)$ ($i=1,2,3,5,6,8$) as used by Diu and Le Bellac (14) for discussing $\pi N\to VN$, where V stands for any vector meson. Off the mass-shell (iė for $k^2\neq m_V^2$), the B_i's will be functions of s,t and k^2 . To relate these amplitudes to the photoproduction invariants A_i's, we assume that $B_i(s,t;\, k^2)$ are smooth in k^2 ($\equiv$squared vector meson mass); then the following relations can be shown to be valid at $k^2=0$ (the photon limit) and high s:

$$B_1= -A_1;\ \frac{B_2}{k.q} = -\frac{2B_3}{s}=A_2 \qquad (5.12)$$
$$B_5= sA_4 +k.q\ A_3\ ;\quad B_6= 2A_4\ ;\quad B_8= A_3$$

where q is the four momentum of the pion. In this derivation we have used an extrapolation in the vector meson mass as done in Refs. (31-34). Vector meson dominance is a special consequence of eqns. (5.12) .

Eqns. (3.1) and (3.4) of Ref. (14) enable us to express the relations between the CGLN invariants A_i and the t-channel helicity amplitudes (THA) for the process $\pi N\to\omega N$. If $\rho_{mn}^{(t)}$ denotes the density matrix element in the t-frame, then it is determined in terms of the THA's. The combinations $(\rho^{(t)}_{11} \pm \rho^{(t)}_{1\,-1})\frac{d\sigma}{dt}$ are asymptotically dominated by t-channel exchanges with positive (upper sign) and negative (lower sign) normalities respectively. We can express them in terms of the CGLN invariants as:

$$[\rho^{(t)}_{11} + \rho^{(t)}_{1\,-1}]\frac{d\sigma}{dt} = \frac{(2\gamma_\omega/e\ )^2}{16\ \pi}[|A^{(0)}|^2 - t|D^{(0)}|^2]$$

$$[\rho^{(t)}_{11} - \rho^{(t)}_{1\,-1}]\frac{d\sigma}{dt} = \frac{(2\gamma_\omega/e\ )^2}{16\ \pi\tau^2_\omega}|(t+m^2_\omega-\mu^2)A^{(\rho P)} - t(m^2_\omega+\mu^2-t)B^{(B)}|^2 \tag{5.13}$$

where γ_ω is the γ-ω coupling constant, $\frac{e^2}{4\pi} = \frac{1}{137}$; m_ω and μ are the ω and the pion masses and

$$\tau^2_\omega = [(m_\omega+\mu)^2-t][(m_\omega-\mu)^2-t] \tag{5.14}$$

Now the important point to notice is that at $t= -(m^2_\omega-\mu^2)$ $=-.59\ GeV^2$, the contribution to $[\rho^{(t)}_{11} - \rho^{(t)}_{1\,-1}]\frac{d\sigma}{dt}$ from the ρ-P cut vanishes[34,35]. So a knowledge of this quantity at this point directly determines the magnitude of the B exchange. It should be remarked that the point $t=-(m^2_\omega-\mu^2)$ is in the physical region of the process $\pi N \rightarrow \omega N$, so that this method of determining the B exchange involves only experimental quantities and does not rest on assumptions about extrapolation to $t=m^2_B$ or strong π-B exchange degeneracy.

It is known that vector dominance relates directly the photoproduction quantities to the density matrix elements of $\pi N \to \omega N$ (and $\pi N \to \rho N$) in the s- (or helicity) frame[6]. However our determination of the B exchange contribution is based on the t-frame quantity $[\rho^{(t)}_{11} - \rho^{(t)}_{1\,-1}] \frac{d\sigma}{dt}$. Because of the special form of vector dominance relations shown in eqns. (5.12), we have been able to express the t-frame quantities $[\rho^{(t)}_{11} \pm \rho^{(t)}_{1\,-1}]\frac{d\sigma}{dt}$ directly in terms of the photoproduction quantities (eqn. (5.13)). These relations involve <u>invariant</u> amplitudes for both $\pi N \to \omega N$ and $\gamma N \to \pi N$. This is the main reason we have proceeded in § 5.1 through the Reggeization of the CGLN invariants.

For the process $\pi N \to \rho N$, isospin invariance tells us that the ω exchange contribution can be isolated in the following combination of differential cross-sections[36]:

$$X_\omega(s,t) = \frac{d\sigma}{dt}(\pi^+ p \to \rho^+ p) + \frac{d\sigma}{dt}(\pi^- p \to \rho^- p) - \frac{d\sigma}{dt}(\pi^- p \to \rho^0 n) \tag{5.15}$$

It is known that this exchange couples to the π-ρ system only when the ρ helicity is ± 1[37]. So it follows that

$$X_\omega(s,t) = 2\, \rho^{(t)}_{11} \frac{d\sigma}{dt} \tag{5.16}$$

So the left hand side of eqn. (5.15) is evaluated from the formulae (5.13) with B=0, and replacing all ρ and ρ-P indices by the corresponding ω and ω-P indices.

5.4 Requirements of the Dual Absorptive Model

We shall use the basic requirement that

$$\mathrm{Im}\ f_{\mu\lambda}(s,t) \sim J_n(R\sqrt{-t})\ ;\quad R\sim 1 \text{ fermi}\ ;\ n= |\lambda-\mu| \qquad (5.17)$$

of the DAM in order to place restrictions on the t-structure of the imaginary parts of our SHA, and implicitly, on the magnitude of our Regge cuts. We shall require that, at any given energy, the combination of Regge pole and cut contributions forming our SHA has an imaginary part with approximately the t-structure (zeroes, maxima, minima) of the corresponding Bessel function.

We first consider the amplitude with isospin index (0) (iė ρ, ρ-P and B exchange contributions). Then Table 5.2 and the DAM requirement (5.17) imply that for the single-flip amplitudes (n=1):

$$\mathrm{Im}\ f^{(0)}_{\frac{1}{2},\frac{3}{2}}(s,t)=\mathrm{Im}\ f^{(0)}_{-\frac{1}{2},\frac{1}{2}}(s,t)=\frac{\sqrt{2s}}{16\pi}\sqrt{-t}\ \mathrm{Im}(D^{(\rho)}+D^{(\rho P)}) \sim J_1(R\sqrt{-t}) \qquad (5.18)$$

Also Table 5.2 implies that for the non-flip amplitude (n=0);

$$\mathrm{Im}\ f^{(0)}_{\frac{1}{2},\frac{1}{2}}(s,t)=-\frac{\sqrt{2s}}{16\ \pi}\ \mathrm{Im}(A^{(\rho)}+2A^{(\rho P)}+tB^{(B)}) \sim J_0(R\sqrt{-t}) \qquad (5.19)$$

and for the double-flip amplitude (n=2)

$$\mathrm{Im}\ f^{(0)}_{-\frac{1}{2},\frac{3}{2}}(s,t)=\frac{\sqrt{2s}}{16\ \pi}\ \mathrm{Im}\ (A^{(\rho)}-tB^{(B)}) \sim J_2(R\sqrt{-t}) \qquad (5.20)$$

Next consider the amplitudes

with isospin index (+) (ie ω and ω-P exchanges). For the n=1 amplitudes, the requirement corresponding to eqn. (5.18) is obtained from Table 5.2 as

$$\mathrm{Im}\ f^{(+)}_{-\frac{1}{2},\frac{1}{2}}(s,t)=\mathrm{Im}\ f^{(+)}_{\frac{1}{2},\frac{3}{2}}(s,t)=\frac{\sqrt{2s}}{16\pi}\sqrt{-t}\ \mathrm{Im}(D^{(\omega)}+D^{(\omega P)})\sim J_1(R\sqrt{-t}) \tag{5.21}$$

Here the n=0 and the n=2 amplitudes are much smaller in magnitude (see § 5.5b). In any case, the corresponding DAM requirements can be easily obtained from Table 5.2.

5.5 Fits, Parameter Values and DAM requirements

Our fits to the experimental data are presented in Figs. 6-14. The Regge pole and the Regge cut parameters used are given in Tables 5.3 and 5.4.

a) Features of the Fits produced

i) $\frac{d\sigma}{dt}$ for $\gamma p\to\pi^0 p$: Both our models account fairly well for the t-structure and the energy variation of the data (Fig. 6). The expected dip at $t\simeq -.55$ GeV^2 is observed in both the models. Model C_1 consistently gives a slightly stronger dip than what is actually observed.

ii) Polarised photon asymmetry Σ for $\gamma p\to\pi^0 p$: Both models reproduce this parameter quite successfully (Fig.7)

iii) The ratio $R=\frac{d\sigma}{dt}(\gamma n\to\pi^0 n)/\frac{d\sigma}{dt}(\gamma p\to\pi^0 p)$: Both the models are again quite successful in fitting the data (Fig. 8).

Model C_1 gives a flat t-structure, while Model C_2 shows a dip at $t \simeq -.55$ GeV^2. This ratio is quite sensitive to the relative magnitudes of the isovector and the isoscalar photon contributions, and in general, quite difficult to obtain correctly.

iv) Polarised target asymmetry T for $\gamma p \to \pi^0 p$: Both Models C_1 and C_2 are unsuccessful in fitting the data for T, in particular at $|t| \leq .5$ GeV^2, where they predict $T>0$ (Fig.9). They also predict a change of sign in T at $t \simeq -.5$ GeV^2, not supported by the present data. However, another set of parameters in the framework of the model C_1 (called C_1' in Tables 5.3 and 5.4) produces better results; at small $|t|$, T is still positive, but at larger $|t|$, reasonable agreement is obtained. This model also gives large negative T ($\simeq -.42$) at $t \simeq -.6$ GeV^2, in agreement with experiment (Fig. 9, cross-dashed curve). With these particular parameters certain other quantities (e.g. the ratio of maximum to minimum value of $\frac{d\sigma}{dt}$ ($\gamma p \to \pi^0 p$, Fig. 6 at 9 GeV) are in less satisfactory agreement. However most of the predictions are qualitatively the same as of Model C_1 (see polarised photon asymmetry Σ at 6 GeV, Fig. 7; the $\gamma p \to \eta p$ differential cross-section at 6 GeV, Fig. 10; and the quantity $X_\omega(s,t)$ at 8 GeV, Fig. 11).

v) $\frac{d\sigma}{dt}$ for $\gamma p \to \eta p$: Model C_1 shows a shoulder at $t \simeq -.55$ GeV^2 (Fig. 10). This feature is not supported (but also not definitely excluded) by the present data. Model C_2 on the other hand, shows no such shoulder or dip.

vi) $X_\omega(s,t)$ for $\pi N \rightarrow \rho N$: From the ω and the ω-Pomeron contribution to π^0 photoproduction, we can obtain $X_\omega(s,t)$ (eqn. (5.15)) by using vector dominance. As we see in Fig. 11, both the models C_1 and C_2 fit the existing data quite well.

vii) The quantities $\rho^{(t)}_{1\,1} \frac{d\sigma}{dt}$, $[\rho^{(t)}_{1\,1} - \rho^{(t)}_{1\,-1}] \frac{d\sigma}{dt}$, and $[\rho^{(t)}_{1\,1}+\rho^{(t)}_{1\,-1}] \frac{d\sigma}{dt}$ for $\pi^+ n \rightarrow \omega p$: Comparisons with experimental data are shown in Figs. 12,13 and 14. Model C_2 semms to fit the data for the first two quantities quite well. Model C_1 shows a dip at $t \simeq -.55$ GeV^2 for $\rho^{(t)}_{11} \frac{d\sigma}{dt}$. For the quantity $[\rho^{(t)}_{1\,1}+\rho^{(t)}_{1\,-1}]$ $\frac{d\sigma}{dt}$, the experimental information is quite imprecise and precludes any definitive statements about the presence or the absence of dips at $t \simeq -.55$ GeV^2. Model C_1 again shows a dip, while Model C_2 exhibits no such dip. At smaller $|t|$, Model C_1 seems to fit the data better.

b) <u>Values of Constants</u>

In both the models, the $\rho N\bar{N}$ coupling is dominantly s-helicity flip (see value of $G_4^{(\rho)}/G_1^{(\rho)}$ in Table 5.3). The $\omega N\bar{N}$ coupling on the other hand is by far dominantly non-flip (see value of $G_1^{(\omega)}/G_4^{(\omega)}$). We need

$G_1^{(\omega)}/G_4^{(\omega)} > 0$ to fit the data. Theoretical considerations(18) give a small negative value for this ratio. Notice that other high energy models(6,18) have also been forced to use positive (and rather large) values for this ratio in order to fit the data. In our fits, the required $G_1^{(\omega)}/G_4^{(\omega)}$ (= .1 ~.05) is quite small. Also $\gamma N \to \pi^0 N$ is dominated by ω exchange (as seen from the values of the ratio $G_1^{(\rho)}/G_4^{(\omega)}$ used in our fits) . The expected values of the constants $G_i^{(\rho)}$ and $G_i^{(\omega)}$ have been calculated in terms of the $\rho N\bar{N}$ and $\omega N\bar{N}$ couplings and the decay widths $\Gamma(\rho\to\pi\gamma)$ and $\Gamma(\omega\to\pi\gamma)$. However, these are only order of magnitude estimates, and our fitted values compare well with them. (see also Table 8.2).

In the η photoproduction fits, we see that SU(6) predictions compare favourably with our parameters values. The values of $\frac{\gamma_\rho^2}{4\pi}$ and $\frac{\gamma_\omega^2}{4\pi}$ as determined from our fits of $X_\omega(s,t)$ for $\pi N\to\rho N$ and the t-frame density matrix elements for $\pi^+ n\to\omega p$ are also quite consistent with the experimentally determined magnitudes of these quantities.

The trajectories ρ, ω and B are constrained to pass through the masses of the corresponding particles. λ_B is taken to be $\simeq .7\ \mathrm{GeV}^{-2}$, so that the B trajectory becomes exchange degenerate to the pion trajectory. To account for the t-variation of the experimental $[\rho_{11}^{(t)}-\rho_{1-1}^{(t)}]\frac{d\sigma}{dt}$ for $\pi^+ n\to\omega p$, we were forced to introduce an extra t-dependence in the B meson residue ($\beta_2^{(B)} = G_2^{(B)}\ e^{\beta t}$). So the exchange degeneracy is weak.

c) Requirements of the DAM

As we discussed in §5.4, the Dual Absorptive Model requires that the imaginary parts of the single-flip amplitudes $f^{(0)}_{-\frac{1}{2},\frac{1}{2}}$ and $f^{(0)}_{\frac{1}{2},\frac{3}{2}}$ behave like $J_1(R\sqrt{-t})$, with $R \simeq 1$ fermi. This means that in addition to vanishing at $t = 0$, each of them has a zero near $t \simeq -.55$ GeV^2. Fig. 15 shows that this requirement is well satisfied for both the ρ and the ω exchanges in both our models. Since vector exchanges are involved, we expect from our discussions in chapter 4 that the corresponding cut contributions are weak. This is indeed the case as seen from Table 5.3 (values of $\tilde{\lambda}^{(\rho),(\omega)}_{\frac{1}{2},\frac{3}{2}}$).

As discussed in the third section of this chapter, the non-flip amplitude $f^{(0)}_{\frac{1}{2},\frac{1}{2}}$ is proportional to the combination $[A^{(\rho)}+2A^{(\rho P)}+tB^{(B)}]$. So, the imaginary part of this combination should behave like $J_0(R\sqrt{-t})$, having a first zero at $t \simeq -.2$ GeV^2, a local maximum at $t \simeq -.6$ GeV^2 and a second zero at $t \simeq -1.2$ GeV^2 . As shown in Fig. 16, both models show the first zero around $t \simeq -.15$ GeV^2 , but the maximum and the second zero are displaced towards smaller $|t|$. This tendency is more evident for Model C_2 .

Similarly the combination $[-A^{(\rho)}+tB^{(B)}]$ is proportional to the double-flip amplitude $f^{(0)}_{-\frac{1}{2},\frac{3}{2}}$. Hence its imaginary part is proportional to $J_2(R\sqrt{-t})$, and consequently it has zeroes at t=0 and t≃-1 GeV^2. Model C_2 satisfies this requirement quite well (Fig. 17), but Model C_1 has its second zero at a smaller value of $|t|$.

Since the $\omega N\bar{N}$ coupling is dominantly non-flip, the ω contribution to $f^{(+)}_{\frac{1}{2},\frac{1}{2}}$ and $f^{(+)}_{-\frac{1}{2},\frac{3}{2}}$ are quite small. So we do not discuss the DAM requirements for these two helicity amplitudes. Again, in view of our discussions of chapter 4, we expect the corresponding cut contributions to be quite large. This is again seen from Table 5.3 (values of $\tilde{\lambda}^{(\rho),(\omega)}_{\frac{1}{2},\frac{1}{2}}$).

The real parts of the corresponding s-channel helicity amplitudes are also shown in Figs. 18 and 19. The real parts of both $f^{(0)}_{-\frac{1}{2},\frac{1}{2}}$ and $f^{(+)}_{-\frac{1}{2},\frac{1}{2}}$ (Fig. 18) look alike in both models C_1 and C_2 . These amplitudes show structures somewhat resembling $J_1(R\sqrt{-t})$ but with the zero shifted towards small $|t|$. For Re $f^{(0)}_{\frac{1}{2},\frac{1}{2}}$, none of the two models give anything resembling $J_0(R\sqrt{-t})$ (Fig. 19). For Model C_2 , Re $f^{(0)}_{-\frac{1}{2},\frac{3}{2}}$ looks like $J_2(R\sqrt{-t})$ (Fig. 19), but Model C_1 gives a different structure. Of course, the DAM does not impose any constraints on the real parts of the amplitudes.

Table 5.1 Combinations of SHA with Definite Normality (*)

Normality σ → / Isospin Index ↓	+	−	+	−
	$\{f_{\frac{1}{2},\frac{3}{2}}+f_{-\frac{1}{2},\frac{1}{2}}\}$ x $(-8\pi/\sqrt{2s})$	$\{f_{\frac{1}{2},\frac{3}{2}}-f_{-\frac{1}{2},\frac{1}{2}}\}$ x $(-8\pi/\sqrt{2s})$	$\{f_{\frac{1}{2},\frac{1}{2}}-f_{-\frac{1}{2},\frac{3}{2}}\}$ x $(-8\pi/\sqrt{2s})$	$\{f_{\frac{1}{2},\frac{1}{2}}+f_{-\frac{1}{2},\frac{3}{2}}\}$ x $(-8\pi/\sqrt{2s})$
(+) ω-like	$-\sqrt{-t}(D^{(\omega)}+D^{(\omega P)})$	0	$A^{(\omega)}+A^{(\omega P)}$	$A^{(\omega P)}$
(0) $(\rho+B)$-like	$-\sqrt{-t}(D^{(\rho)}+D^{(\rho P)}$	0	$A^{(\rho)}+A^{(\rho P)}$	$A^{(\rho P)}+tB^{(B)}$

(*) This table is directly obtained from equations (A.II.3) and (A.II.4).

Table 5.2 Residue Functions and Contributions to s-channel Helicity Amplitudes

	Residue functions $\beta_i^{(R)}(t)$				Contributions to s-channel helicity amplitudes x $(-16\pi/\sqrt{2s})$		
Exchanges	$\beta_1(t)$	$\beta_2(t)$	$\beta_3(t)$	$\beta_4(t)$	$f_{-\frac{1}{2},\frac{1}{2}} = f_{\frac{1}{2},\frac{3}{2}}$	$f_{\frac{1}{2},\frac{1}{2}}$	$f_{-\frac{1}{2},\frac{3}{2}}$
ρ	$-tG_1^{(\rho)}$	$G_1^{(\rho)}$	0	$G_4^{(\rho)}$	$-\sqrt{-t}\ D^{(\rho)}$	$A^{(\rho)}$	$-A^{(\rho)}$
ω	$-tG_1^{(\omega)}$	$G_1^{(\omega)}$	0	$G_4^{(\omega)}$	$-\sqrt{-t}\ D^{(\omega)}$	$A^{(\omega)}$	$-A^{(\omega)}$
B	0	$G^{(B)}e^{bt}$	0	0	0	$tB^{(B)}$	$tB^{(B)}$
ρ-Pomeron					$-\sqrt{-t}\ D^{(\rho P)}$	$2A^{(\rho P)}$	negligible
ω-Pomeron					$-\sqrt{-t}\ D^{(\omega P)}$	$2A^{(\omega P)}$	negligible

Table 5.3 Fitted and Expected Values

Parameters	Fitted Values					Expected Values (*)	References
	C_1(DAM)	C_1(WCM)	C_2(DAM)	C_2(WCM)	C_1'(DAM)		
$G_4^{(\omega)}$ ($\mu b^{\frac{1}{2}}GeV^{-2}$)	97	79	118	118	94	95	(18)(40)(41) (42) and SU(6)
$\frac{G_1^{(\omega)}}{G_4^{(\omega)}}$ (GeV^{-1})	0.1	0.03	0.05	0.05	0.05	-0.07	(18)(39)(42)
$\frac{G_1^{(\rho)}}{G_4^{(\omega)}}$ (GeV^{-1})	0.39	0.45	0.25	0.25	0.25	0.225	(18)(40)(41) (42) and SU(6)
$\frac{G_4^{(\rho)}}{G_1^{(\rho)}}$ (GeV)	0.35	0.24	0.45	0.45	0.45	0.50	(18)(38) (39)(42)
$\frac{g_{\gamma\pi\omega}}{g_{\gamma\eta\omega}} = \frac{1}{\sqrt{H}}$	-4.54	-3.22	-4.0	-2.96	-3.86	-3.0	SU(6)
$\frac{g_{\gamma\pi\omega}g_{\gamma\eta\rho}}{g_{\gamma\eta\omega}g_{\gamma\pi\rho}} = h$	9.0	8.87	9.0	9.0	9.0	9.0	SU(6)
$\gamma_\omega^{\ 2}/4\pi$	5.4	5.2	5.4	10.1	4.9	3.7±0.65	(43)
$\gamma_\rho^{\ 2}/4\pi$	0.45	0.55	0.6	0.6	1.5	0.52±0.03	(43)

(*) See discussions at the end of §8.3(c) and Table 8.2.

Table 5.4 Other Parameters

Parameters	C_1(DAM)	C_1(WCM)	C_2(DAM)	C_2(WCM)	C_1'(DAM)
$\lambda_\rho=\lambda_\omega$ (GeV^{-2})	0.86	0.88	0.90	0.90	0.90
λ_B (GeV^{-2})	0.68	0.70	0.70	0.70	0.70
λ_P (GeV^{-2})	0.40	0.39	0.30	0.30	0.10
$s_{o\rho}$ (GeV^2)	1.31	1.49	$(6\lambda_\rho)^{-1}$	$(6\lambda_\rho)^{-1}$	$(\lambda_\rho)^{-1}$
$s_{o\omega}$ (GeV^2)	0.83	0.63	$(\lambda_\omega)^{-1}$	$(\lambda_\omega)^{-1}$	$(\lambda_\omega)^{-1}$
s_{oB} (GeV^2)	0.80	0.63	$(\lambda_B)^{-1}$	$(\lambda_B)^{-1}$	$(\lambda_B)^{-1}$
$s'_{o\rho}$ (GeV^2)	$s_{o\rho}$	$s_{o\rho}$	$(\lambda_\rho)^{-1}$	$s_{o\rho}$	$s_{o\rho}$
$s'_{o\omega}$ (GeV^2)	$s_{o\omega}$	$s_{o\omega}$	$s_{o\omega}$	$s_{o\omega}$	$s_{o\omega}$
$\tilde{\lambda}^{(\rho P)}_{\frac{1}{2},\frac{1}{2}}$	4.1	1.0	3.5	1.0	4.25
$\tilde{\lambda}^{(\omega P)}_{\frac{1}{2},\frac{1}{2}}$	3.8	1.0	3.5	1.0	4.25
$\tilde{\lambda}^{(\rho P)}_{-\frac{1}{2},\frac{1}{2}}$	1.5	1.0	1.0	1.0	1.0
$\tilde{\lambda}^{(\omega P)}_{-\frac{1}{2},\frac{1}{2}}$	1.5	1.0	1.0	1.0	1.0
A_o (GeV^{-2})	2.40	2.35	0	0	4.0
$G^{(B)}/G_4^{(\omega)}$	-1.62	-2.11	-2.54	-2.54	-0.96
b (GeV^{-2})	4.4	3.79	4.87	4.87	4.4
σ_{tot} (mb)	24	24	24	24	24

CHAPTER 6

CALCULATIONS WITH THE WCM AND COMPARISON WITH THE DAM RESULTS

In this chapter, we shall discuss the Weak Cut Model (WCM) results for the same quantities for which the DAM results were presented in the last chapter. We shall also suggest some tests for experimentally distinguishing between the DAM and the WCM. We shall also discuss the implications of our calculations.

6.1 Weak Cut Model

a) Amplitudes in the WCM

The contribution to the CGLN invariants A_i in the forward direction from the Regge trajectory R (ρ, ω and B exchanges) is taken to be the same as in the DAM (eqn. (5.2)) :

$$A_i^{(R)}(s,t) = \beta_i^{(R)}(t)\ \pi\ \frac{1 - e^{-i\pi\alpha_R(t)}}{\Gamma[\alpha_R(t)]\ \ \mathrm{Sin}[\pi\alpha_R(t)]}\ \left(\frac{s}{s_R}\right)^{\alpha_R(t)-1} \tag{6.1}$$

The explicit forms of the residues $\beta_i^{(R)}(t)$ have been shown in Table 5.1. As usual, s_R is the energy scale.

For the cut contributions, we remember that (see chapter 3 and Appendix I) the WCM is defined by taking

$$\tilde{\lambda}^{(RP)}_{\frac{1}{2},\frac{1}{2}} = \tilde{\lambda}^{(RP)}_{-\frac{1}{2},\frac{1}{2}} = 1.0 \tag{6.2}$$

and

$$s_{0R} = s'_{0R} \tag{6.3}$$

Of course in C_1(WCM) we take $A_0 \neq 0$, while in C_2(WCM) we have $A_0 = 0$ (see Appendix I).

It is easy to see that in this model, the analyticity constraint (5.3) is satisfied exactly in the same way as in the case of the DAM.

b) Features of Fits produced

The fits to the experimental data are shown in Figs. 6-14. The corresponding Regge pole and Regge cut parameters have already been given in Tables 5.3 and 5.4.

i) $\frac{d\sigma}{dt}$ for $\gamma p \to \pi^0 p$: As in the DAM, both Models C_1 and C_2 account fairly well for both the t-structure and the energy variation of the data (Fig. 6). However, the WCM always gives a slightly stronger dip at $t \simeq -.55$ GeV^2 compared with the corresponding DAM.

ii) Polarised photon asymmetry Σ for $\gamma p \to \pi^0 p$: Again both models are quite successful in explaining the data (Fig.7).

iii) The ratio $R = \frac{d\sigma}{dt}(\gamma n \to \pi^0 n) / \frac{d\sigma}{dt}(\gamma p \to \pi^0 p)$: At 4 GeV, the ratio R comes out somewhat high. At 8 GeV, the fit is quite good.

iv) Polarised target asymmetry T for $\gamma p \to \pi^0 p$: Both models fail quite badly. Model C_1 gives a small positive value for this quantity in the small $|t|$ region. T changes sign at $t \simeq -.55$ GeV^2, and assumes a small negative and practically constant value upto $|t| \leq 1$ GeV^2 (Fig. 9). Model C_2 predicts a very small T for all $|t| \leq 1$ GeV^2 (not shown in Fig. 9).

v) $\frac{d\sigma}{dt}$ for $\gamma p \to \eta p$: Model C_1(WCM) exhibits a shoulder at $t \simeq -.55$ GeV^2, just like the corresponding C_1(DAM). Model C_2 (WCM), on the other hand, does not exhibit any dip at $t \simeq -.55$ GeV^2 and fits the data quite well (Fig. 10)

vi) $X_\omega(s,t)$ for $\pi N \to \rho N$: Both the models fit the data quite well. The results are very similar to the corresponding DAM results (see Fig. 11; the WCM results are not shown).

vii) The quantities $\rho^{(t)}_{11} \frac{d\sigma}{dt}$, $[\rho^{(t)}_{11} - \rho^{(t)}_{1-1}] \frac{d\sigma}{dt}$ and $[\rho^{(t)}_{11} + \rho^{(t)}_{1-1}] \frac{d\sigma}{dt}$ for $\pi^+ n \to \omega p$: For the first two quantities, both models show strong dips near t= 0 (Fig. 12 and 13). At larger values of $|t|$, both models show reasonably good agreement with the data, although for the quantity $\rho^{(t)}_{11} \frac{d\sigma}{dt}$, Model C_2(WCM) seems to produce the better fit. For the quantity $[\rho^{(t)}_{11} + \rho^{(t)}_{1-1}] \frac{d\sigma}{dt}$, both the Weak Cut Models predict strong dips around $t \simeq -.55$ GeV^2 .

c) Values of Constants

Both $\frac{d\sigma}{dt}$ and Σ for $\gamma p \to \pi^0 p$ and $X_\omega(s,t)$ for $\pi N \to \rho N$ are effectively determined by the single-flip amplitude which is dominated by ω exchange. Since the DAM and the WCM are quite similar for single-flip amplitudes and the parameters used for ω exchange corresponding to this helicity amplitude in both the DAM and the WCM are also similar, the corresponding results are predictably similar.

In our discussions in § 3.2. we pointed out that if vector exchanges dominate, then the WCM should produce an unwanted dip in $\frac{d\sigma}{dt}$ for $\gamma p \to \eta p$ around $t \simeq -.55$ GeV^2 . Model C_2(WCM) does not give this dip. Model C_1 (WCM) produces a shoulder around this point, but this is weaker than that produced by C_1(DAM). The reason for this is that in both the WCM's, we have introduced a relatively large B contribution. This is also evident from an examination of the quantity $[\rho^{(t)}_{1\,1} - \rho^{(t)}_{1\,-1}]\frac{d\sigma}{dt}$ (Fig. 13) at $t \simeq -.6$ GeV^2.

At this point, this quantity is exclusively determined by the amount of B contribution, and we see that this is somewhat overestimated in both the WCM's. Moreover, in order to obtain the proper normalisation for $\rho^{(t)}_{1-1}\frac{d\sigma}{dt}$, $[\rho^{(t)}_{1\,1} - \rho^{(t)}_{1\,-1}]\frac{d\sigma}{dt}$ and $[\rho^{(t)}_{1\,1} + \rho^{(t)}_{1\,-1}]\frac{d\sigma}{dt}$, the model C_2(WCM) has to use a value of $\frac{\gamma_\omega^2}{4\pi}$, which is about 3 times larger than the experimentally observed value (Table 5.3).

6.2 Conclusions and Predictions

The Dual Absorptive Model imposes the requirement that the imaginary parts of the different helicity amplitudes be peripheral. It, however, does not specify how to achieve this objective. In this work, we have introduced suitable amounts of Regge cuts (Reggeon-Pomeron cuts to be exact) in addition to the corresponding Regge pole contributions in order to obtain the required peripherality. These Regge cut contributions have been calculated through the absorption prescription (eqn. (3.18)). So, our principal motivation for carrying out this calculation is to examine whether the absorption prescription is a proper tool for implementing the DAM requirements.

We have seen that both the models C_1(DAM) and C_2(DAM) are in reasonable agreement with the data (except with those for the parameter T). It is true that C_1(DAM) predicts shoulders at $t \simeq -.55$ GeV^2 for the quantities $\frac{d\sigma}{dt}(\gamma p\to\eta p)$ and $\rho^{(t)}_{11}\frac{d\sigma}{dt}$,$[\rho^{(t)}_{11}+\rho^{(t)}_{1-1}]\ \frac{d\sigma}{dt}$ for $\pi^+ n\to\omega p$. No dips are experimentally observed for these at this point. However, the corresponding data contain large errors (in particular for the last quantity). So the presence of a small shoulder cannot be ruled out.

Both models C_1(DAM) and C_2(DAM) seem to be in disagreement with the present data on the polarised target asymmetry T. Parameters corresponding to Model C_1'(DAM) give better numerical results, but the t-dependence remains basically the same. It should be pointed out here that other Regge cut model calculations through the absorption prescription, as carried out by Gault et al[6] and Worden[44] as well as the WCM (see §6.1), also give similar results. So far, the parameter T has been measured only at one energy, and the data contain large errors. If more precise and thorough measurements confirm the present data, then the conclusion will be that the absorption prescription is not a suitable method for calculating the Regge cut corrections to reggeized vector exchanges.

We can speculate here about the reasons for the seeming failure of the absorption prescription. It is true that we have imposed the DAM requirements on the imaginary parts of the helicity amplitudes in a reasonably satisfactory manner. It should be remembered that these requirements are to be satisfied irrespective of the particular method chosen to calculate the Regge cut contributions. However, for the corresponding real parts, only for the n=1 amplitudes does the DAM implicitly predict any definite t-behaviour (eqn. (4.3)). For the n=0 (and the n=2) amplitudes, these real parts are determined in a model dependent way (in this case, the absorption prescription). Since of all the quantities we have tried to fit, T is the most sensitive to the real parts of the amplitudes, the shapes of the real parts of n=0 and n=2 amplitudes in our models should be blamed for the disagreement with the data. Notice that Re $f^{(0)}_{\frac{1}{2}\frac{1}{2}}$ (Fig. 19) of our models do not look at all like the real part of the n=0 amplitude of Halzen-Michael and Kelly[25] analyses.

It is also possible that the DAM requirements should not be imposed through the introduction of Regge cuts in the first place. However, the theoretical basis of the existence of these cuts have been well established [16,17]. So, such a possibility demands a proper evaluation of the relative importance of Regge cuts for different hadronic interactions.

Another motivation for doing this work is as follows. If we accept that, at least in photoproduction, the absorption prescription is suitable for calculating Regge cut contributions, we would like to see if we can experimentally distinguish between the DAM and the WCM on the basis of the existing data or from some yet unmeasured quantities.

The present data on $\frac{d\sigma}{dt}$ and for $\gamma p \to \pi^0 p$ and the corresponding ratio R do not really prefer one model over the other. The same is true for the differential cross-section for $\gamma p \to \eta p$. The predictions for the polarised photon asymmetry Σ for η production for all models at 4 GeV are shown in Fig. 20. We see that the WCM (both C_1 and C_2) predicts a strong dip in Σ at $t \simeq -.5$ GeV^2, and, in general, this quantity should show a strong t-dependence, while the DAM (again both C_1 and C_2) gives only a small shoulder at that point. So an accurate measurement of this quantity will help in distinguishing between the DAM and the WCM. The ratio $R = \frac{d\sigma}{dt}(\gamma n \to \eta n)/\frac{d\sigma}{dt}(\gamma p \to \eta p)$ is also shown in Fig. 20. The predictions are very similar in both the models.

A more precise determination of the small t-behaviour ($t \sim 0$) of the quantities $\rho^{(t)}_{11} \frac{d\sigma}{dt}$ and $[\rho^{(t)}_{11} - \rho^{(t)}_{1-1}] \frac{d\sigma}{dt}$ for $\pi^+ n \to \omega p$ will be very useful for our purpose. The WCM gives strong dips near $t=0$, a feature not predicted by the DAM. But the most clear distinction can be obtained from the behaviour of the quantity $[\rho^{(t)}_{11} + \rho^{(t)}_{1-1}] \frac{d\sigma}{dt}$ near $t \simeq -.55$ GeV^2. The WCM predicts a strong dip at this point, while the DAM does not give this dip, or at best produces a small shoulder. Unfortunately, due to the inaccuracy of the present data, definite conclusions about the presence or the absence of this dip cannot be made.

PART C : CHARGED PION PHOTOPRODUCTION

CHAPTER 7

REVIEW OF EXISTING MODELS

In this part of the thesis, we shall discuss different aspects of photoproduction of π^+ and π^-. The important features observed in the case of charged pion photoproduction are:

a) Both π^+ and π^- cross-sections show sharp forward peaks of width $\sim\mu^2$(μ = pion mass).

b) The ratio $R = \frac{d\sigma}{dt}(\gamma n \to \pi^- p) / \frac{d\sigma}{dt}(\gamma p \to \pi^+ n)$ has a value R=1 in the forward direction (t=0) and then drops rapidly and shows a broad dip around $t \simeq -.4$ GeV^2.

c) Unlike π^0 photoproduction, charged pion photoproduction does not show any dip around $t \simeq -.55$ GeV^2.

d) The polarised photon asymmetry Σ (defined in eqn. (2.17)) for both π^+ and π^-, rises rapidly from $\Sigma=0$ at t=0 to $\Sigma \sim 1$ at $t \sim -\mu^2$. After this initial increase, Σ drops for both $\pi^\pm$, the drop for π^- being faster than that for π^+.

e) The polarised target asymmetry T (defined in eqn. (2.18)) has been measured for the process $\gamma p \to \pi^+ n$. The data show that T, starting from zero at t=0, becomes large negative with increasing $|t|$. For $|t| \geq .5$GeV^2, T decreases in absolute value.

f) In the backward direction, the π^+ differential cross-section drops smoothly with increasing $|u|$, and exhibits no dip structure. There is yet no experimental information for backward $\gamma n \to \pi^- p$.

The photoproduction of charged pions involves the isotopic spin combinations $A_i^{(-)} \pm A_i^{(0)}$. The Regge exchanges in the t-channel corresponding to these amplitudes are shown in Table 2.1. The asymptotic expressions for the forward and the backward cross-sections in terms of the CGLN invariants are given in eqns. (2.20) and (2.21) respectively.

Pion exchange dominates the cross-section in the extreme forward direction ($t \sim 0$) and this is demonstrated by the sharp forward peak of width $\sim \mu^2$. We shall now proceed with a brief review of the most important theoretical models advanced for the understanding and the description of charged pion photoproduction.

7.1 Electric Born Model

The forward structure of charged pion photoproduction can be explained on the basis of a gauge invariant perturbation theory model (Electric Born Model). This consists of an elementary pion exchange in the t-channel and nucleon contributions in the s- and u-channels; the nucleon anomalous magnetic moment is ignored. The corresponding Feynman diagrams for $\gamma p \to \pi^+ n$ are shown in Figs. 21 a,b,c. The elementary pion exchange alone (Fig. 20a) is not gauge invariant; the nucleon exchange diagrams (b) and (c) must in addition be considered in order to obtain a gauge invariant contribution.

If we only consider the electric and the normal magnetic moment couplings between the photon and the nucleon, then elementary Feynman diagram calculations give the following contributions to the different CGLN amplitudes:

$$A^{(+)}=A^{(0)}=\tfrac{1}{2}eg\left[\frac{1}{s-M^2}+\frac{1}{u-M^2}\right] \quad ; \quad A^{(-)}=\tfrac{1}{2}eg\left[\frac{1}{s-M^2}-\frac{1}{u-M^2}\right]$$

$$B^{(+)}=B^{(0)}=eg\,\frac{1}{(s-M^2)(u-M^2)} \quad ; \quad B^{(-)}=eg\,\frac{s-u}{(s-M^2)(u-M^2)(t-\mu^2)} \tag{7.1}$$

In the asymptotic limit $s\to\infty$, t small, it is clear from (7.1) that the amplitudes $A^{(-)}$ and $B^{(-)}$ dominate over $A^{(0)}$ and $B^{(0)}$. So for small $|t|$ we can write

$$\frac{d\sigma_\perp}{dt}\simeq\frac{1}{8\pi}\,|A^{(-)}|^2;\quad \frac{d\sigma_\parallel}{dt}\simeq\frac{1}{8\pi}\,|A^{(-)}+tB^{(-)}|^2\quad;\quad \frac{d\sigma}{dt}=\tfrac{1}{2}\left(\frac{d\sigma_\perp}{dt}+\frac{d\sigma_\parallel}{dt}\right) \tag{7.2}$$

Thus at $t=0$:

$$\frac{d\sigma_\perp}{dt}=\frac{d\sigma_\parallel}{dt} \tag{7.3}$$

This condition is essentially a restatement of the analyticity constraint eqn. (2.26).

Form (7.1), we see that $A^{(-)}$ increases very slowly with $|t|$, and so $\frac{d\sigma_\perp}{dt}$ is almost constant in the forward direction. So the t-structure of $\frac{d\sigma}{dt}$ is to explained solely on the variation of $\frac{d\sigma_\parallel}{dt}$ with t. For calculating $\frac{d\sigma_\parallel}{dt}$, we note that the Electric Born Model gives

$$A^{(-)}+tB^{(-)} = \tfrac{1}{2}eg \frac{s-u}{(s-M^2)(u-M^2)} \frac{t+\mu^2}{t-\mu^2} \qquad (7.4)$$

This shows that $\frac{d\sigma_\parallel}{dt}$ starts from a finite value ($= \frac{d\sigma_\perp}{dt}$) at t=0 and drops off to zero at $t=-\mu^2$ and then rises again. The quantities $\frac{d\sigma_\perp}{dt}$, $\frac{d\sigma_\parallel}{dt}$ and $\frac{d\sigma}{dt}$ are plotted in Fig. 22. The Electric Born Model qualitatively reproduces the forward peak in $\frac{d\sigma}{dt}$. However for $|t|>\mu^2$, $\frac{d\sigma}{dt}$ as calculated from this model, starts increasing again, in total disagreement with the experimental data, which show a smooth decrease, more in tune with conventional Regge behaviour. Quantitatively, the Electric Born Model agrees reasonably well with the experimental cross-section in the region $|t|\leq\mu^2$.

From (7.3) and (7.4), it is also evident that the polarised photon asymmetry Σ rises from $\Sigma=0$ at t=0 (where $\frac{d\sigma_\perp}{dt} = \frac{d\sigma_\parallel}{dt}$) to $\Sigma=1$ at $t=-\mu^2$(where $\frac{d\sigma_\parallel}{dt} = 0$). Also since the amplitudes $A_i^{(0)}$ are small compared to $A_i^{(-)}$, the ratio R=1 at t~0 as experimentally observed. All versions of the pion exchange model (including pion parity doublet and Regge cut models , and not just the Electric Born model) explain the forward structure of $\frac{d\sigma}{dt}$, Σ and R in a similar way. The change in $\frac{d\sigma}{dt}$ comes almost entirely from the rapid t-variation of $\frac{d\sigma_\parallel}{dt}$, while $\frac{d\sigma_\perp}{dt}$ is essentially constant in t.

7.2 Regge Cut (Absorption) Model

The analyticity properties of the CGLN amplitudes lead to the requirement that at t=0, the singularity free PCTHA's must satisfy (eqn. (2.26))

$$\tilde{f}^{++}_{11}(s,0) = M\ \tilde{f}^{-+}_{01}(s,0) \qquad (7.5)$$

While discussing the photoproduction of π^0 and η mesons, we showed (§ 5.1) how the ρ and B trajectories satisfy this condition (by evasion). In the present case, we have two additional trajectories, π and A_2, which contribute to $\tilde{f}^{-+(-)}_{01}$ and $\tilde{f}^{++(-)}_{11}$ respectively (the superscript (-) denotes the i-spin index). As in the case of the ρ trajectory, A_2 gives a contribution that vanishes at t=0 ($\tilde{f}^{++(A_2)}_{11}$ (s,t) $\to$ 0, as $t\to 0$; evasive solution).

The simplest possibility is that the pion as well gives a contribution that vanishes at t=0,iė which at small $|t|$ behaves as:

$$\tilde{f}^{-+(\pi)}_{01}(s,t) \simeq \beta_\pi(t)\ \frac{t}{t-\mu^2} \qquad \left(\frac{s}{s_0}\right)^{\alpha_\pi(t)-1} \qquad (7.6)$$

where $\beta_\pi(t)$ is a smoothly varying function of t ($\beta_\pi(0)\neq 0$). However, as already mentioned, there is a sharp forward peak in the differential cross-section for charged pion production, and this peak has a width $\sim\mu^2$ and should presumably be explained on the basis of pion exchange. A pion contribution vanishing at t=0 will give a dip instead of a peak. So, we have to have some additional non-vanishing contribution at t=0. This can be done by generating through the Bessel transform of eqn. (3.18) a pion-Pomeron Regge cut, like the ρ-Pomeron and the ω-Pomeron cuts of chapter 5. This cut (having no definite normality σ) contributes to both $\tilde{f}_{01}^{-+}$ and $\tilde{f}_{11}^{++}$ with contributions

$$M\, \tilde{f}_{01}^{-+(\pi P)}(s,0) \;=\; \tilde{f}_{11}^{++(\pi P)}(s,0)$$

thus satisfying the constraint (7.5). So, we have

$$\begin{aligned} \tilde{f}_{01}^{-+}(s,t) &= \tilde{f}_{01}^{-+(\pi)}(s,t) + \tilde{f}_{01}^{-+(\pi P)}(s,t) \\ \tilde{f}_{11}^{++}(s,t) &= \tilde{f}_{11}^{++(\pi P)}(s,t) \end{aligned} \qquad (7.7)$$

(leaving out contributions from other exchanges like A_2 etc.)

The sign of $\tilde{f}_{01}^{-+(\pi P)}$ is so chosen that it interferes destructively with $\tilde{f}_{01}^{-+(\pi)}$. This destructive interference produces the sharp forward peak as shown in Fig. 23.

Notice that such a picture is in complete agreement with elementary pion exchange plus absorption corrections[20]. At small $|t|$, Regge and elementary pions are practically indistinguishable; and the effect of of the Regge cuts is very much the same as that of the absorption corrections.

Models based on the above Regge cut mechanism account quite well for the experimental situation in charged pion photoproduction[5].

7.3 Pion Parity Doublet Model

This model does not use any Regge cuts. $\tilde{f}^{-+(-)}_{01}$ receives its entire contribution from the exchange of the pion Regge trajectory, and this contribution is non-vanishing in the forward direction. In order to satisfy the analyticity constraint (7.5), the existence of another trajectory $\alpha_{\pi'}(t)$, which has positive parity, but has all other quantum numbers the same as those of the pion trajectory ('parity doublet conspiracy'), is assumed. $\alpha_{\pi'}(t)$ contributes to $\tilde{f}^{++}_{11}(s,t)$, and if $\alpha_{\pi}(0)= \alpha_{\pi'}(0)$ and $\beta_{\pi}(0)= \frac{1}{M} \quad \beta_{\pi'}(0)$ ($\neq 0$), (where $\beta_{\pi}(t)$ and $\beta_{\pi'}(t)$ are the residue functions of the π and π' contributions to $\tilde{f}^{-+}_{01}$ and $\tilde{f}^{++}_{11}$ respectively), then (7.5) is satisfied. Also, both $\tilde{f}^{-+}_{01}(s,t)$ and $\tilde{f}^{++}_{11}(s,t)$ give finite contributions to the differential cross-section at t=0. Good fits were obtained by Ball, Frazer and Jacob[45] to charged pion photoproduction using such a model. Similar mechanisms were also used to explain the forward structure of $np \rightarrow pn$[46,47], where similar problems with analyticity constraints arise as well.

For quite some time, this model received much attention, because the existence of such a parity doublet was predicted in the Toller classification of Regge trajectories. Particle theorists were initially led to this classification by group theoretical methods[48.49], and later by means of analyticity and factorisation[50]. However, certain serious difficulties in connection with factorisation and the forward structure of the reaction $\pi^+ p \rightarrow \rho^0 \Delta^{++}$[51,52] and with the soft pion limit[53], as well as the fact that the existence of particles corresponding to quantum numbers of π' has not been unambiguously established, made this model rather unpopular.

7.4 Pseudomodel[54]

Both the model with a pion parity doublet conspiracy and the model with an evasive pion and pion absorption cut are consistent with Finite Energy (FE) and Continuous Moment (CM) sum rules, as the works of Bietti et al[55], DiVecchia et al[56] and Jackson and Quigg[54] indicate. This suggeste that one can attempt to explain the forward structure of this reaction essentially on the basis of its low energy features and the sum rules, without postulating any specific high energy model . This approach[54] leads to quite successful fits to the differential cross-section and the polarised photon asymmetry Σ for $|t| \leq .45 \text{GeV}^2$('pseudomodel').

Sum rules are applied by Jackson and Quigg to the t-channel helicity amplitudes $H_i (i=1,4)$, which are related to the PCTHA $f_{\mu\lambda}^{\sigma,\sigma_c}(s,t)$ of §2.3 as follows:

$$\tilde{f}^{++}_{01} = \sqrt{2}H_1 ; \quad \tilde{f}^{-+}_{01} = \frac{\sqrt{2}H_2}{t-\mu^2} ; \quad \tilde{f}^{++}_{11} = \frac{1}{\sqrt{2}} H_3 \quad ; \tilde{f}^{--}_{11} = -2\sqrt{2}\, H_4 \qquad (7.8)$$

The contributions of the trajectories π, B, ρ, A_2 and A_1 to the H_i's can be easily deduced from (7.8) and Table 2.1, In the forward direction, the contributions from ρ,B and A_1 are negligible, and we consider only contributions from π and A_2, both of which have even signature.

Now if ϕ_i denotes the low energy side of the sum rule for the amplitude H_i, then the $\gamma^{th.}$ CMSR is given by

$$\phi_i(\gamma, \nu_{max}, t) = -\frac{\mu}{\pi} \int_0^{\nu_{max}} d\nu \left(\frac{\nu}{\nu_{max}}\right)^{\gamma} \text{Im}\,[e^{-\frac{1}{2}i\pi\gamma} H_i(\nu, t)] \qquad (7.9)$$

where $\nu = \frac{s-M^2}{2\ M}$ = incident photon energy in the lab frame.

Eqns. (7.8) and (7.9) establish the connection between the ϕ_i's(γ, ν_{max}, t) and the H_i's. These in turn relate the ϕ_i's to the CGLN invariants A_i's through (2.24). Some algebra gives (using eqn. (2.20)), in the forward direction ($t \sim 0$):

$$\begin{aligned} (s-M^2)^2 \frac{d\sigma_\perp}{dt} &= \frac{1}{4\pi\mu^2} [\ |\phi'_3|^2 - |\phi'_1|^2] \\ (s-M^2)^2 \frac{d\sigma_\parallel}{dt} &= \frac{M^2}{\pi\mu^2} \left[\frac{|\phi'_2|^2}{(t-\mu^2)^2} - |\phi'_4|^2 \right] \end{aligned} \qquad (7.10)$$

where $\phi'_i = \lim_{t\to 0} \phi_i(\gamma=0, \nu_{max}, t)$

The ϕ'_i's in (7.10) are completely supplied by low energy data. Eqns. (7.10) were obtained without using any specific model for the H_i's in the right hand side of eqn. (7.9). This model fits the differential cross-section of π^+ photoproduction quite well upto $t \simeq -.45$ GeV^2 . Its predictions for polarised photon asymmetry Σ also agree with the experimental data quantitatively upto $t \sim -\mu^2$ and qualitatively upto $t \simeq -.45$ GeV^2 (54).

7.5 The Veneziano Model

We have seen that the gauge invariant Electric Born Model is quite successful in explaining the features of charged pion photoproduction in the extreme forward direction. However, as we mentioned in §7.1, for $|t|>\mu^2$, this model predicts a differential cross-section $\frac{d\sigma}{dt}$ increasing with $|t|$, while the experimental $\frac{d\sigma}{dt}$ decreases smoothly, and is compatible with conventional Regge behaviour. It is of interest to formulate a model which will be compatible with the Electric Born Model at small $|t|$, while giving the desired Regge behaviour at large $|t|$.

The Veneziano representation is one framework, through which this objective can be achieved. In the next chapter, we shall explicitly build up a Veneziano model with π, A_2, ρ and A_1 exchanges in the t-channel and N_α , N_γ and Δ exchanges in the s- and u-channels, and shall try to account for the different features of charged pion photoproduction. In the limit $s\to\infty$, t small, the Veneziano model for any particular CGLN invariant amplitude will give an energy dependence ~ $s^{\alpha(t)-1}$, where $\alpha(t)$ is the Regge trajectory dominating the amplitude. At small $|t|$, where the pion contribution dominates, the corresponding amplitudes will have a power behaviour ~ $s^{\alpha_\pi(0)-1}$ ~ s^{-1} as $\alpha_\pi(0) \simeq 0$. If we look at the Born expression (7.4), we see that at $t \sim 0$, $A^{(-)}+tB^{(-)}$ has the same power behaviour $\sim s^{-1}$. To ensure that the Veneziano model also produces the Electric Born results quantitatively, we shall impose the constraints that the residues of the Veneziano model expression for the amplitudes $A^{(-)}+tB^{(-)}$ at the pion and the nucleon poles be the same as those obtained from the Electric Born model at the same points.

There are two other advantages of using the Veneziano model. Firstly being a dual model, it satisfies FESR's, at least approximately[57]. Secondly, being crossing symmetric, it can be used, at least in principle, to describe charged pion photoproduction in both the forward and the backward directions. The application of the model to backward $\gamma p \to \pi^+ n$ will be taken up in §8.5.

CHAPTER 8

CALCULATIONS WITH THE VENEZIANO MODEL

In this chapter, we shall formulate a Veneziano model for the different CGLN invariant amplitudes and apply this model to explain the various features of charged pion photoproduction in both forward and backward directions.

In the last chapter, we discussed the pseudomodel of Jackson and Quigg. We saw that as far as the explanation of the forward peak in $\pi^{\pm}$ photoproduction is concerned,the pion parity doublet model and the evasive pion model with absorptive pion-Pomeron cuts are equivalent. The incorporation of absorptive corrections in a crossing symmetric (Veneziano type) framework is quite a complicated problem, while the pion parity doublet model can be formulated in a straight forward and simple way. So in our formulation of the Veneziano model, we shall adopt the pion parity doublet approach.

The parity partner of the pion, π', will contribute to the singularity free PCTHA $\tilde{f}_{11}^{++(-)}(s,t)$. Now, $\tilde{f}_{11}^{++(-)}(s,t)$ also receives contributions from A_2 exchange in the t-channel and from baryon resonances in the s- and u-channels. If only a finite number of resonances are considered, then in the high s limit, the corresponding contribution has the behaviour $\tilde{f}_{11}^{++(-)} \sim \sum_n s^{-n}$, where n is an integer. In the

Veneziano approach, the number of resonances are infinite, and the corresponding infinite sum can be considered to give a contribution $\tilde{f}_{11}^{++(-)}(s,t) \sim s^{\alpha_{\pi'}(t)-1}$, where $\alpha_{\pi'}(t)$ denotes the Regge trajectory of π' (conspirator).

In the second portion of this thesis, when we were considering π^0 and η photoproduction, we used a substantial B meson (σ=-) contribution to the amplitude $B^{(0)}$. This contribution is evasive, iė it vanishes at t=0. In the extreme forward direction (t~0), pion exchange (σ=-) dominates charged pion photoproduction (contribution to $B^{(-)}$), and is taken to be non-evasive. An analysis by Diebold[58] of the experimental data shows that the combinations ($\pi\pm B$) which contribute to $\pi^{\pm}$ photoproduction, are essentially dominated by the pion contribution in the forward direction. Since the present analysis will be confined to small $|t|$, we shall construct our Veneziano amplitudes simply by neglecting the B exchange.

8.1 Parity Doublets, Walker Residues

Near an s-channel resonance, say at $s=s_0$, each of the CGLN invariants A_i has a behaviour of the form $\frac{g^{(i)}(t)}{s-s_0}$ where $g^{(i)}(t)$ is a polynomial in t. If the highest spin of all resonant states at $s=s_0$ is J, then the degree of $g^{(i)}(t)$ in t is related to J. We consider the case that the highest spin J resonance has a definite normality $\sigma(=P(-)^J)$, and we denote by $A_J^{(i)}$ the coefficients of the leading terms of $g^{(i)}(t)$. Then it can be shown that[10]:

$$\text{Res. } A \simeq A_J\ t^{J-\frac{1}{2}} \quad ; \quad \text{Res. } B \simeq B_J\ t^{J-\frac{3}{2}}$$

$$\text{Res. } (C+D) \simeq (C_J+D_J)\ t^{J-\frac{1}{2}} \quad ; \quad \text{Res. } (C-D) \simeq (C_J-D_J)\ t^{J-\frac{3}{2}} \tag{8.1}$$

The symbol $\simeq$ means we are only considering the leading t-behaviour. Then from eqns. (2.11), which connect the amplitudes F_i's to A_i's, we obtain the degrees of F_i's as

$$F_1 \sim t^{J-\frac{1}{2}} \ ; \ F_2 \sim t^{J-\frac{1}{2}} \ ; F_3 \sim t^{J-\frac{3}{2}} \ ; F_4 \sim t^{J-\frac{3}{2}} \tag{8.2}$$

Now the s-channel regularised helicity amplitudes $\bar{f}_{\mu\lambda}$ (i=1,4) are related to the F_i's as follows (see eqn. (2.13)):

$$\bar{f}_{\frac{1}{2},\frac{3}{2}} = -\frac{1}{\sqrt{2}}\{F_3+F_4\} \quad ; \quad \bar{f}_{\frac{1}{2},\frac{1}{2}} = \sqrt{2}\ \{F_2-F_1+\tfrac{1}{2}(1-\text{Cos }\theta_s)(F_3-F_4)\}$$

$$\bar{f}_{-\frac{1}{2},\frac{3}{2}} = \frac{1}{\sqrt{2}}\{F_3-F_4\} \quad ; \quad \bar{f}_{-\frac{1}{2},\frac{1}{2}} = \sqrt{2}\ \{F_2+F_1+\tfrac{1}{2}(1+\text{Cos }\theta_s)(F_3+F_4)\} \tag{8.3}$$

Then it can be shown that[10]

$$\bar{f}_{\frac{1}{2},\frac{3}{2}} \simeq \sigma\bar{f}_{-\frac{1}{2},\frac{3}{2}} \quad ; \quad \bar{f}_{\frac{1}{2},\frac{1}{2}} \simeq \sigma\bar{f}_{-\frac{1}{2},\frac{1}{2}} \tag{8.4}$$

From (8.3), this implies that

$$F_3 \simeq 0 \quad ; \quad 2F_1+F_4+\cos\theta_s \simeq 0 \qquad (\sigma=+) \qquad (8.5)$$

$$F_4 \simeq 0 \quad ; \quad 2F_2+F_3+\cos\theta_s \simeq 0 \qquad (\sigma=-) \qquad (8.6)$$

These two equations, coupled with (8.2), give

$$F_3 \simeq 0 \quad ; \quad F_1 \simeq 0 \qquad (\sigma=+) \qquad (8.7)$$

$$F_4 \simeq 0 \quad ; \quad F_2 \simeq 0 \qquad (\sigma=-) \qquad (8.8)$$

Using the relationship between the F_i's and the A_i's (eqn. (2.11)), we immediately obtain from (8.7) and (8.8)

$$\left.\begin{array}{l}(W-M)B_J + (C_J-D_J) = 0 \\ 2A_J+ B_J + (W-M)(C_J+D_J) = 0\end{array}\right\} \qquad (\sigma=+) \qquad (8.9)$$

and

$$\left.\begin{array}{l}(W+M)B_J - (C_J-D_J) = 0 \\ 2A_J+ B_J - (W+M)(C_J+D_J) \quad 0\end{array}\right\} \qquad (\sigma=-) \qquad (8.10)$$

Notice that if $W \longleftrightarrow -W$, eqns. (8.9)$\longleftrightarrow$(8.10). This is an explicit statement of the MacDowell symmetry[59].

These last two eqns. are satisfied when the resonance with spin J has a definite normality. If a resonance with spin J has $\sigma=+$ [$-$] and does not satisfy eqn. (8.9) [(8.10)] , then it means that it recieves contributions from a resonance at the same $s(=s_0)$ and with spin J, but with opposite normality; then we have a parity doublet. Since the evidence for the presence of parity doublets is very scanty, in our construction of the Veneziano amplitudes, we shall eliminate parity doublets, at least from the experimentally known (lower mass) baryon states.

Walker[12] has calculated the residue functions at various baryon poles in the s-channel from the low energy photoproduction data. For a given resonance of spin J, the residues A_J and B_J can be calculated from Walker's data in a straightforward manner (see Appendix III). Then if the resonance has $\sigma=+$ [$-$], we can use eqn. (8.9) [(8.10)] to calculate C_J and D_J. This automatically eliminates any contribution from the parity partners[10]. The corresponding results are shown in Table 8.1. So, we shall construct our Veneziano amplitudes in such a way that they reproduce the Walker residues of the low spin baryon resonances.

8.2 Explicit Veneziano Representations for the CGLN Invariants

While considering the baryon exchanges in the s- and the u-channels, we shall assume an exchange degenerate N_α-N_γ[60,61] trajectory, but a non-degenerate Δ_δ trajectory. The pion, its parity partner π',A_1 and A_2 all couple to the isovector part of the photon, and as such, the corresponding exchanges in the s- and the u-channels will include all three baryon trajectories - N_α ,N_γ and Δ_δ. On the other hand, ρ couples to the isoscalar part of the photon, and so only the N_α and N_γ trajectories are allowed in the crossed channels.

The pion exchange in the t-channel and N_α , N_γ and Δ_δ exchanges in the s- and u-channels contribute to the combination $A^{(-)}+tB^{(-)}$ $(\sigma=-)$, and the simplest form(62) for such a contribution is

$$A^{(-)}+tB^{(-)}=\beta_1\left\{\frac{B[-\alpha_\pi(t),\tfrac{1}{2}-\alpha_N(s)]}{[\tfrac{1}{2}-\alpha_\pi(t)-\alpha_N(s)]} - (s\longleftrightarrow u)\right\}$$

$$+\ \beta_2\ \{B[1-\alpha_\pi(t),\tfrac{1}{2}-\alpha_\Delta(s)] - (s\longleftrightarrow u)\}$$

$$+\ \beta_3\ \{B[\tfrac{1}{2}-\alpha_N(s),\tfrac{1}{2}-\alpha_\Delta(u)] - (s\longleftrightarrow u)\} \tag{8.11}$$

where $B(x,y) \equiv \dfrac{\Gamma(x)\Gamma(y)}{\Gamma(x+y)}$

The trajectory $\alpha_{\pi'}(t)$ contributes to $\tilde{f}^{++}_{11}$ $(=MA - \frac{t}{2}D)$. The analyticity constraint (eqn.(2.26)) involves $\tilde{f}^{++}_{11}(s,0)$. This means that, in terms of CGLN invariants, only the π' contribution to $A^{(-)}$ $(\sigma=+)$ is to be adjusted in order to satisfy eqn. (2.26). For simplicity, we assume that π' contributes only to $A^{(-)}$. $A^{(-)}$ $(\sigma=+)$ also receives contributions from A_2. A_2 satisfies (2.26) by evasion, which implies that the contribution of A_2 to $A^{(-)}$ must vanish as $t\to 0$. So we can write the following Veneziano expression for $A^{(-)}$:

$$
\begin{aligned}
A^{(-)} = \frac{t}{2M^2}\, a_1' \; & \{B[1-\alpha_{A_2}(t),\ \tfrac{3}{2} - \alpha_N(s)] \; - (s \longleftrightarrow u)\} \\
+ a_1 \; & \{B[1-\alpha_{\pi'}(t),\ \tfrac{1}{2} - \alpha_N(s)] \; - (s \longleftrightarrow u)\} \\
+ a_2 \; & \{B[1-\alpha_{\pi'}(t),\ \tfrac{1}{2} - \alpha_\Delta(s)] \; - (s \longleftrightarrow u)\} \\
+ a_3 \; & \{B[\tfrac{1}{2} - \alpha_N(s),\ \tfrac{1}{2} - \alpha_\Delta(u)] \; - (s \longleftrightarrow u)\}
\end{aligned} \tag{8.12}
$$

For the amplitudes $C^{(-)}$ (receiving contribution from A_1 in the t-channel) and $D^{(-)}$ (receiving contributions from A_2 in the t-channel), we have to remember (see eqn. (A.II.12)) that in the asymptotic limit $s \to \infty$, u fixed

$$
C + D \sim s^{\alpha(u) - \frac{3}{2}} \quad ; \quad C - D \sim s^{\alpha(u) - \frac{1}{2}} \tag{8.13}
$$

Also, the models for amplitudes $C^{(-)}$ and $D^{(-)}$ have to be so constructed that the residues of the low baryon resonances as given by Walker (see Table 8.1) are correctly accounted for. We simply take

$$
\begin{aligned}
C^{(-)} = \; & c_1\{\, B[1-\alpha_{A_1}(t),\ \tfrac{1}{2} - \alpha_N(s)] \; + \; (s \longleftrightarrow u)\} \\
+ \; & c_2\{\, B[1-\alpha_{A_1}(t),\ \tfrac{3}{2} - \alpha_N(s)] \; + \; (s \longleftrightarrow u)\} \\
+ \; & c_3\{\, B[1-\alpha_{A_1}(t),\ \tfrac{3}{2} - \alpha_\Delta(s)] \; + \; (s \longleftrightarrow u)\} \\
+ \; & c_4\{\, B[\tfrac{3}{2} - \alpha_N(s),\ \tfrac{3}{2} - \alpha_\Delta(u)] \; + \; (s \longleftrightarrow u)\}
\end{aligned} \tag{8.14}
$$

and

$$
\begin{aligned}
D^{(-)} = \; & d_1\{\; B[1-\alpha_{A_2}(t),\tfrac{1}{2} - \alpha_N(s)] - (s\longleftrightarrow u)\} \\
+ \; & d_2\{\; B[1-\alpha_{A_2}(t),\tfrac{3}{2} - \alpha_N(s)] - (s\longleftrightarrow u)\} \\
+ \; & d_3\{\; B[1-\alpha_{A_2}(t),\tfrac{3}{2} - \alpha_\Delta(s)] - (s\longleftrightarrow u)\} \\
+ \; & d_4\{\; B[\tfrac{3}{2} -\alpha_N(s),\tfrac{3}{2} - \alpha_\Delta(u)] - (s\longleftrightarrow u)\}
\end{aligned}
\tag{8.15}
$$

For the ρ exchange contribution, we again remember that ρ satisfies eqn. (2.26) by evasion, and hence the contribution from ρ to $A^{(0)}$ goes to zero as $t\to 0$. So we write

$$
\begin{aligned}
A^{(0)} = \; & \frac{t}{2\,M}\, c\, \{\; B[1-\alpha_\rho(t),\, \tfrac{7}{2} - \alpha_N(s)] + (s\longleftrightarrow u)\} \\
& + \sum_{k=1}^{3} \gamma_k \frac{\Gamma[(2k-1)/2- \alpha_N(s)]\;\Gamma[(2k-1)/2- \alpha_N(u)]}{\Gamma\,[\; k- \alpha_N(s) - \alpha_N(u)]}
\end{aligned}
\tag{8.16}
$$

The contributions from the exchange degenerate N_α-N_γ trajectories have been written in this particular form, because we want our model to correctly reproduce the Walker residues for $N_\alpha(938)$, $N_\gamma(1519)$ and $N_\alpha(1672)$ resonances (see next section).

There are no known t-channel Regge exchanges contributing to $C^{(0)}$. The corresponding residue at the nucleon pole is proportional to $(\mu_p+\mu_n)$ and is very small. (μ_p and μ_n are the anomalous magnetic moments of the proton and the neutron respectively). Residues of other baryon resonances are also very small. So we take

$$
C^{(0)} = 0 \tag{8.17}
$$

For constructing a model for $D^{(0)}$, we note that since $C^{(0)} + D^{(0)} \sim s^{\alpha(u)-\frac{3}{2}}$, $D^{(0)}$ cannot receive any contribution from the nucleon pole. So the simplest representation for $D^{(0)}$ is

$$D^{(0)} = d \{ B[1-\alpha_\rho(t), \tfrac{5}{2} - \alpha_N(s)] + (s \longleftrightarrow u) \} \tag{8.18}$$

This contributes only to the lower daughters of $\alpha_N(s)$.

8.3 Determination of Constants

The constants in the Veneziano amplitudes written down in the previous section are determined through the following requirements:

a) Exchange non-degeneracy of Δ_δ

The Δ_δ trajectory has a definite signature ξ_Δ given by

$$\xi_\Delta = 1 - e^{-i\pi(\alpha_\Delta - \frac{1}{2})}$$

If we calculate the Δ exchange contributions to the amplitudes $A^{(-)}+tB^{(-)}$, $A^{(-)}$, $C^{(-)}$ and $D^{(-)}$ (eqns. (8.11), (8.12), (8.14) and (8.15)) in the asymptotic limit $s\to\infty$, u fixed, then it is easily seen that in order to obtain the correct signature factor, we must have

$$\beta_2 = \beta_3 \quad ; \quad a_2 = a_3 \quad ; \quad c_3 = c_4 \quad ; \quad d_3 = -d_4 \tag{8.19}$$

b) Asymptotic Behaviour of $C^{(-)}+D^{(-)}$ in the backward direction

In the asymptotic limit $s\to\infty$, u fixed, $C^{(-)}+D^{(-)} \sim s^{\alpha(u)-\frac{3}{2}}$ (see eqn. (A.II.12)). Imposing this condition on eqns. (8.14) and (8.15), one immediately obtains

$$c_1 = d_1 \tag{8.20}$$

c) Comparison with Elementary Particle exchanges in the t-channel

In our model, we have t-channel exchanges of π,π', A_1, A_2 and ρ Regge trajectories. We require that the residues at the poles (physical particles) are given in terms of the (approximately known) couplings of the exchanged and the external particles.

i) Pion exchange: The results of the elementary pion exchange in the t-channel have already been considered in the Electric Born model (§7.1). Comparing the residue at $t=\mu^2$ given by the Electric Born model with that obtained from (8.11), we have

$$\beta_1 = -\lambda^2\mu^2 eg \tag{8.21}$$

ii) ρ exchange: An elementary ρ exchange in the t-channel gives the following contributions[10];

$$A^{(0)} = -\frac{t}{2M} \quad g_\rho^{(2)} \quad \frac{g_{\gamma\pi\rho}}{m_\rho} \quad \frac{1}{t-m_\rho^2} \tag{8.22}$$

$$D^{(0)} = \quad g_\rho^{(1)} \quad \frac{g_{\gamma\pi\rho}}{m_\rho} \quad \frac{1}{t-m_\rho^2} \tag{8.23}$$

and

$$A^{(0)}+tB^{(0)} = 0$$

m_ρ is the mass of the ρ meson, $g_{\gamma\pi\rho}$ is the ρ coupling to the $\gamma\pi$ vertex and is related to the width $\Gamma(\rho\to\pi\gamma)$ in the following fashion:

$$\frac{g^2_{\gamma\pi\rho}}{4\pi} = 24\ m_\rho^{-1}\ (1 - \frac{\mu^2}{m_\rho^2})^{-3}\ \Gamma(\rho\to\pi\gamma) \tag{8.24}$$

where we have considered an interaction of the form

$$\mathcal{L} = \frac{g_{\gamma\pi\rho}}{m_\rho}\, e_{\kappa\lambda\mu\nu}\varepsilon^{\kappa}_{\rho}\varepsilon^{\lambda}_{\gamma}\ \ k^\mu\ Q^\nu$$

$g_\rho^{(1)}$ and $g_\rho^{(2)}$ are the $\rho N\bar{N}$ couplings defined through the vertex function

$$\langle p_2|j_{\mu\nu}|p_1\rangle = u(\bar{p}_2)(g_\rho^{(1)}\gamma_\mu + \frac{1}{2M}\ g_\rho^{(2)}\sigma_{\mu\nu}Q^\nu)\ u(p_1)$$

where Q is the four momentum of ρ.

Comparing the residues at $t=m_\rho^2$ obtained from eqns. (8.16) and (8.18) with those obtained from (8.22) and (8.23), we have

$$c = \frac{\lambda}{m_\rho}\ g_{\gamma\pi\rho}\ g_\rho^{(2)} \tag{8.25}$$

$$d = -\frac{\lambda}{2m_\rho}\ g_{\gamma\pi\rho}\ g_\rho^{(1)} \tag{8.26}$$

iii) A_2 exchange: An elementary A_2 exchange in the t-channel gives the following contributions [10]:

$$A^{(-)} = -\frac{t}{2M} g_{A_2}^{(2)} \frac{e g_{\gamma\pi A_2}}{\mu} \frac{s}{t-m_{A_2}^2} \tag{8.27}$$

$$D^{(-)} = g_{A_2}^{(1)} \frac{e g_{\gamma\pi A_2}}{\mu} \frac{s}{t-m_{A_2}^2} \tag{8.28}$$

and

$$A^{(-)} + tB^{(-)} = 0$$

Again , m_{A_2} is the mass of the A_2, $g_{\gamma\pi A_2}$ is the coupling of the A_2 meson to the $\gamma\pi$ vertex. This is again related to the width $\Gamma(A_2\to\pi\gamma)^{(2)}$ as

$$\Gamma(A_2\to\pi\gamma) = \frac{g_{\gamma\pi A_2}^2 e^2}{40\,\pi} \frac{M^2}{\mu^2} k^5$$

where k is the C.M. momentum in the $\pi\gamma$ system, and the interaction used for the $\gamma\pi A_2$ vertex is of the form[10];

$$\mathcal{L} = g_{\gamma\pi A_2} e_{\kappa\lambda\mu\nu} A_{A_2}^{\kappa\sigma} k^\mu Q^\nu k^\sigma \varepsilon_\gamma^\lambda$$

The couplings $g_{A_2}^{(1)}$ and $g_{A_2}^{(2)}$ are the $A_2 N\bar{N}$ couplings defined from the vertex function

$$\langle p_2|j_{\mu\nu}|p_1\rangle = \bar{u}(p_2)[\tfrac{1}{2} g_{A_2}^{(2)} M^{-2}\{P_\mu P_\nu - \tfrac{1}{3} P^2(g_{\mu\nu} - \frac{Q_\mu Q_\nu}{Q^2})\}$$

$$-\tfrac{1}{2}(g_{A_2}^{(1)} + g_{A_2}^{(2)}) M^{-1}\{\gamma_\mu P_\nu + \gamma_\nu P_\mu - \tfrac{2}{3}(\gamma.P)(g_{\mu\nu} - \frac{Q_\mu Q_\nu}{Q^2})\}]u(p_1)$$

where Q is the four momentum of A_2 and $P = \tfrac{1}{2}(p_1+p_2)$

Again, comparison of the residues at $t=m_{A_2}^2$ of eqns. (8.12) and (8.14) with (8.27) and (8.28) gives

$$a_1' = \frac{M}{2\mu} \; e g_{\gamma\pi A_2} \; g_{A_2}^{(2)} \tag{8.29}$$

$$d_1 + d_2 + d_3 = -\frac{1}{2\mu} \; e g_{\gamma\pi A_2} \; g_{A_2}^{(1)} \tag{8.30}$$

The value of the constants $g_\rho^{(1)}$, $g_\rho^{(2)}$, $g_{A_2}^{(1)}$, $g_{A_2}^{(2)}$ and of the decay rates $\Gamma(\rho\to\pi\gamma)$, $\Gamma(A_2\to\pi\gamma)$ used in our calculations are presented in Table 8.2 (second column). This table also presents the expected values of the same quantities, as determined experimentally or in certain phenomenological analyses (third column).

We want to point out here that the constants $g_\rho^{(1)}$, $g_\rho^{(2)}$ and $g_{\gamma\pi\rho}$ are related to the residue constants $G_1^{(\rho)}$ and $G_4^{(\rho)}$ of part B (Table 5.3) as follows:

$$G_1^{(\rho)} = -\frac{\lambda_\rho}{2} \frac{g_\rho^{(2)}}{2M} \frac{g_{\gamma\pi\rho}}{m_\rho} \; ; \qquad G_4^{(\rho)} = \frac{\lambda_\rho}{2} \; g_\rho^{(1)} \frac{g_{\gamma\pi\rho}}{m\rho} \tag{8.31}$$

Then we easily verify the consistency between the expected values of Tables 5.3 and 8.2. The value of $g_\rho^{(1)}/g_\rho^{(2)} = 0.27$ corresponds to $G_4^{(\rho)}/G_1^{(\rho)} = 0.5$ GeV. Also, $\Gamma(\rho\to\pi\gamma) = 0.2$ MeV leads through eqn. (8.24) and $G_1^{(\rho)}/G_4^{(\omega)} = 0.225$ GeV^{-1} to $G_4^{(\omega)} \simeq 95$ $\mu b^{\frac{1}{2}}$ GeV^{-2}.

d) Comparison with Walker Residues at low baryon resonances

We again require that our model

be consistent with the residues for low baryon resonances as calculated by Walker (Table 8.1).

i) Nucleon Residue: Comparing the residue of $A^{(-)}+tB^{(-)}$ (eqn. (8.11)) at nucleon pole ($s=M^2$) with that obtained from the Electric Born model (§7.1) and using eqn. (8.21), we have

$$\beta_2 = \tfrac{1}{2}\lambda eg \tag{8.32}$$

Eqns. (8.21) and (8.32) ensure that our Veneziano model for pion exchange becomes identical to the Electric Born model at small $|t|$.

Requiring the correct residue at the nucleon pole in $C^{(-)}$ (or $D^{(-)}$) gives

$$c_1=d_1 = \frac{\mu_p - \mu_n}{2M}\lambda eg \tag{8.33}$$

A similar requirement for the amplitude $A^{(0)}$ gives

$$\gamma_1 = \tfrac{1}{2}\lambda eg \tag{8.34}$$

ii) Other Baryon Resonances: Consistency with Walker residues for $N_\gamma(1519)$ and $N_\alpha(1672)$ in $C^{(-)}-D^{(-)}$ give

$$c_1[\alpha_{A_1}(0)-\alpha_{A_2}(0)]+c_2-d_2+c_3+d_3=-0.31\ eg \tag{8.35}$$

$$c_1[\alpha_{A_1}(0)-\alpha_{A_2}(0)]+c_2-d_2-c_3-d_3=-0.78\ eg \tag{8.36}$$

γ_2 and γ_3 (in $A^{(0)}$) are also determined from the Walker residues at $N_\gamma(1519)$ and $N_\alpha(1672)$.

Consideration of $\Delta(1236)$ residues in $A^{(-)}$ (eqn. (8.12)) and $C^{(-)} - D^{(-)}$ give

$$a_2 = -0.29 \text{ eg} \tag{8.37}$$

$$c_3 - d_3 = 0.99\lambda\text{eg} \tag{8.38}$$

Notice that in our model, the entire contribution of A_1 to $C^{(-)}$ is completely determined without involving any free parameters for the unknown $A_1N\bar{N}$ coupling.

e) Analyticity Constraint

The analyticity constraint (2.26) together with eqns. (8.11) and (8.12) give

$$a_1 + a_2 = -\tfrac{1}{2}\lambda\text{eg} \tag{8.39}$$

In Table 8.1, we have given the Walker residues for different amplitudes. The residues marked with asterisks have been used in this section to evaluate the constants of our Veneziano model. For the other residues, we show two values. The values outside the brackets are those given by Walker, while those inside the brackets are those calculated by our model.

8.4 The Forward Direction

The asymptotic limit in the forward direction is given by $s \to \infty$, t fixed. If we denote by $T_i(s,t)$ this asymptotic limit of the left hand side of eqns.

(8.11), (8.12), (8.14), (8.15), (8.16) and (8.18), then we have

$$T_i(s,t)=\sum_k \beta_i^k(t)\ \Gamma[1-\alpha^k(t)][1\pm e^{-i\pi\alpha^k(t)-1}]\ (\lambda s)^{\alpha^k(t)-1} \qquad (8.40)$$

where k denotes the sum over the different Regge trajectories contributing to T_i. The β_i^k's are completely specified in terms of the constants evaluated in the last section. The residues $\beta_i^{k}{}'(t)$ are shown in Table 8.3(without curly brackets).

Using these asymptotic expressions in formulae (2.18), (2.15), (2.21) and (2.8), we calculate the differential cross-sections, the polarised photon asymmetry Σ, the target asymmetry T and the ratio $R=\frac{d\sigma}{dt}(\gamma n\to\pi^- p)/\frac{d\sigma}{dt}(\gamma p\to\pi^+ n)$. The results of this calculation have been shown in Figs. 24,25, 26 and 27. In section 8.1, we remarked that π' can have a contribution to $D^{(-)}$ as well. This can be introduced without affecting the leading baryon resonances (ie without making changes in eqns. (8.32) to (8.38) to fit the Walker residues). Such a contribution, which was taken to be of the same order of magnitude as the contribution of π' to $A^{(-)}$, has been incorporated in our calculation (see Table 8.3).

The important points to notice are the following:

a) The forward peak (of width~μ^2) is due to non-evasive pion exchange. This peak is produced by a sharp variation of $A^{(-)}+tB^{(-)}$ $(\sigma=-)$ near $t=0$.

b) The experimentally observed rapid drop of the ratio R with increasing $|t|$ is explained on the basis of a significant ρ exchange to $A^{(0)}$ and $D^{(0)}$, which contributes with opposite signs to $\gamma p\to\pi^+ n$ and $\gamma n\to\pi^- p$ (eqn. (2.8). An evasive ρ exchange also means that at $t=0$ there is no ρ contribution, and $R=1$.

c) The rapid rise of $\Sigma(\pi^{\pm})$ from $\Sigma=0$ at $t=0$ to $\Sigma\simeq 1$ at $|t|=\mu^2$ is again explained by the fact that $\frac{d\sigma_\perp}{dt}$ varies smoothly at small $|t|$, while $\frac{d\sigma_\parallel}{dt}$, which is dominated by the pion exchange, drops very fast for $0\leq -t\leq \mu^2$ (see discussion in the last paragraph of 7.1).

d) The faster drop of $\Sigma(\pi^-)$ compared to the drop for $\Sigma(\pi^+)$ for $|t|>\mu^2$ is again explained on the basis of an increasing ρ exchange which interferes destructively with the other $\sigma=+$ contributions in $\frac{d\sigma}{dt}(\gamma n\to\pi^- p)$.

e) The calculated values of the polarised target asymmetry T agree quite well with the experimental values for $|t|\leq\mu^2$. For $|t|\geq\mu^2$, the magnitude of T drops off much faster than what is indicated by the data (*).

(*) It should be remarked that the experimental data on T ($\gamma p\to\pi^+ n$) became known to us after the completion of all the work reported in this part of this thesis (and published in Ref. (10)). Thus our results (Fig. 27) actually constitute a prediction of the Veneziano model under discussion.

f) At $|t| \geq .35\ GeV^2$, the present model is inadequate. Our exchange has a NWSZ (Chapter 3), and this will produce an unwarranted dip in the cross-section around $t \simeq -.55\ GeV^2$. Unless we have significant ρ-Pomeron Regge cuts (and/or strong B meson exchange), we cannot eliminate this dip. This also explains why the agreement with different experimental quantities like $\Sigma(\pi^{\pm})$, R, T gets poorer at larger $|t|$ values.

g) The pion contribution in the Veneziano model has been adjusted so that it reproduces the Electric Born results at small $|t|$. However, the Electric Born model gives differential cross-sections slightly lower than the actually observed ones. In order to fit the forward cross-section more accurately, we can add a satellite term of the form

$$\beta_4 \ \{ B[1-\alpha_\pi(t), \tfrac{3}{2} - \alpha_N(s)] \quad - \quad (s \longleftrightarrow u)\} \tag{8.41}$$

to the amplitude $A^{(-)}+tB^{(-)}$ of (8.11). This does not affect the residues of the poles at $t=\mu^2$ and the leading baryon resonances. The contribution of π' to $A^{(-)}$, or, more precisely, eqn. (8.39) has to be modified accordingly so that eqn. (2.26) can still be satisfied. The modified residues are also given in Table 8.3 inside brackets. We see that the fits of the resulting cross-sections and the asymmetry ratios improve immediately.

8.5 The Backward Direction

The asymptotic limit in the

backward direction is given by $s\to\infty$, u fixed. The formulae for the differential cross-sections in this limit are given in eqns. (2.21). For $\gamma p\to\pi^+ n$, these involve the combinations $(A^{(-)}+A^{(0)})$; $s(B^{(-)}+B^{(0)})$; $s(C^{(-)}+C^{(0)}+D^{(-)}+D^{(0)})$ and $(C^{(-)}+C^{(0)}-D^{(-)}-D^{(0)})$.

Let us then introduce the quantities $X^{(i)}$ as follows:

$$X^{(1)}= A^{(-)}+A^{(0)} \quad ; \quad X^{(2)}= \lambda s(B^{(-)}+B^{(0)})$$
$$X^{(3)}=\lambda s(C^{(-)}+C^{(0)}+D^{(-)}+D^{(0)}); \; X^{(4)}=\lambda s(C^{(-)}+C^{(0)}-D^{(-)}-D^{(0)}) \tag{8.42}$$

Now using eqns. (8.11)-(8.18) it is quite straight forward to show that

for i=1,2

$$X^{(i)}(s,u)=\sum_{N_\alpha,N_\gamma}\{x^{(i)}_{B_1}\Gamma[\tfrac{1}{2}-\alpha_B(u)]+x^{(i)}_B\Gamma[\tfrac{3}{2}-\alpha_B(u)]\}\xi_B(u)(\lambda s)^{\alpha_B(u)-\frac{1}{2}}$$
$$+\quad x^{(i)}_{\Delta_1}\Gamma[\tfrac{1}{2}-\alpha_\Delta(u)]\xi_\Delta(u)\;(\lambda s)^{\alpha_\Delta(u)-\frac{1}{2}} \tag{8.43}$$

and for i=3

$$X^{(3)}(s,u)=\sum_{N_\alpha,N_\gamma,\Delta} x^{(3)}_{B_2}\Gamma[\tfrac{3}{2}-\alpha_B(u)]\xi_B(u)(\lambda s)^{\alpha_B(u)-\frac{1}{2}} \tag{8.44}$$

and for i=4

$$X^{(4)}(s,u)=\sum_{N_\alpha,N_\gamma} x^{(4)}_{B_1}\,\Gamma[\tfrac{1}{2}-\alpha_B(u)]\xi_B(u)(\lambda s)^{\alpha_B(u)-\frac{1}{2}} \tag{8.45}$$

where

$\xi_B(u)= 1 \pm e^{-i\pi[\alpha_B(u)-\frac{1}{2}]}$ is the signature factor of the corresponding baryon trajectory. The constants $x_{B_k}^{(i)}$'s in the above expressions are again completely specified in terms of the constants evaluated in §8.3. These are shown in Table 8.4 (inside parenthesis). Thus no free parameters are used and the $x_{B_k}^{(i)}$'s are consistent with the Walker residues.

With these expressions we can estimate the differential cross-sections as well as the residues of some higher baryon resonances. The differential cross-section in the backward direction consistently comes out to be one order of magnitude larger than the experimentally observed value. The main reason for this was found to be an excessive Δ contribution to $X^{(3)}$, ie a very large $x_{\Delta_2}^{(3)}$. Relatively large contributions from $x_{N_1}^{(4)}$ (connected to the nucleon pole) and $x_{\Delta_1}^{(2)}$ are also observed.

In order to obtain a fit to the differential cross-section, while correctly accounting for the Walker residues, we use a Veneziano model with satellite terms. We write

$$X^{(i)}(s,t) = \sum_{N_\alpha, N_\gamma} \{x_{B_1}^{(i)}\Gamma[\tfrac{1}{2}-\alpha_B(u)] + x_{B_2}^{(i)}\Gamma[\tfrac{3}{2}-\alpha_B(u)]\}\xi_B(u)(\lambda s)^{\alpha_B(u)-\frac{1}{2}}$$
$$+ \sum_{k=1}^{3} x_{\Delta_k}^{(i)}\Gamma[\tfrac{2k-1}{2}-\alpha_\Delta(u)] \quad \xi_\Delta(u)(\lambda s)^{\alpha_\Delta(u)-\frac{1}{2}} \tag{8.46}$$

This shows that we are adding

one or two satellites to each baryon trajectory. Some of the $x_{B_k}^{(i)}$'s are again determined from the Walker residues. We treat the other $x_{B_k}^{(i)}$'s as free parameters and vary them in order to obtain the best fit. These values have also been shown in Table 8.4 (without parenthesis). The fit to the differential cross-section obtained in this fashion is shown in Fig. 28. This has χ^2=35.5 for 32 data points.

Table 8.1 Coefficients of the Leading Powers of t of the Residues at the lowest Baryon Resonances

Baryon Resonance	Residues in units of eg.X(proper power of GeV)							
	$A^{(-)}$	$B^{(-)}$	$C^{(-)}$	$C^{(-)}-D^{(-)}$	$A^{(o)}$	$B^{(o)}$	$C^{(o)}$	$C^{(o)}-D^{(o)}$
$N_\alpha(\frac{1}{2}^+, 938)$	$-\frac{1}{2}$ *	$(t-\mu^2)^{-1}$ *	$\frac{\mu_p-\mu_n}{2M}$ *	0 *	$-\frac{1}{2}$ *	$(t-\mu^2)^{-1}$ $[\frac{1}{2}(t-\mu^2)^{-1}]$	$\frac{\mu_p+\mu_n}{2M}$ [0]	0 *
$N_\alpha(\frac{5}{2}^+, 1672)$	-0.72 [-0.64]	1.06 [0.76]	0.26 [0.50]	-0.78 *	-0.06 *	0.097 [0.06]	0 [0]	0 *
$N_\gamma(\frac{3}{2}^-, 1519)$	-0.39 [-0.31]	0.53 [-0.194]	0.22 [0.982]	-0.31 *	-0.05 *	0.03 [0.05]	0.05 [0]	-0.017 [0]
$\Delta(\frac{3}{2}^+, 1236)$	-0.58 *	0.91	-0.056 [0]	1.98 *	0 [0]	0 [0]	0 [0]	0 [0]

Table 8.2 Used and Expected Values

Parameters	Values used in calculations of Chapter 8	Expected values	References
$g_\rho^{(2)}$	g	$0.86g$	(18)(38)(39)(41)(42)
$g_\rho^{(1)}/g_\rho^{(2)}$	0.24	0.27	(18)(42)
$\Gamma(\rho\to\pi\gamma)$	0.2 MeV	<.5 MeV	(40)
$g_{A_2}^{(2)}$	$g_\rho^{(2)}$	$g_\rho^{(2)}$	(22)(10)
$g_{A_2}^{(1)}/g_{A_2}^{(2)}$	$g_\rho^{(1)}/g_\rho^{(2)}$	$g_\rho^{(1)}/g_\rho^{(2)}$	(22)(10)
$\Gamma(A_2\to\pi\gamma)$	0.15 MeV	0.5 MeV	(63)

Table 8.3 Residue Functions $\beta_i^k(t)$'s of eqn. (8.40)

Meson trajectories used: $\alpha_\pi(t)=-\mu^2+t=\alpha_{\pi'}(t)=\alpha_{A_1}(t);\alpha_\rho(t)=.415+t;\alpha_{A_2}(t)=.35+t$

Isospin index	Regge Exchange	Residue functions $\beta_i^k(t)$ (units eg × (proper power of GeV))			
		A	A + tB	C	D
(-)	π		$\frac{\mu^2 + 0.5\ \alpha_\pi(t)}{-\alpha_\pi(t)}$ $\{\frac{\mu^2 + 0.6\ \alpha_\pi(t)}{-\alpha_\pi(t)}\}$		
	A_2	0.386t			-0.174
	A_1			0.96	
	π'	0.5 {0.6}			1.0
(o)	ρ	-0.722t			0.325

Table 8.4 The parameters $x^{(i)}_{B_k}$'s of eqn.(8.46) in units of eg.

Baryon trajectories used: $\alpha_{N_\alpha}(s)=\alpha_{N_\gamma}(s)\equiv\alpha_N(s)=-.59+s$; $\alpha_\Delta(s)=-.0277+s$

	$x^{(i)}_{N_\alpha 1}$	$x^{(i)}_{N_\alpha 2}$	$x^{(i)}_{N_\gamma 1}$	$x^{(i)}_{N_\gamma 2}$	$x^{(i)}_{\Delta 1}$	$x^{(i)}_{\Delta 2}$	$x^{(i)}_{\Delta 3}$
$x^{(1)}$	.0 (.0)	-.3362 (-.3362)	-.6124 (.0)	-.4433 (.1691)	.1458 (.0)	.1422 (.288)	.1082 (.0)
$x^{(2)}$	.0 (.0)	.4285 (.4285)	-.0052 (.0)	-.2502 (-.245)	.0141 (.0)	-.4437 (-.4578)	.172 (.0)
$x^{(3)}$	.0 (.0)	.4890 (.4890)	.5579 (.0)	.4179 (-.14)	-.1091 (.0)	.8909 (1.0)	-.5783 (.0)
$x^{(4)}$	1.022 (1.022)	.2545 (.2545)	.2922 (.0)	.4530 (.1608)	.2006 (.0)	.1446 (-.056)	-.3306 (.0)

CHAPTER 9

CONCLUSIONS

In the last chapter, we used the Veneziano model, a crossing-symmetric dual model, to study charged pion photoproduction both in the forward and backward directions. The model we have formulated essentially does not involve any free parameters. The coefficients of all the leading terms were determined in terms of the known couplings of the t-channel exchanges to the $N\bar{N}$ and $\gamma\pi$ vertices and some of the experimentally known residues (Walker residues (12)) of the low energy resonances contributing to pion photoproduction. The Veneziano model so formulated makes definite predictions about residues of other resonances. Comparison with the other Walker residues shows that these are in good agreement.

In the forward direction we separately consider two distinct t-regions: the region $0 \le |t| \lesssim \mu^2$ and the region around $t \simeq -.55\ \mathrm{GeV}^2$. The dominating contribution in the first region comes from the pion exchange. The principal feature in this domain is the sharp forward peak in the differential cross-section. As we have discussed, this forward peak is usually explained on the basis of the rapid t-variation of $\frac{d\sigma_{\parallel}}{dt}$ in the extreme forward direction. Our model also employs this mechanism to explain this peak.

Since all other experimental features (e.g. structure of the polarised photon asymmetry Σ , the ratio $R= \frac{d\sigma}{dt}(\gamma n\to\pi^- p)/\frac{d\sigma}{dt}(\gamma p\to\pi^+ n)$) are strongly related to the t-behaviour of the differential cross-section, our model justifiably produces good fits for the parameters Σ ,T and R in this region.

In the other important t-region ($t\simeq-.55$ GeV^2), charged pion production data do not exhibit any dip in the differential cross-section. The dominating contribution in this region comes from the ρ and the A_2 exchanges. Since the ρ contribution in our model has a NWSZ at $t\simeq-.55$ GeV^2, detailed calculations give a dip at this point. From our discussions of η photoproduction and of the process $\pi N\to\omega N$ in the second part of this thesis, we expect that a substantial ρ-Pomeron cut will be required to get rid of this unwarranted dip. A reasonable B contribution (which we have neglected in this case) will also help. The unsuitability of a pure pole model with NWSZ's in this region is also clearly demonstrated by the worsening agreement between our results and the experimental data for the parameters Σ ,T and R as $|t|$ gradually increases. However,as we stated in the beginning of Chapter 8, we did not want to go into the complication of introducing Regge cuts in the framework of a simple Veneziano model, and exclusively devoted ourselves to explain the experimental features in the very small $|t|(\lesssim\mu^2)$ region.

In the backward direction, π^+ photoproduction recieves leading contributions from N_α, N_γ and Δ_δ exchanges in the u-channel. No dip is exhibited in $\frac{d\sigma}{du}$ at $u \simeq -.2$ GeV^2, which corresponds to a non-sense wrong signature point for the N_α trajectory. The absence of this dip is explained in our model through strong N_α-N_γ exchange degeneracy. These same three exchanges contribute to backward π^+p scattering. The differential cross-section in this case, however, shows a dip around $u \simeq -.2$ GeV^2, and this is attributed to the NWSZ of the N_α trajectory. These two explanations might seem contradictory. However, there are two important differences between $\gamma p \to n\pi^+$ and $\pi^+ p \to p\pi^+$. In the case of photoproduction of pions, four independent helicity amplitudes (one non-flip, two single-flips and one double-flip) are involved, while πN scattering is described in terms of two independent helicity amplitudes (one single-flip, one non-flip). Also photoproduction demands that gauge invariance be satisfied, a requirement which has no parallel in hadronic processes like πN scattering. It has been shown by Roy[60] that gauge invariance and duality require that the contributions of the N_α and the N_γ trajectories to the particular combination of the two single-flip amplitudes proportional to the CGLN invariant B be strongly exchange degenerate. It has also been pointed out[64] that the elastic couplings of the resonant states $N_\gamma(1520)$ and $D_{15}(1670)$ are known from phase shift analyses, and these are roughly about $\frac{1}{2}$ of those of $N_\alpha(938)$ and $\Delta_\delta(1236)$. If similar large residue functions are considered in the physical region of πN backward scattering (negative u values), the pronounced dip in $\frac{d\sigma}{du}$ in backward π^+p would be considerably smaller. So, it is the presence of the strong dip in backward π^+p scattering which really needs a better explanation.

The other important point to notice is that the Veneziano model, which reproduces the extreme forward cross-sections and the Walker residues so well, gives backward cross-sections which exceed the experimentally observed ones by about one order of magnitude. For $\pi N \rightarrow \pi N$, the Veneziano approach encounters exactly the same difficulties[65]. To solve this problem, we added certain satellite terms involving several free parameters while taking care not to disturb the agreement with Walker residues. The free parameters were adjusted to obtain the best fit to $\frac{d\sigma}{du}$. We notice that the best fit values of these free parameters are, roughly, of the same order of magnitude as the Walker residues. Moreover, they imply definite predictions about residues of higher πN resonances contributing to photoproduction. No experimental information is presently available to check these predictions.

PART D : APPENDICES

APPENDIX I

In this appendix, we shall calculate explicitly the contributions from the ρ-Pomeron and the ω-Pomeron Regge cuts. We shall start with eqn. (3.18), which states

$$f_{\mu\lambda}^{(RP)}(s,t) = \tilde{\lambda}_{\mu\lambda}^{(R)} \int_0^{-\infty} d\tau\, f_{\mu\lambda}^{(R)}(s,\tau)\tfrac{1}{2}Ce^{\frac{1}{2}A(t+\tau)}\, I_n(A\sqrt{t\tau}) \qquad \text{(A.I.1)}$$

where R stands for the ρ or the ω.

We take the Pomeron contribution in the forward direction as

$$f^P(s,t) = i\,\frac{\sigma_t}{16\pi}\; s\; e^{A_0 t}\left(e^{-\frac{1}{2}i\pi}\,\frac{s}{s_0}\right)^{\lambda_P t} \qquad \text{(A.I.2)}$$

where the Pomeron trajectory

$$\alpha_P(t) = 1 + \lambda_P t \qquad \text{(A.I.3)}$$

and s_0 is the energy scale. A_0 is directly determined by fitting the elastic scattering data (essentially πN elastic scattering in this case). Comparing (A.I.2) with eqn.(3.9), we immediately obtain

$$A = 2A_0 + 2\,\lambda_P(\ln\frac{s}{s_0} - \tfrac{1}{2}i\pi) \qquad \text{(A.I.4)}$$

Also

$C = \dfrac{\sigma_t}{4\pi A}$ as in (3.11)

The exact Regge pole exchange expressions for the CGLN invariants A_i have been written down in §5.1. In order that the integral in (A.I.1) can be evaluated analytically, we shall use a simplified version of these expressions and take

$$A_i^{(R)} \simeq \beta_i^{(R)}(t)\ \pi\ \alpha_R(t)\ \left(e^{-\frac{1}{2}i\pi}\ \frac{s}{s_0}\right)^{\alpha_R(t)-1} \tag{A.I.5}$$

where $\beta_i^{(R)}(t)$ are given in Table 5.2. This simplification is a reasonably good approximation of (5.2) in the range of importance $(0 \le |t| \le 1\ \mathrm{GeV}^2)$.

Let us now define the following quantities:

$$B(s') = \ln\left(\frac{s}{s'}\right) - \tfrac{1}{2}i\pi\ ; \quad b^2 = 2A + \lambda B\ ; \quad x = \frac{iA\sqrt{-t}}{b} \tag{A.I.6}$$

$$R(s,s';t) = \frac{\sigma_t}{16}\ \left(e^{-\frac{1}{2}i\pi}\ \frac{s}{s'}\right)^{\alpha(0)-1}\ e^{\frac{1}{2}At - x^2} \tag{A.I.7}$$

$$W_1(s,s';t) = \frac{1}{\left[\frac{A}{2} + \lambda B\right]^2}\ \left[\ \alpha(0) L_1^0(x^2) - \frac{8\lambda}{b^2} L_2^0(x^2)\right] \tag{A.I.8}$$

$$W_4(s,s';t) = \frac{A}{\left[\frac{A}{2} + \lambda B\right]^2}\ \left[\alpha(0) L_0^1(x^2) - \frac{4\lambda}{b^2}\ L_1^1(x^2)\right] \tag{A.I.9}$$

$L_n^{\alpha}(y)$ are the generalised Laguerre polynomials(66) defined as follows:

$$L_n^{\alpha}(y) = \sum_{m=0}^{n} \binom{n-\alpha}{n-m}\ \frac{(-y)^m}{m!} \tag{A.I.10}$$

It is now easy to show that (A.I.1) leads to [66] the following results :

$$f^{(RP)}_{\frac{1}{2},\frac{1}{2}} = 2\ \tilde{\lambda}^{(R)}_{\frac{1}{2},\frac{1}{2}}\ \beta_1^{(R)}\ \left[-\frac{\sqrt{2}}{16\pi}\sqrt{s}\ \right]\ W_1(s,s_0;t)\ R(s,s_0;t) \qquad \text{(A.I.11)}$$

$$f^{(RP)}_{-\frac{1}{2},\frac{1}{2}} = f^{(RP)}_{\frac{1}{2},\frac{3}{2}} = \sqrt{-t}\ \ \tilde{\lambda}^{(R)}_{\frac{1}{2},\frac{3}{2}}\ \beta_4^{(R)}\ \frac{\sqrt{2}}{16\pi}\sqrt{s}\ \ W_4(s,s_0;t)\ R(s,s_0;t)$$

$$\text{(A.I.12)}$$

Notice that the exact calculations give the same scale s_0 for both $W_{1,4}$ and R.

Also from Table 5.2, we obtain

$$A^{(RP)} = \tfrac{1}{2}\left[-\frac{16\pi}{\sqrt{2s}}\right]\ f^{(RP)}_{\frac{1}{2},\frac{1}{2}} \qquad \text{(A.I.13)}$$

$$D^{(RP)} = \frac{1}{\sqrt{-t}}\ \frac{16\ \pi}{\sqrt{2s}}\ \ f^{(RP)}_{\frac{1}{2},\frac{3}{2}} \qquad \text{(A.I.14)}$$

There are two important observations about (A.I.11) and (A.I.12). In most important models leading to branch points in complex angular momentum plane, including those studied by Mandelstam[67], Polkinghorne[16] and Gribov et al[68], a Reggeon-Pomeron cut contribution has an energy dependence of the form (apart from ln s terms) $s^{\alpha_c(t)-1}$, where $\alpha_c(t) = \alpha(0) + \dfrac{\lambda\lambda_P}{\lambda\ \lambda_P}\ t$. However, from eqn. (A.I.7), we see that our Regge cut expressions contain the factor

$$(e^{-\frac{1}{2}i\pi} \; s)^{\alpha(0)-1} e^{\frac{1}{2}At-x^2}$$

Substituting the values of A and x^2 , we obtain the corresponding energy dependence as

$$(s \; e^{-\frac{1}{2}i\pi})^{\alpha(0)+\lambda' t-1} \tag{A.I.15}$$

where

$$\lambda' = \frac{\lambda\lambda_P \left[1+ \frac{A_0}{\lambda_P\{\ln(s/s_0)-\frac{1}{2}i\pi\}}\right]}{\lambda+\lambda_P\left[1+ \frac{A_0}{\lambda_P\{\ln(s/s_0)-\frac{1}{2}i\pi\}}\right]} \tag{A.I.16}$$

We see that in the limit $\ln(s/s_0)\to\infty$ (ie extremely high s)

$$\lambda' \to \frac{\lambda\lambda_P}{\lambda+\lambda_P}$$

However for energies of interest $\alpha(0)+\lambda' t \neq \alpha_c(t)$

Furthermore, when the energy dependence of the cut is $s^{\alpha_c(t)-1}$, well known applications of s-u crossing and of Phragmen-Lindelhoff theorem[27-29] demand that the phase of the leading contribution be determined by a factor of the form $e^{-\frac{1}{2}i\pi[\alpha_c(t)-1]}$ (≡ the cut signature factor). With eqn. (A.I.16), the phase is determined by the factor $e^{-\frac{1}{2}i\pi[\alpha(0)+\lambda' t-1]}$, which again reduces to $e^{-\frac{1}{2}i\pi[\alpha_c(t)-1]}$ only at extremely high s.

Nevertheless, we notice that if in our model of the Pomeron contribution, we take $A_0=0$, then $\lambda'=\frac{\lambda\lambda_P}{\lambda+\lambda_P}$, so that even at relatively low s, the energy dependence becomes $s^{\alpha_c(t)-1}$ and the phase is controlled by $e^{-\frac{1}{2}i\pi\,[\alpha_c(t)-1]}$

Thus in view of the uncertainties concerning the features of the Pomeron contribution and of the great importance of nonleading terms at energies of interest, we carry out calculations with two different Regge cut models:

i) Model C_1 : Here we use the exact formulae (A.I.11) and (A.I.12) with $A_0\neq 0$.

ii) Model C_2 : Here we take $A_0=0$. However we allow different energy scales s_0 and s_0' for the functions R and $W_{1,4}$ respectively . Again, this is easily seen to leave unaffected the leading (in powers of ln s) contributions of the Regge cuts, but does affect the non-leading contributions.

The preceding discussions make it clear that to the very leading order in s and ln s, both our cut models have the correct asymptotic ($\sim s^{\alpha_c(t)-1}/(\ln s)^n$) behaviour and the correct asymptotic phase, as required by s-u crossing and the Phragmen-Lindelhoff theorem.

APPENDIX II

In this appendix, we shall give a brief outline of the derivation of the formulae (2.20), (2.21), (2.22) and (2.23) and shall also obtain the asymptotic behaviour of the CGLN invariants A_i. We follow the notation of Chapter 2.

For this purpose, some useful relations are

$$E_1+M=\frac{(\sqrt{s}+M)^2}{2\sqrt{s}} \quad ; \quad E_2+M=\frac{(\sqrt{s}+M+\mu)(\sqrt{s}+M-\mu)}{2\sqrt{s}} \quad ; \quad \nu_1=\frac{1}{4M}[s+u-2M^2]$$

Using these relations in (2.11), the following limits are obtained in the forward direction ($s\to\infty$, t fixed):

$$\begin{aligned} &F_1+F_2\simeq\frac{s}{8\pi}D \quad ; \quad F_1-F_2\simeq\frac{\sqrt{s}}{8\pi}A \\ &F_3+F_4\simeq\frac{s}{16\pi}(C-D) \quad ; \quad F_3-F_4\simeq\frac{s\sqrt{s}}{16\pi}B \end{aligned} \tag{A.II.1}$$

So from (2.13), we immediately obtain

$$\begin{aligned} &f_{\frac{1}{2},\frac{3}{2}}\simeq-\frac{\sqrt{2}}{16\pi}\sqrt{-ts}\,(C-D) \quad ; \quad f_{\frac{1}{2},\frac{1}{2}}\simeq-\frac{\sqrt{2}}{16\pi}\sqrt{s}\,(2A+tB) \\ &f_{-\frac{1}{2},\frac{3}{2}}\simeq-\frac{\sqrt{2}}{16\pi}\sqrt{s}\;tB \quad ; \quad f_{-\frac{1}{2},\frac{1}{2}}\simeq\frac{\sqrt{2}}{16\pi}\sqrt{-ts}\,(C+D) \end{aligned} \tag{A.II.2}$$

The following combinations of SHA are known[12] to be dominated by t-channel exchanges of $\sigma=-$:

$$f_{\frac{1}{2},\frac{3}{2}} - f_{-\frac{1}{2},\frac{1}{2}} \simeq -\frac{\sqrt{2}}{8\pi}\sqrt{-ts}\ C$$

$$f_{\frac{1}{2},\frac{1}{2}} + f_{-\frac{1}{2},\frac{3}{2}} \simeq -\frac{\sqrt{2}}{8\pi}\sqrt{s}\ (A+tB) \qquad \text{(A.II.3)}$$

while exchanges of $\sigma=+$ dominates the combinations:

$$f_{\frac{1}{2},\frac{3}{2}} + f_{-\frac{1}{2},\frac{1}{2}} \simeq \frac{\sqrt{2}}{8\pi}\sqrt{-ts}\ D$$

$$f_{\frac{1}{2},\frac{1}{2}} - f_{-\frac{1}{2},\frac{3}{2}} \simeq -\frac{\sqrt{2}}{8\pi}\sqrt{s}\ A \qquad \text{(A.II.4)}$$

Since according to Stichel's theorem[15] (§2.4), $\frac{d\sigma_{\parallel}}{d\Omega}$ ($\frac{d\sigma_{\perp}}{d\Omega}$) is dominated by exchanges with $\sigma=-$ (+), we immediately see that (see eqn. (2.14)):

$$\frac{d\sigma_{\parallel}}{d\Omega} \sim \left|f_{\frac{1}{2},\frac{3}{2}} - f_{-\frac{1}{2},\frac{1}{2}}\right|^2 + \left|f_{\frac{1}{2},\frac{1}{2}} + f_{-\frac{1}{2},\frac{3}{2}}\right|^2$$

$$\frac{d\sigma_{\perp}}{d\Omega} \sim \left|f_{\frac{1}{2},\frac{3}{2}} + f_{-\frac{1}{2},\frac{1}{2}}\right|^2 + \left|f_{\frac{1}{2},\frac{1}{2}} - f_{-\frac{1}{2},\frac{3}{2}}\right|^2 \qquad \text{(A.II.5)}$$

The substitution of (A.II.2), (A.II.3) and (A.II.4) in (2.14), (2.16) and (2.18) gives eqns. (2.20), (2.22) and (2.23) respectively.

Similarly in the backward direction ($s\to\infty$, u fixed) :

$$F_1+F_2 \simeq \frac{1}{16\pi}[2MA+s(C+D)\ (u+M^2)(C-D)]\ ;F_1-F_2 \simeq \frac{1}{16\pi}[2A+2M(C-D)]$$

$$F_3+F_4 \simeq \frac{1}{16\pi}[C-D]\ ;\quad F_3-F_4 \simeq \frac{1}{16\pi}[B+\frac{M}{s}\ (C-D)] \qquad \text{(A.II.6)}$$

whence

$$f_{\frac{1}{2},\frac{3}{2}} \simeq \frac{\sqrt{2}}{16\pi}\, u(C-D) \quad ; \; f_{\frac{1}{2},\frac{1}{2}} \simeq \frac{\sqrt{2}}{16\pi}\sqrt{-u} \quad [2A+sB-M(C-D)]$$

$$f_{-\frac{1}{2},\frac{3}{2}} \simeq \frac{\sqrt{2}}{16\pi}\sqrt{-u} \quad [sB+M(C-D)]; \; f_{-\frac{1}{2},\frac{1}{2}} \simeq \frac{\sqrt{2}}{16\pi}\,[2MA+s(C+D)+M^2(C-D)] \tag{A.II.7}$$

Eqn. (2.21) follows immediately.

For ascertaining the asymptotic behaviour of the A_i's, we remember that according to Regge pole theory

$$f_{\mu\lambda} \sim s^{\alpha(t)-\frac{1}{2}} \quad ; \; f_{\mu\lambda} \sim s^{\alpha(u)-\frac{1}{2}} \tag{A.II.8}$$

So from (2.11),

$$F_2+F_1 \sim s^{\alpha(t)} \quad ; F_2-F_1 \sim s^{\alpha(t)-\frac{1}{2}}$$

$$F_3+F_4 \sim s^{\alpha(t)} \quad ; F_3-F_4 \sim s^{\alpha(t)+\frac{1}{2}} \qquad t \text{ fixed} \tag{A.II.9}$$

and

$$F_2+F_1 \sim s^{\alpha(u)-\frac{1}{2}} \quad ; F_2-F_1 \sim s^{\alpha(u)}$$

$$F_3+F_4 \sim s^{\alpha(u)+\frac{1}{2}} \quad ; F_3-F_4 \sim s^{\alpha(u)} \qquad u \text{ fixed} \tag{A.II.10}$$

Combining (A.II.9) with (A.II.1),

$$A \sim s^{\alpha(t)-1} \; ; \; B \sim s^{\alpha(t)-1} \; ;$$

$$(C-D) \sim s^{\alpha(t)-1} ; (C+D) \sim s^{\alpha(t)-1} \qquad \text{for } s\to\infty, \; t \text{ fixed.} \tag{A.II.11}$$

Similarly from (A.II.10) and (A.II.6),

$$A \sim s^{\alpha(u)-\frac{1}{2}} \; ; \; B \sim s^{\alpha(u)-\frac{3}{2}} \qquad s \to \infty \text{ ,u fixed} \qquad \text{(A.II.12)}$$

$$(C-D) \sim s^{\alpha(u)-\frac{1}{2}} \; ; \; (C+D) \sim s^{\alpha(u)-\frac{3}{2}}$$

APPENDIX III

In this appendix, we shall give an outline of the determination of the residues corresponding to A_J and B_J (§8.1) from Walker's residues (Table III of Ref. (12)).

The angular dependence of the amplitudes F_i (see eqn.(2.11)) has been given in terms of electric and magnetic transition amplitudes $E_{\ell\pm}$ and $M_{\ell\pm}$. In his paper, Walker has given the relations between the quantities $E_{\ell\pm}$ and $M_{\ell\pm}$ and the partial helicity amplitudes $A_{\ell\pm}$ and $B_{\ell\pm}$. These are

$$E_{0+}=A_{0+} \quad ; \quad M_{1-}=A_{1-}$$

and for $\ell\geq 1$

$$E_{(\ell+1)-}=-\frac{1}{\ell+1}[A_{(\ell+1)-}-\tfrac{1}{2}(\ell+2)B_{(\ell+1)-}] \;;M_{(\ell+1)-}=\frac{1}{\ell+1}[A_{(\ell+1)-}-\tfrac{1}{2}\ell B_{(\ell+1)-}]$$

$$E_{\ell+}=\frac{1}{\ell+1}[A_{\ell+}+\ell B_{\ell+}] \quad ; \quad M_{\ell+}=\frac{1}{\ell+1}[A_{\ell+}-\tfrac{1}{2}(\ell+2)B_{\ell+}] \tag{A.III.1}$$

If the leading term in $P_\ell(x)$ is given by

$$P_\ell(x)\simeq \tau_\ell x^\ell\equiv\frac{(2\ell)!}{2^\ell(\ell!)^2}\, x^\ell \tag{A.III.2}$$

then using (A.III.1) in (2.12),we obtain for

i) a resonance with $\sigma=+$, $J=\ell-\frac{1}{2}$

$$\mathrm{Res}\ F_1 \simeq [A_{\ell-}+\tfrac{1}{2}(\ell+1)B_{\ell-}]\ (\ell-1)\ \tau_{\ell-1}\ (\tfrac{t}{2kq})^{\ell-2}$$

$$\mathrm{Res}\ F_2 \simeq [A_{\ell-}+\tfrac{1}{2}(\ell-1)B_{\ell-}]\ \ell\ \tau_{\ell}\ (\tfrac{t}{2kq})^{\ell-1}$$

$$\mathrm{Res}\ F_3 \simeq B_{\ell-}(\ell-1)(\ell-2)\ \tau_{\ell-1}\ (\tfrac{t}{2kq})^{\ell-3} \qquad \text{(A.III.3)}$$

$$\mathrm{Res}\ F_4 \simeq -B_{\ell-}\ell(\ell-1)\ \tau_{\ell}\ (\tfrac{t}{2kq})^{\ell-2}$$

and for

ii) a resonance with $\sigma=-$, $J=\ell+\frac{1}{2}$

$$\mathrm{Res}\ F_1 \simeq (A_{\ell+}-\tfrac{1}{2}\ell B_{\ell+})\ (\ell+1)\ \tau_{\ell+1}\ (\tfrac{t}{2kq})^{\ell}$$

$$\mathrm{Res}\ F_2 \simeq [A_{\ell+}-\tfrac{1}{2}(\ell+2)B_{\ell+}]\ \ell\ \tau_{\ell}\ (\tfrac{t}{2kq})^{\ell-1}$$

$$\mathrm{Res}\ F_3 \simeq B_{\ell+}\ \ell(\ell+1)\ \tau_{\ell+1}\ (\tfrac{t}{2kq})^{\ell-1} \qquad \text{(A.III.4)}$$

$$\mathrm{Res}\ F_4 \simeq -B_{\ell+}\ \ell(\ell-1)\ \tau_{\ell}\ (\tfrac{t}{2kq})^{\ell-2}$$

If we now define the quantity Λ as follows

$$\Lambda = \frac{4\pi}{\sqrt{s_0}-M}\ \frac{1}{\sqrt{(E_1+M)(E_2+M)}} \qquad \text{(A.III.5)}$$

then , substituting (A.III.) and (A.III.) in (2.11) we have at a resonance at $s=s_0$

i) $\sigma=+$, $J=\ell-\frac{1}{2}$

$$\text{Res } A_J \simeq -t^{\ell-1}\ \Lambda\ \frac{E_2+M}{q}(2kq)^{-\ell+1}\ \ell\tau_\ell\ (\sqrt{s}_0-M)[A_{\ell-}+\tfrac{1}{2}(\ell-1)(1+\frac{2M}{\sqrt{s}})B_{\ell-}]$$

$$\text{Res } B_J \simeq t^{\ell-2}\ \Lambda\ \frac{E_2+M}{q}\ (2kq)^{-\ell+2}\ \ell(\ell-1)\ \tau_\ell\ B_{\ell-} \tag{A.III.6}$$

and ii) $\sigma=-$, $J=\ell+\frac{1}{2}$

$$\text{Res } A_J \simeq t^{\ell}\ \Lambda\ (2kq)^{-\ell}\ (\ell+1)\ \tau_\ell\ (\sqrt{s}_0+M)[A_{\ell+}-\tfrac{1}{2}\ell(1-\frac{2M}{\sqrt{s}})B_{\ell+}]$$

$$\text{Res } B_J \simeq t^{\ell-1}\ \Lambda\ \frac{1}{q}\ (2kq)^{-\ell+1}\ \ell(\ell+1)\ \tau_{\ell+1}\ B_{\ell+} \tag{A.III.7}$$

REFERENCES

1. R.C.Arnold - Phys. Rev. 153 (1967) P.1523
   R.C.Arnold and M.L.Blackmon - Phys. Rev. 176 (1968) P.2082
   G.Cohen-Tannoudji, A.Morel and H.Navelet - Nuovo Cim. 48A (1967) P.1075
2. M.L.Blackmon,G.Kramer and K.Schilling - Nucl.Phys. B12 (1969) P.495
3. M.L.Blackmon,G.Kramer and K.Schilling - Phys. Rev. 183 (1969) P.1452
4. A.P.Contogouris and J.P.Lebrun - Nuovo Cim. 64A (1969) P.627
5. F.Henyey, G.L.Kane,J.Pumplin and M.H.Ross - Phys. Rev. 182 (1969) P.1579
6. F.D.Gault,A.D.Martin and G.L.Kane - Nucl. Phys. B32 (1971) P.429
7. M.H.Ross,F.Henyey and G.L.Kane - Nucl. Phys. B23 (1970) P.269
8. H.Harari - Phys.Rev. Lett. 26 (1971) P.140
   H.Harari - in 'Proceedings of International Conference on Duality and Symmetry in Hadron Physics' - edited by E.Gotsman - Weizmann Science Press (1971)
   H.Harari and M.Davier - Phys. lett. 35B (1971) P.239
9. E.N.Argyres, A.P.Contogouris,S.Ray and M.Svec - to be published in Nucl. Phys. B.
10. E.N.Argyres,A.P.Contogouris,C.S.Lam and S.Ray - Nuovo Cim. 4A (1971) P.156
11. G.F.Chew,M.L.Goldberger,F.E.Low and Y.Nambu - Phys. Rev. 106 (1957) P.1345

12.R.L.Walker - Phys. Rev. 182 (1969) P.1729

13.M.Gell-Mann,M.L.Goldberger,F.E.Low,E.Marx and F.Zachariasen Phys. Rev. 133B (1964) P.145

14.B.Diu and M.Le-Bellac - Nuovo Cim. 53A (1968) P.158

15.P.Stichel - Z. Phys. 180 (1964) P.140
R.P.Bajpai - Nucl. Phys. B26 (1971) P.231

16.R.J.Eden,P.V.Landshoff,D.I.Olive and J.C.Polkinghorne - 'The Analytic S Matrix' - Cambridge (1966)

17. P.D.B.Collins and E.J.Squires - 'Regge Poles in Particle Physics' - Springer Tracts in Modern Physics- Vol. 45 - Springer Verlag (1967)

18. A.Dar,T.L.Watts and V.F.Weiskopff - Phys. Lett. 30B (1969) P.264

19. A.Dar,T.L.Watts and V.F.Weiskopff - Nucl. Phys. B13 (1969) P.477

20. K.Gottfried and J.D.Jackson - Nuovo Cim. 34 (1964) P.735

21. N.J.Sopkovich - Nuovo Cim. 26 (1962) P.186

22. V.D.Barger and D.B.Cline - 'Phenomenological Theories of High Energy Scattering' - Benjamin (1969)

23. A.P.Contogouris - in 'Photon-Hadron Interactions' - Springer Tracts in Modern Physics - Vol. 63 - Springer Verlag (1972)

24. G.Giacomelli - in 'Proceedings of Amsterdam International Conference on Elementary Particles' - edited by A.G.Tenner and M.J.G.Veltman - North Holland (1972) P.23

25. C.Michael and F.Halzen - Phys. Lett. 36B (1971) P.367
R.L.Kelly - Carnegie-Mellon University Preprint (1972)

26. R.Dolen,D.Horn and C.Schmid - Phys.Rev. 166 (1969) P.1768

27. R.J.Eden - 'High Energy Collisions of Elementary Particles' - Cambridge (1967)

28. A.Logunov,Nguyen Van Hien,I.T.Todorov and O.A.Krustalev - Phys. Lett. 7 (1963) P.69

29. L.Van Hove - Rev. Mod. Phys. 36 (1964) P.655

30. R.H.Dalitz and D.Sutherland - Nuovo Cim. 37 (1965) P.1777 and 38 (1965) P.1945

31. J.J.Sakurai - Invited talk at the Japan-U.S. Seminar on Elementary Particle Physics with Bubble Chamber Detectors (SLAC), University of California, Los Angelos Preprint (1971)
C.F.Cho and J.J.Sakurai - Phys. Rev. D2 (1970) P.517

32. M.Le-Bellac and G.Plaut - Nuovo Cim. 64A (1969) P.95

33. B.H.Kellet - University of Manchester Preprints DNLP/P68 and 76 (1971)

34. M.Le-Bellac and G.Plaut - Lett. Nuovo Cim. 1 (1969) P.721

35. M.Svec - private communication

36. A.P.Contogouris, H.Lubatti and J.Tran Thanh Van - Phys. Rev. Lett. 19 (1967) P.1352

37. G.Eilam, G.Berlad and A.Dar - Nucl.Phys. B27 (1971) P.415

38. S.P.Kharlanov -'Proceedings of the Dubna Conference'- (1964)

39. D.Amaldi,E.Leader and B.Vitale - Phys. Rev. 130 (1963) P.750

40. Particle Data Group - Rev. Mod. Phys 43 (1971) P. S1

41. J.J.Sakurai - Ann. Phys. (N.Y.) 11 (1960) P.1
J.J.Sakurai - Phys. Rev. Lett. 17 (1966) P.1021
J.J.Sakurai - 'Currents and Mesons' - Chicago University Press (1969)

J.R.Dunning,K.W.Chen,A.A.Cone,G.Hartwig,N.F.Ramsey,J.K. Walker and R.Wilson - Phys. Rev. Lett. 13 (1964) P.631

42. L.Stodolsky - Phys. Rev. 134B (1964) P.1099
M.Gell-Mann and F.Zachariasen - Phys. Rev. 124 (1961) P.953
M.K.Bannerji and C.A.Levinson - Phys. Rev. 176 (1968) P.2140

43. J.E.Augustin - Phys. Lett. 28B (1969) P.503

44. R.Worden - Nucl. Phys. B37 (1972) P.253

45. J.S.Ball,W.R.Frazer and M.Jacob - Phys. Rev. Lett. 20 (1968) P.518

46. R.J.N.Phillips - Nucl.Phys. B2 (1967) P.394

47. F.Arbab and J.Dash - University of California Lawrence Radiation report No. UCRL -17585 (1967)

48. M.Toller - Nuovo Cim. 37 (1965) P.631 ; 53A (1968) P.671 and 54A (1968) P.295

49. G.Consenza,A.Sciarrino and M.Toller - Phys. Lett. 27B (19680 P.398 and Nuovo Cim. 62A (1969) P.999

50. A.P.Contogouris - in 'Strong Interaction Physics' - Springer Tracts in Modern Physics - Vol. 57 - Springer Verlag (1971)

51. M.Le-Bellac - Phys. Lett. 25B (1967) P.524

52. E.J.Sqires - in 'Strong Interaction Physics' - Springer Tracts in Modern Physics - Vol. 57 - Springer Verlag (1971)

53. S.Mandalstam - Phys. Rev. 168 (1968) P.1884
R.F.Sawyer — Phys. Rev. Lett. 21 (1968) P.764

54. J.D.Jackson and C.Quigg - Phys. Lett. 29B (1969) P.236 and Nucl. Phys. B22 (1970) P.301

55. A.Bietti,P.DiVecchia,F.Drago and M.L.Paciello - Phys. Lett. 26B (1968) P.457

56. P.DiVecchia,F.Drago,C.Ferro Fontan,R.Odorico and M.L. Paciello - Phys. Lett. 27B (1968) P.296 and P.521

57. G.Veneziano - Nuovo Cim. 57A (1968) P.190

58. R.Diebold - Phys. Rev. Lett. 22 (1969) P.204

59. S.W'MacDowell - Phys. Rev. 116 (1960) P.774

60. D.P.Roy - Phys. Rev. Lett. 23 (1969) P.1417

61. V.Barger and P.Weiler - Phys. Lett. 30B (1969) P.105

62. M.Ahmed,Fayyazuddin and Riazuddin - Phys. Rev. Lett. 23 (1969) P.504

63. Y.Eisenberg,B.Haber,B.Horovitz,E.Peleg,E.E.Ronat,A.Shapiro, G.Vishinsky,G.Yekutielli,J.Ballam,G.B.Chadwick,Z.G.T.Guiragossian, A.Levy,M.Menke,P.Seyboth and G.Wolf - Phys.Rev. Lett. 23 (1969) P.1322

64. E.L.Berger and G.C.Fox - Nucl.Phys. B26 (1971) P.1

65. E.L.Berger and G.C.Fox - Phys. Rev. 188 (1969) P.2120

66. A.Erdelyi (editor) - 'Higher Transcendental Functions' - Vol. 3 - McGraw Hill (1953)

A.Erdelyi (editor) - 'Tables of Integral Transforms' - Vol. 2 - McGraw Hill (1953)

67. S.Mandelstam - Nuovo Cim. 30 (1963) P.1148

68. V.N.Gribov,I.Ya Pomeranchuk and K.A.Ter-Martirosyan - Soviet Journal of Nucl. Phys. 2 (1966) P.258

69. R.L.Anderson,D.Gustavson,J.Johnson,D.Ritson,B.H.Wiik,W.G. Jones,D.Kreinick,F.Murphy and R.Weinstein - Phys. Rev. D1 (1970) P.27

J.Johnson - Report No. SLAC-124 (1970)

70. M.Braunschweig,W.Braunschweig,D.Heismann,K.Lubelsmeyer and D.Schmitz - Phys. Lett. 26B (1968) P.405

71. D.Bellinger,R.Bordelon,K.Cohen,S.B.Deutsch,W.Lobar, D.Luckey, L.S.Osborne, E.Pothier and R.Schwitters - Phys. Rev. Lett. 23 (1969) P.540

R.L.Anderson,G.Gustavson,J.Johnson,I.Overman,D.Ritson, B.H.Wiik,R.Talman and D.Worcester - Phys. Rev. Lett. 26 (1971) P.30

72. G.C.Bolon,D.Bellinger,W.Lobar,D.Luckey,L.S.Osborne and R.Schwitters - Phys. Rev. Lett. 26 (1971) P.30

A.Osborne,A.Browman,K.Hanson,W.Meyer, A.Silverman, E.Taylor and N.Horowitz - Bull. Am. Phys. Soc. 16 (1971) P.1400 and private communication.

73. P.S.L.Booth,G.R.Court,B.Craven,R.Gamet,P.J.Hayman,J.R. Holt,A.P.Hufton,J.N.Jackson,J.H.Norem and W.H.Range - Phys. Lett. 38B (1972) P.339

B.Wiik - in 'Proceedings of 1971 International Symposium on Electron and Photon Interactions at High Energies' - Cornell University (1972)

74. W.Braunschweig,W.Erlewin,H.Frese,K.Lubelsmeyer,H. Meyer-Machsmith,D.Schmitz,A.Schultz von Dratzig and G. Wessels - Phys. Lett. 33B (1970) P.236

J.DeWire,B.Gittelman,R.Loe,E.C.Loh and D.J.Ritchi - Cornell University Preprint - CLNS 170 (1971)

75. D.J.Crennel,H.A.Gordon,M.L.Ioffredo,Kwan-Wy Lai and J.M. Scarr - Phys. Rev. Lett. 27 (1971) P.1674

76. G.Abrams,B.Eisenstein and H.A.Gordon - Phys. Rev. Lett. 23 (1969) P.673

77. N.Armenise,B.Ghidini,V.Picciarelli,A.Romano,A.Silvestri, A.Forino,R.Gessaroli,L.Lendinara,A.Quareni-Vignudelli,A. Cartacci,M.D.Dagliana,G.di Caporiacco,M.Barrier,D.Methel and J.Quinquard - BBFO Collaboration - Nuovo Cim. 65A (1970) P.637

J.A.Mathews,J.D.Prentice,T.S.Yoon,J.T.Carroll,M.W. Firebaugh and W.D.Walter - Phys. Rev. Lett. 26 (1971) P.400

78. R.Diebold - Review Talk at High Energy Physics Conference at Boulder, Colorado - SLAC-673 (1969)

79. K.Lubelsmeyer - in 'Proceedings of International Conference on Electron and Photon Interactions at High Energies' - Liverpool (1969)

80. C.C.Morehouse,M.Borghini,O.Chamberlain,R.Fuzesy,W.Gorn, T.Powell,P.Rebrish,S.Rock,S.Shannon,G.Shapiro,H.Weisberg, A.Boyarski,S.Ecklund,Y.Murata,B.Richter,R.Siemann and R.Diebold - Phys. Rev. Lett. 25 (1970) P.835

81. R.L.Anderson,D.Gustavson,J.Johnson,I.Overman,D.Ritson and B.H.Wiik - Phys. Rev. Lett. 23 (1969) P.721

FIGURE CAPTIONS

Fig. 1. The process $\gamma(k)+N(p_1) \rightarrow \pi(q)+N(p_2)$. The quantities inside the brackets denote the four momenta of the corresponding particles.

Fig. 2. t-channel Regge exchanges for $\gamma+N \rightarrow \pi+N$

Fig. 3. The process $1+2 \rightarrow 3+4$. λ_i denotes the helicity of the i^{th} particle $(i=1,4)$.

Fig. 4. Absorption function $\eta(s,b) = 1-C\,e^{-\frac{b^2}{2A}}$ [eqn.(3.12)]

Fig. 5 Wood-Saxon type absorption function

$$\eta(s,b) = \frac{1}{1+\exp\left[(R-b)/d\right]}$$

In Figs. 6-20, the following notation will be maintained:

——————— : Solid curve : Model C_1(DAM)

– – – – – – – – : Dashed curve : Model C_2(DAM)

–X–X–X– : Cross-dashed curve : Model C_1'(DAM)

—·—·—·—·— : Dot-dashed curve : Model C_1(WCM)

.... : Dotted curve : Model C_2(WCM)

Fig. 6. Differential Cross-sections for $\gamma p \to \pi^0 p$ at 6,9, 12 and 15 GeV. Data as in Ref. (69) and (70). The data points are as follows:

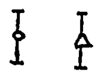 : data from Ref. (70)

 : data from Ref. (69)

Fig. 7. Polarised photom asymmetry Σ for $\gamma p \to \pi^0 p$ at 3 and 6 GeV. Data as in Ref. (71).

Fig. 8. The ratio $R = \frac{d\sigma}{dt}(\gamma n \to \pi^0 n) / \frac{d\sigma}{dt}(\gamma p \to \pi^0 p)$ at 4 and 8 GeV. Data as in Ref. (72).

Fig. 9. Polarised target asymmetry T for $\gamma p \to \pi^0 p$ at 4 GeV. Data as in Ref. (73).

Fig. 10. Differential Cross-sections for $\gamma p \to \eta p$ at 4, 6 and 9 GeV. Data as in Ref. (69) and (74). The data points are as follows :

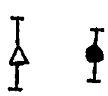 : data from Ref. (74)

 : data from Ref. (69)

Fig. 11. The quantity $X_\omega(s,t)$ for $\pi N \to \rho N$ at 4, 6 and 8 GeV. Data as in Ref. (36) and (75).

Fig. 12. The quantity $\rho^{(t)}_{11}\frac{d\sigma}{dt}$ for $\pi^+ n \to \omega p$ at 4.2, 5.1 and 6.95 GeV. Data as in Ref. (76) and (77).

Fig. 13. The quantity $[\rho^{(t)}_{1\,1} - \rho^{(t)}_{1\,1}]\frac{d\sigma}{dt}$ for $\pi^+ n \to \omega p$ at 4.2, 5.1 and 6.95 GeV. Data as in Ref. (76) and (77).

Fig. 14. The quantity $[\rho^{(t)}_{1\,1} + \rho^{(t)}_{1\,1}]\frac{d\sigma}{dt}$ for $\pi^+ n \to \omega p$ at 5.1 and 6.95 GeV. Data as in Ref. (77).

Fig. 15. Imaginary parts of $f^{(+)}_{-\frac{1}{2},\frac{1}{2}}$ and $f^{(0)}_{-\frac{1}{2},\frac{1}{2}}$ at 5.1 GeV.

Fig. 16. Imaginary parts of $f^{(0)}_{\frac{1}{2},\frac{1}{2}}$ at 5.1 and 12 GeV.

Fig. 17. Imaginary parts of $f^{(0)}_{-\frac{1}{2},\frac{3}{2}}$ at 5.1 and 12 GeV.

Fig. 18. Real parts of $f^{(+)}_{-\frac{1}{2},\frac{1}{2}}$ and $f^{(0)}_{-\frac{1}{2},\frac{1}{2}}$ at 5.1 GeV.

Fig. 19. Real parts of $f^{(0)}_{\frac{1}{2},\frac{1}{2}}$ and $f^{(0)}_{-\frac{1}{2},\frac{3}{2}}$ at 5.1 GeV.

Fig. 20. Predictions for the polarised photon asymmetry Σ , and the ratio $R = \frac{d\sigma}{dt}(\gamma n \to \eta n) / \frac{d\sigma}{dt}(\gamma p \to \eta p)$ at 4 and 9 GeV.

Fig. 21. Feynman diagrams for the gauge invariant pion contribution to the process $\gamma p \to \pi^+ n$. The corresponding four momenta of each part of each Feynman diagram are shown inside brackets. ε is the polarisation vector of the photon and $Q = q-k$; $P = p_1 + k$; $P' = k - p_2$.

Fig. 22. Plots of $\frac{d\sigma_\perp}{dt}$, $\frac{d\sigma_\parallel}{dt}$ and $\frac{d\sigma}{dt}$ as calculated by Electric Born Model for the process $\gamma p \to \pi^+ n$ showing sharp forward peak of width $\sim\mu^2$.

Fig. 23. Sharp forward peak of width $\sim\mu^2$ for the process $\gamma p \to \pi^+ n$ produced through the absorption model.

In Figs. 24-26, the following notation will be maintained:

———————— : Solid curve : Veneziano Model with the term given in eqn. (8.41).

— — — — — — — : Dashed curve: Veneziano Model without this term-

Fig. 24. Forward differential cross-section for $\gamma p \to \pi^+ n$ at 3.4,5,8 and 16 GeV. Data as in Ref. (78). The source of the data points are explained inside the diagram.

Fig. 25. Polarised photon asymmetry Σ for processes $\gamma p \to \pi^+ n$ and $\gamma n \to \pi^- p$ at 3.4 GeV. Data as in Ref. (79).

Fig. 26. The ratio $R=\frac{d\sigma}{dt}(\gamma n\to\pi^- p)/\frac{d\sigma}{dt}(\gamma p\to\pi^+ n)$ at 3.4,5, 8 and 16 GeV. Data as in Ref. (78).

Fig. 27. Polarised target asymmetry T for $\gamma p\to\pi^+ n$ at 5 and 16 GeV. Data as in Ref. (80). Data points are as follows:

5 GeV ; 16 GeV

All calculations done with the term in eqn. (8.41). The two curves are as follows:

: Dashed curve : 5 GeV

: Solid curve : 16 GeV

Fig. 28. Backward differential cross-sections for $\gamma p\to\pi^+ n$ at 4.3,5,9.5 and 14.9 GeV. Parameters used for this calculation correspond to numbers without parenthesis in Table 8.4. Data as in Ref. (81).

DIAGRAMS

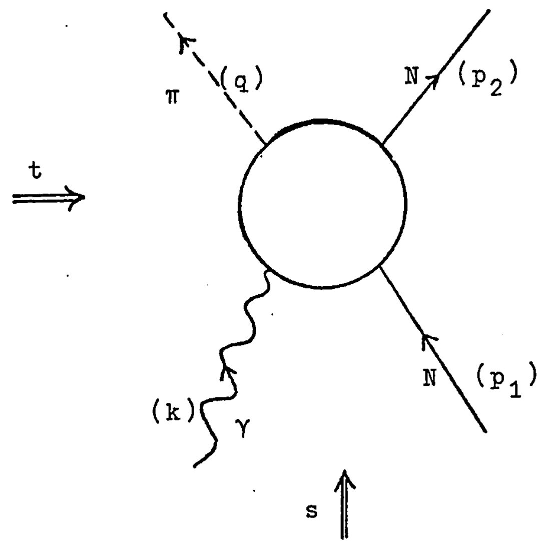

Fig. 1

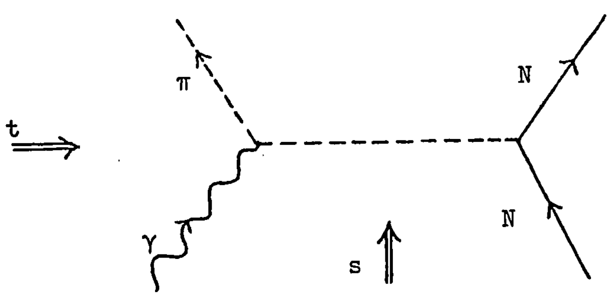

Fig. 2

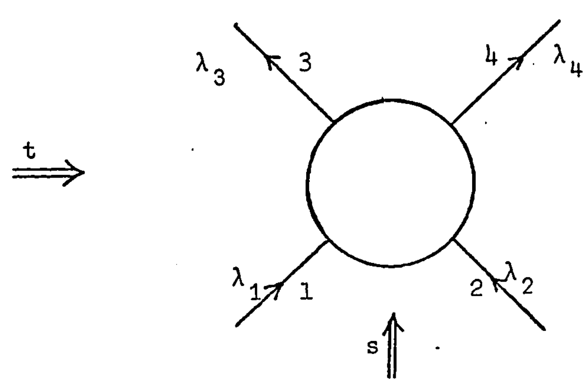

Fig. 3

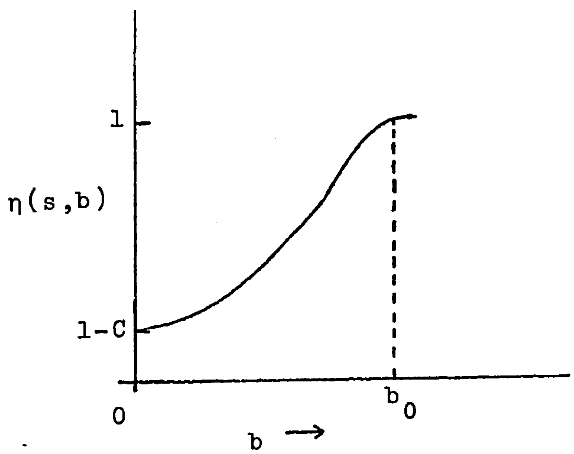

Fig. 4

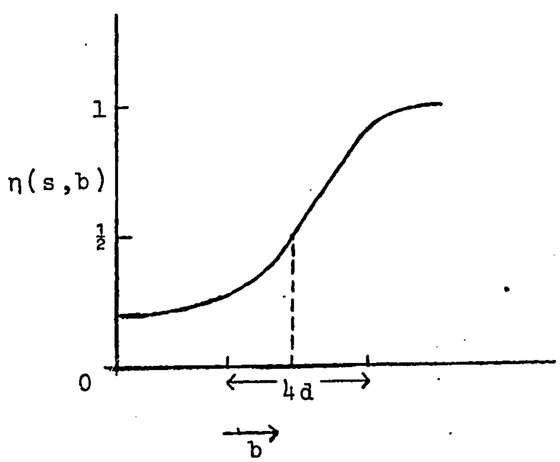

Fig. 5

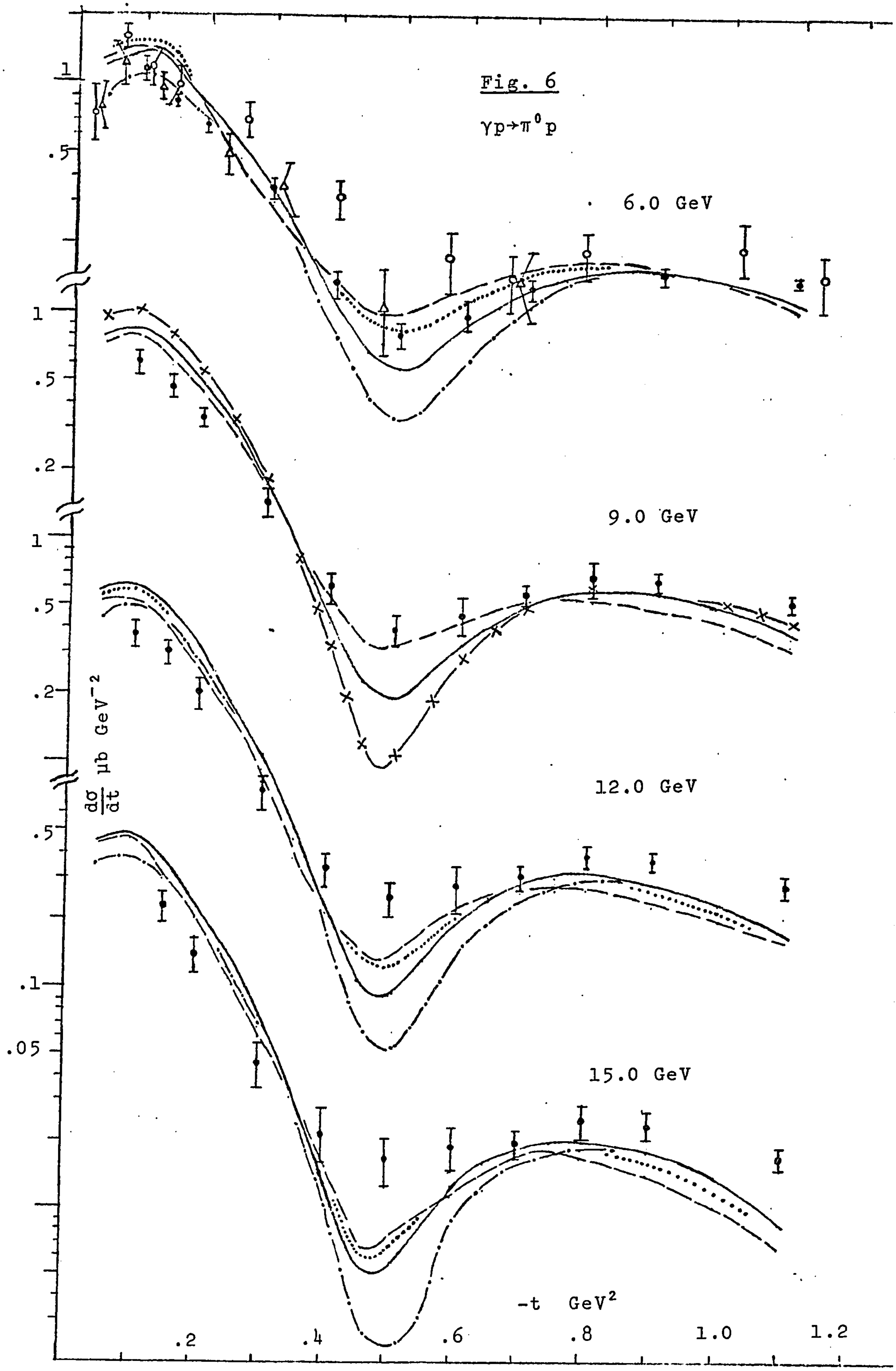

Fig. 6
$\gamma p \to \pi^0 p$
6.0 GeV
9.0 GeV
12.0 GeV
15.0 GeV
$\frac{d\sigma}{dt}$ μb GeV^{-2}
-t GeV^2
1
.5
.2
.1
.05
.2
.4
.6
.8
1.0
1.2

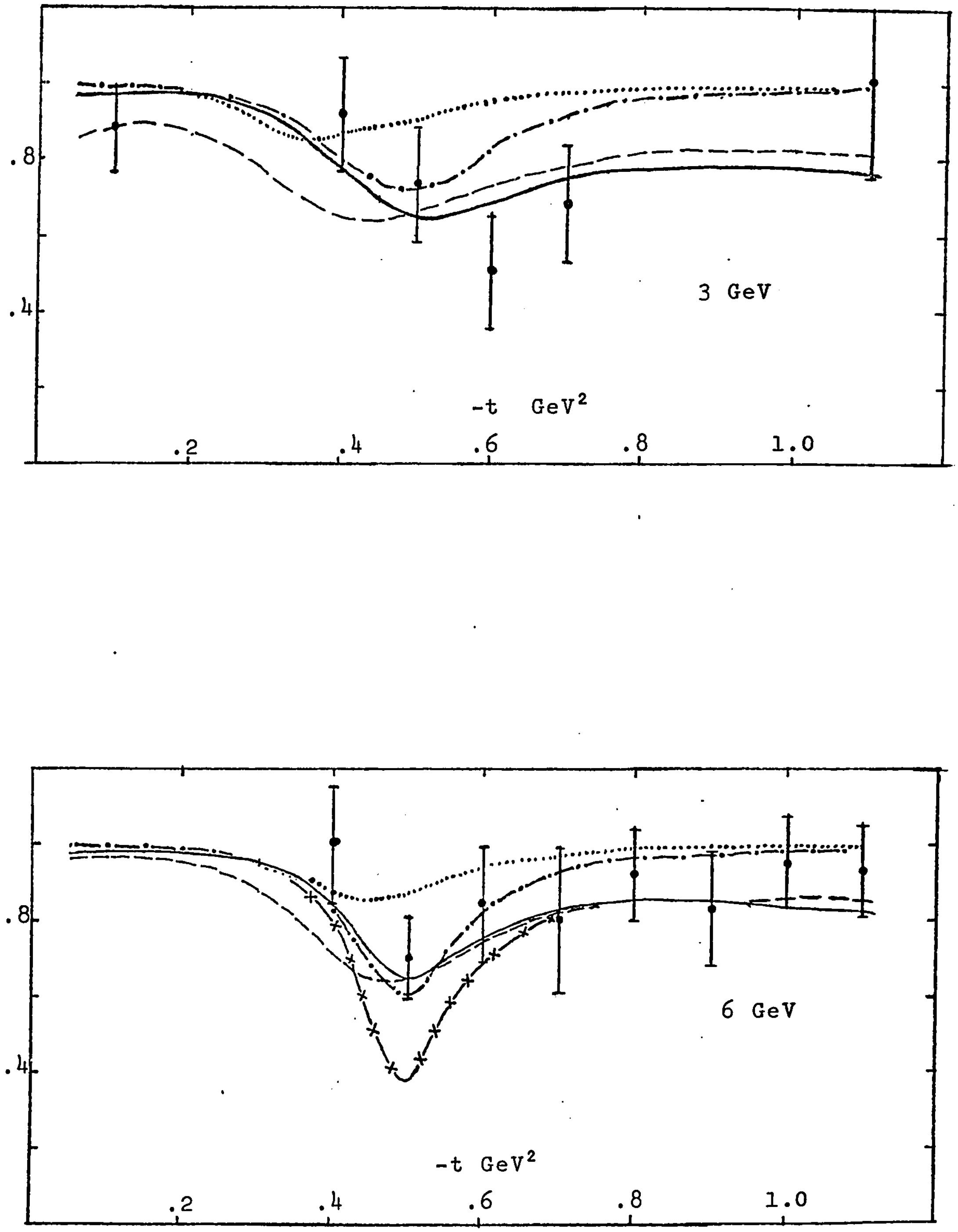

Σ for $\gamma p \to \pi^0 p$

<u>Fig. 7</u>

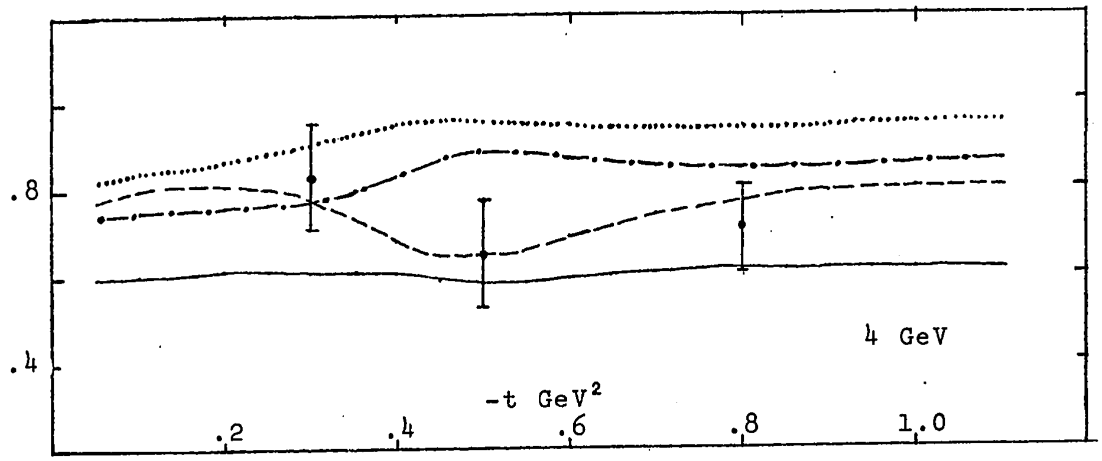

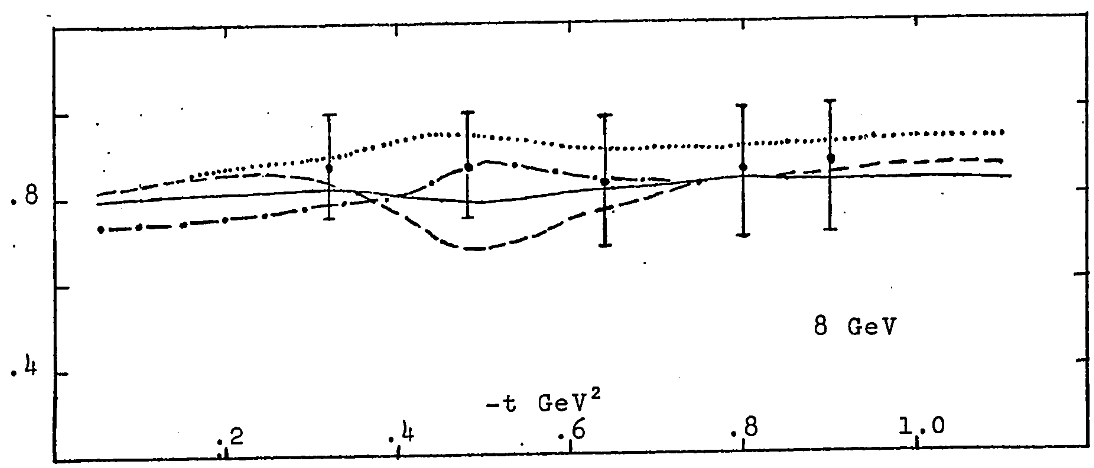

Ratio $R = \frac{d\sigma}{dt}(\gamma n \to \pi^0 n) / \frac{d\sigma}{dt}(\gamma p \to \pi^0 p)$

<u>Fig. 8</u>

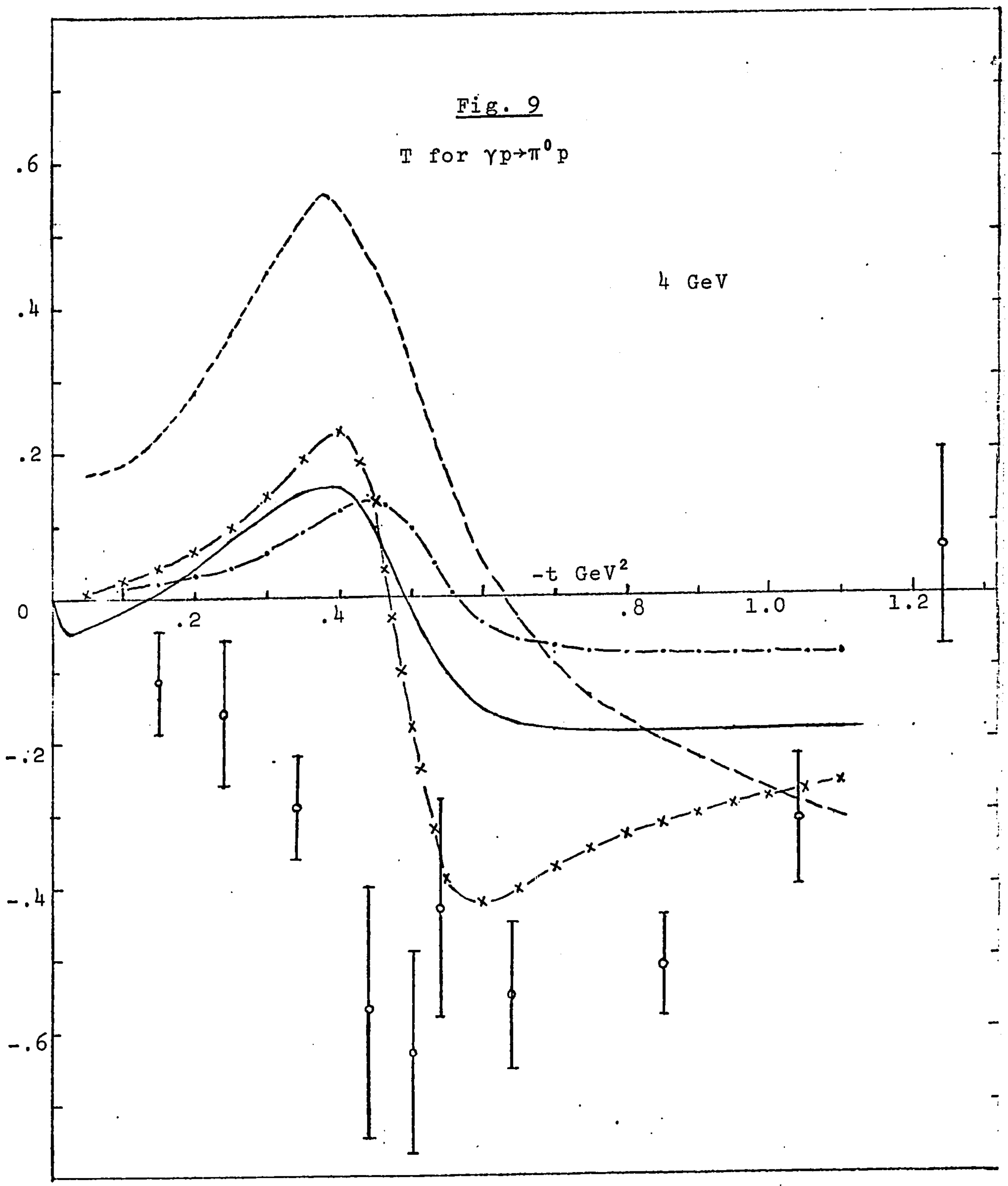
Fig. 9
T for $\gamma p \to \pi^0 p$
4 GeV
-t GeV^2
.6
.4
.2
0
-.2
-.4
-.6
.2
.4
.8
1.0
1.2

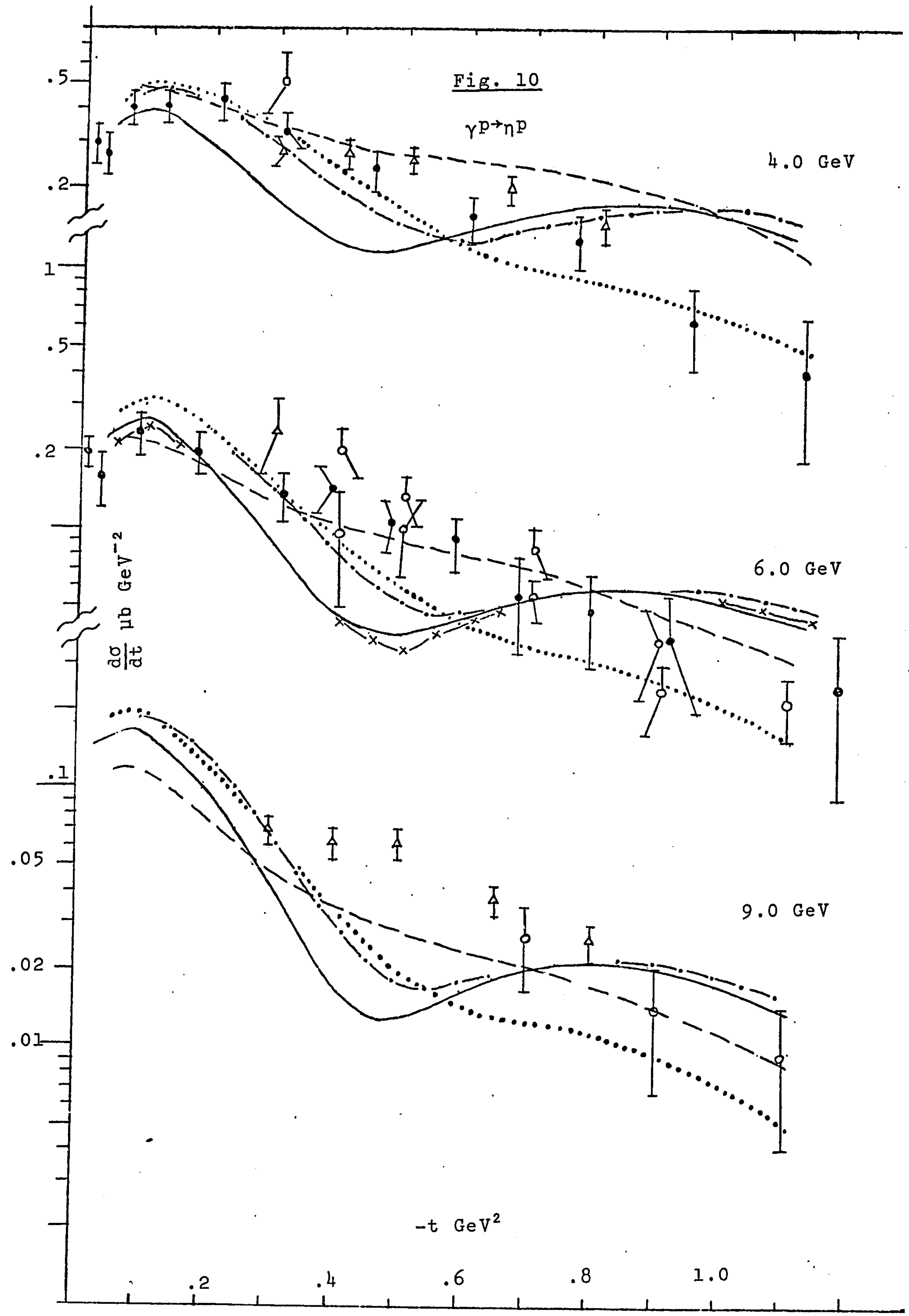
Fig. 10
γp→ηp
4.0 GeV
6.0 GeV
9.0 GeV
dσ/dt μb GeV⁻²
-t GeV²
.5
.2
1
.5
.2
.1
.05
.02
.01
.2
.4
.6
.8
1.0

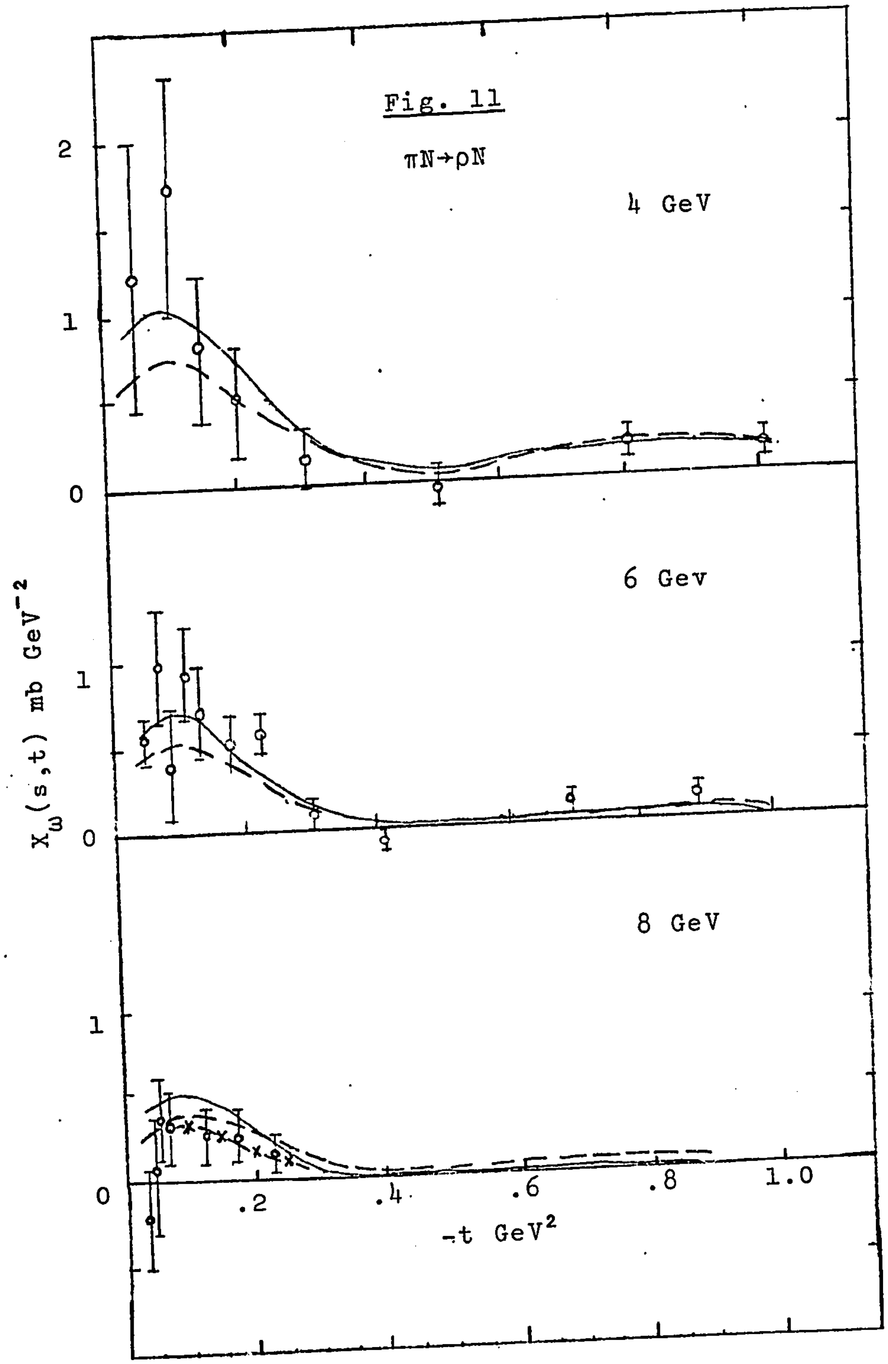

Fig. 11
πN→ρN
4 GeV
6 Gev
8 GeV
$X_\omega(s,t)$ mb GeV^{-2}
2
1
0
.2
.4
.6
.8
1.0
-t GeV^2

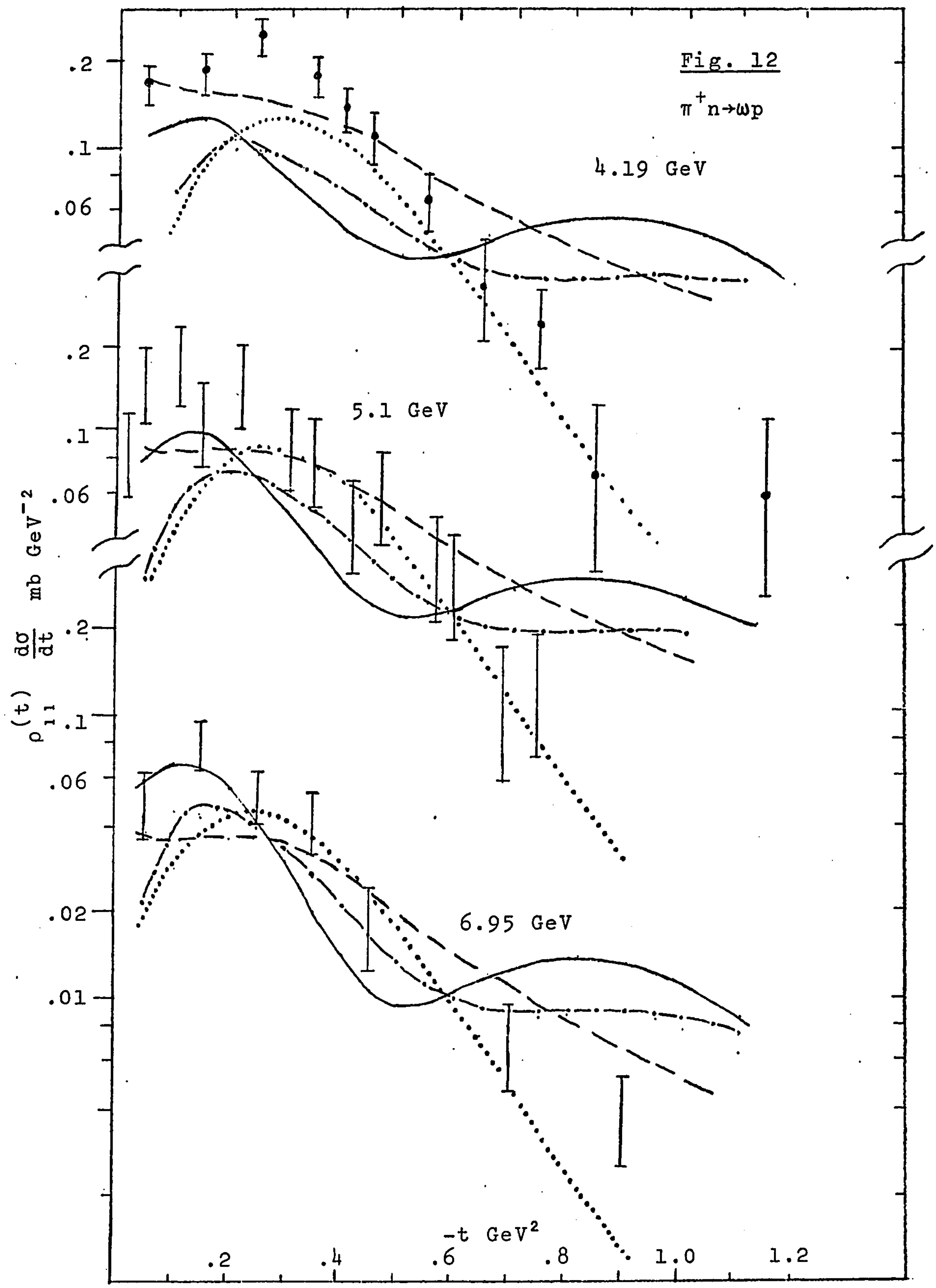
Fig. 12
$\pi^+ n \to \omega p$
4.19 GeV
5.1 GeV
6.95 GeV
$\rho_{11}(t) \frac{d\sigma}{dt}$ mb GeV^{-2}
$-t$ GeV^2
.2
.1
.06
.02
.01
.4
.6
.8
1.0
1.2

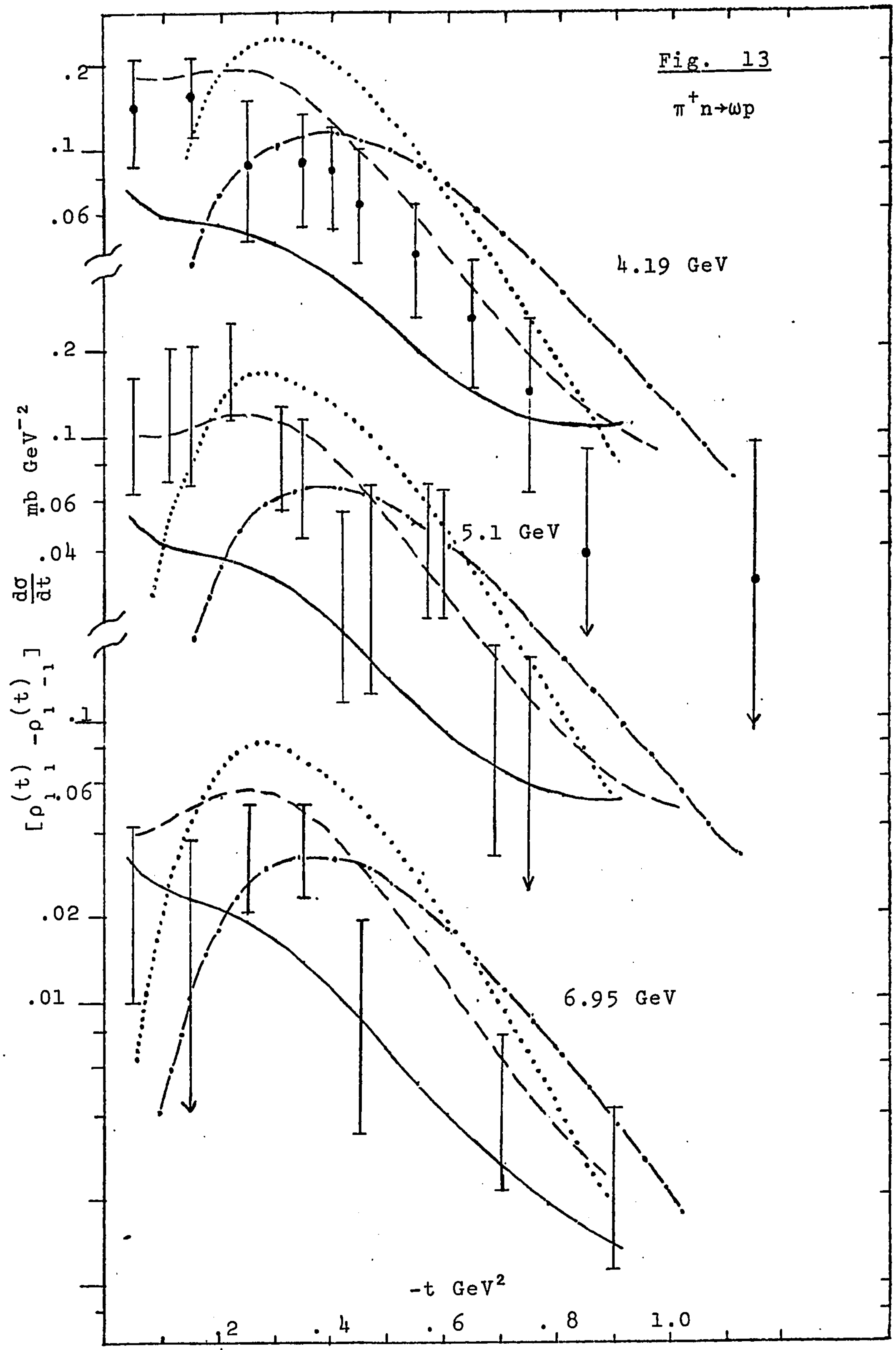

Fig. 13
$\pi^+ n \to \omega p$
4.19 GeV
5.1 GeV
6.95 GeV
$\frac{d\sigma}{dt}$ mb GeV^{-2}
$[\rho^{(t)}_{11} - \rho^{(t)}_{1-1}]$
.2
.1
.06
.04
.02
.01
-t GeV²
.2
.4
.6
.8
1.0

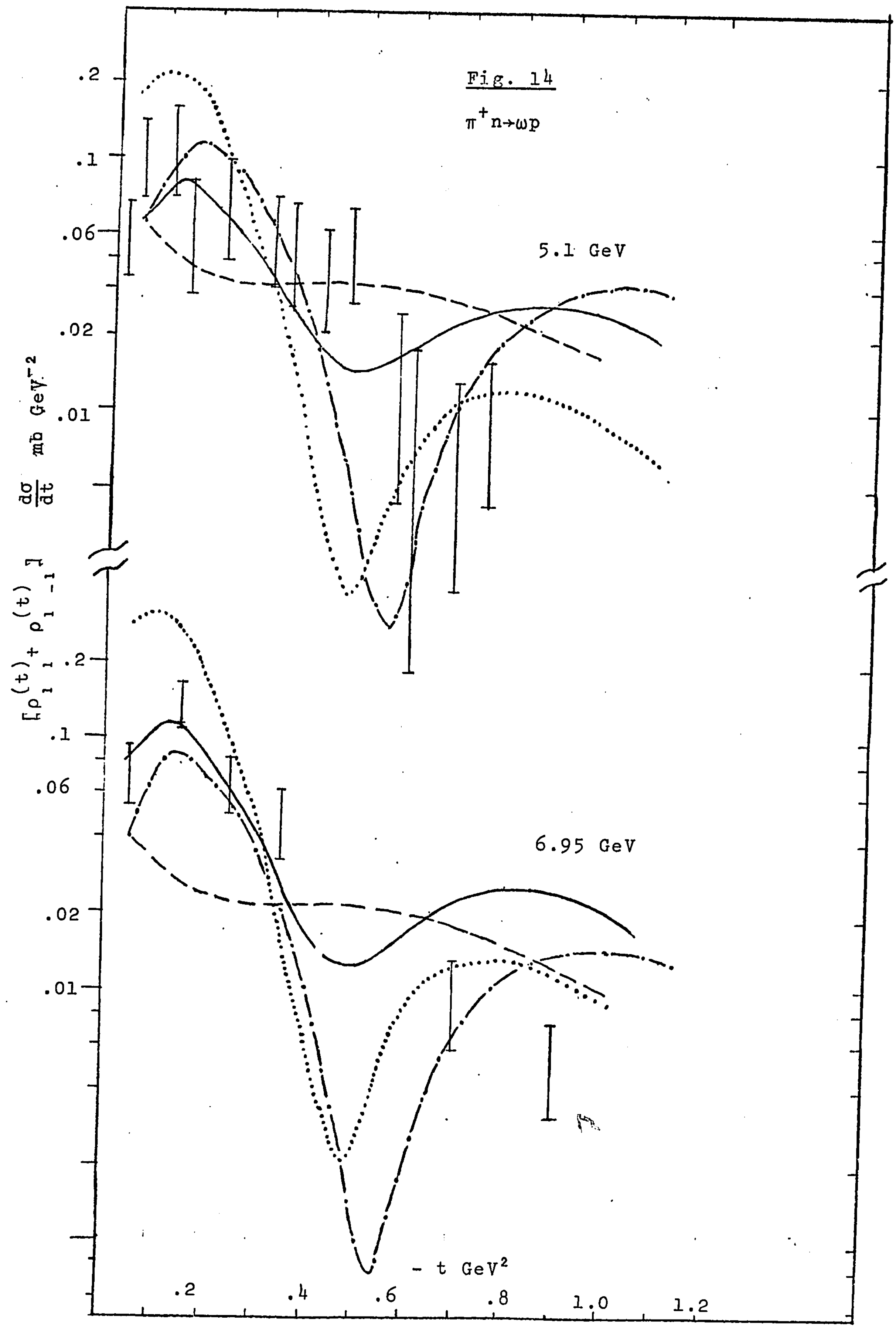

Fig. 14
$\pi^+ n \to \omega p$
5.1 GeV
6.95 GeV
$\frac{d\sigma}{dt}$ mb GeV^{-2}
$[\rho_{11}^{(t)} + \rho_{1\,-1}^{(t)}]$
.2
.1
.06
.02
.01
- t GeV^2
.2
.4
.6
.8
1.0
1.2

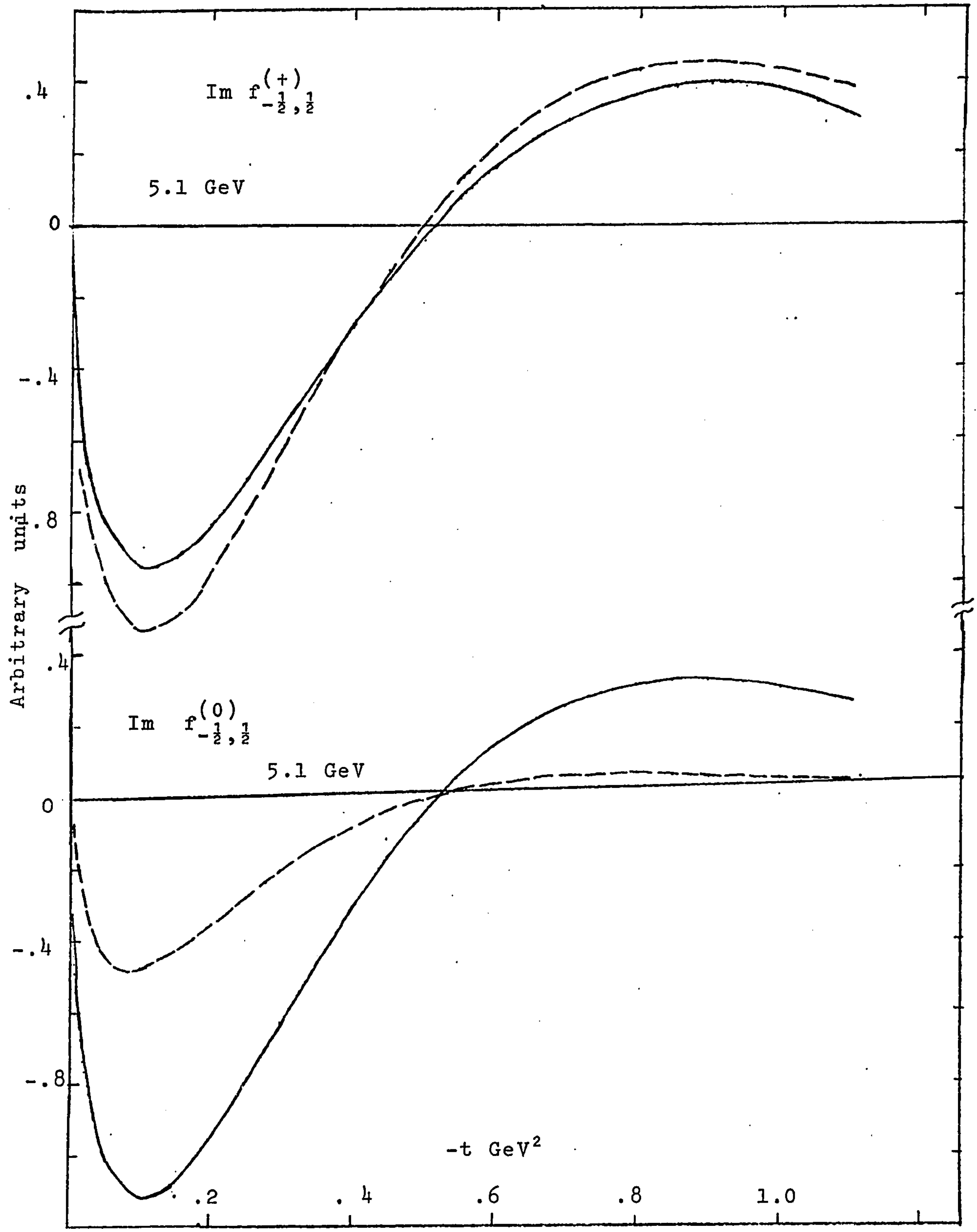

Im $f^{(+)}_{-\frac{1}{2},\frac{1}{2}}$
5.1 GeV
.4
0
-.4
.8
Arbitrary units
.4
Im $f^{(0)}_{-\frac{1}{2},\frac{1}{2}}$
5.1 GeV
0
-.4
-.8
-t GeV^2
.2
.4
.6
.8
1.0

Fig. 15

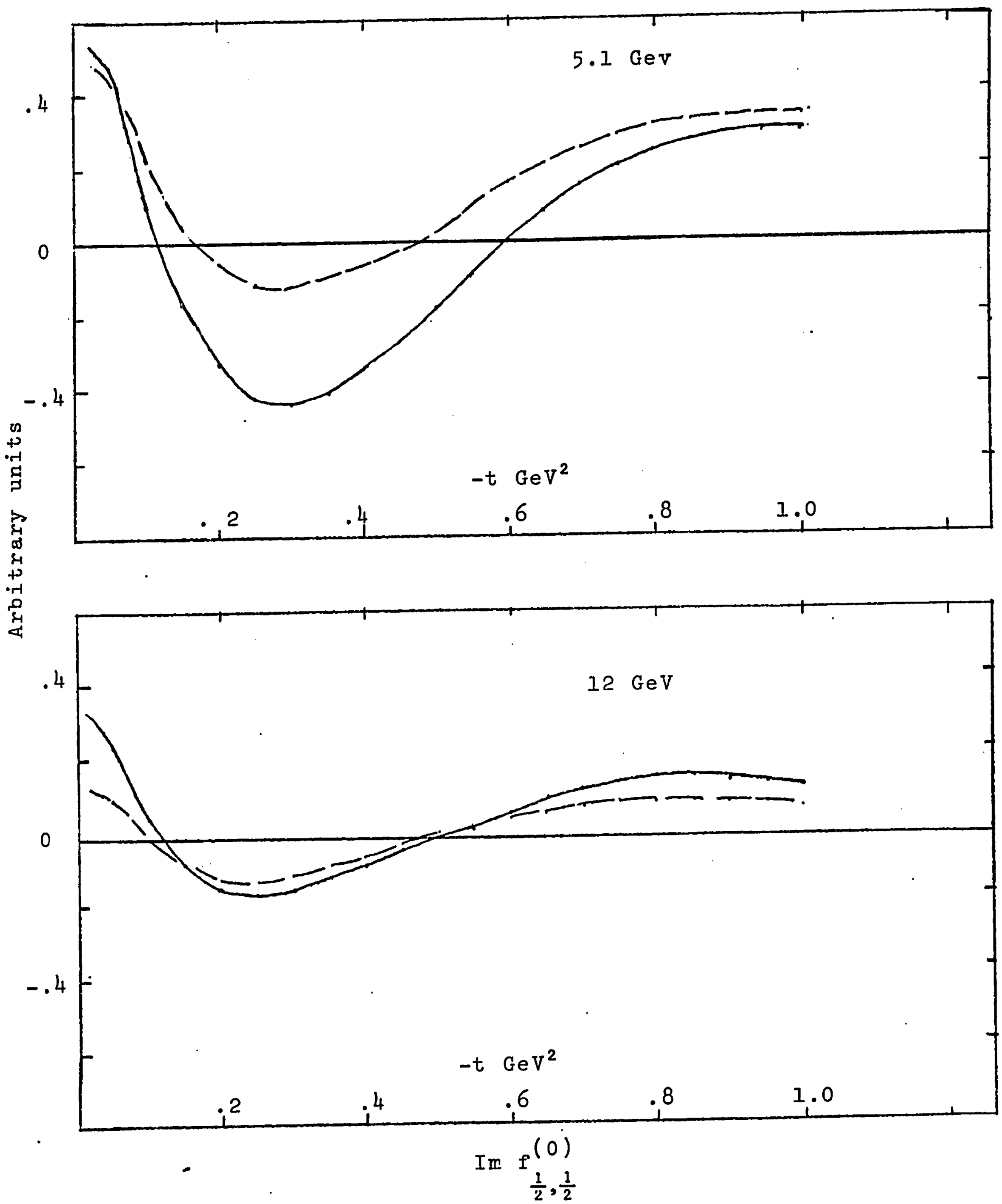
5.1 Gev
12 GeV
.4
0
-.4
Arbitrary units
-t GeV²
.2
.4
.6
.8
1.0
Im $f^{(0)}_{\frac{1}{2},\frac{1}{2}}$

Fig. 16

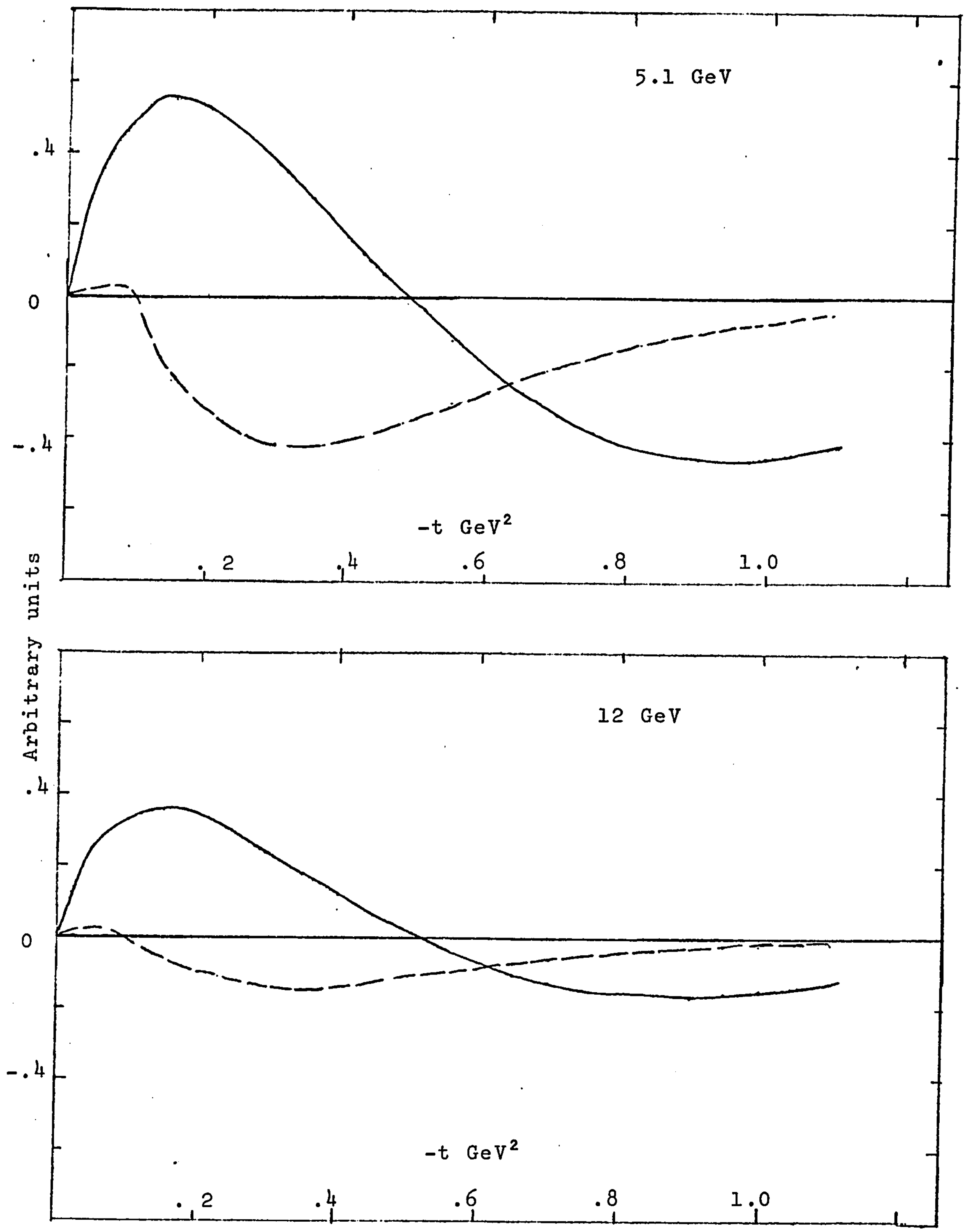

Im $f^{(0)}_{-\frac{1}{2}\,\frac{3}{2}}$

Fig. 17

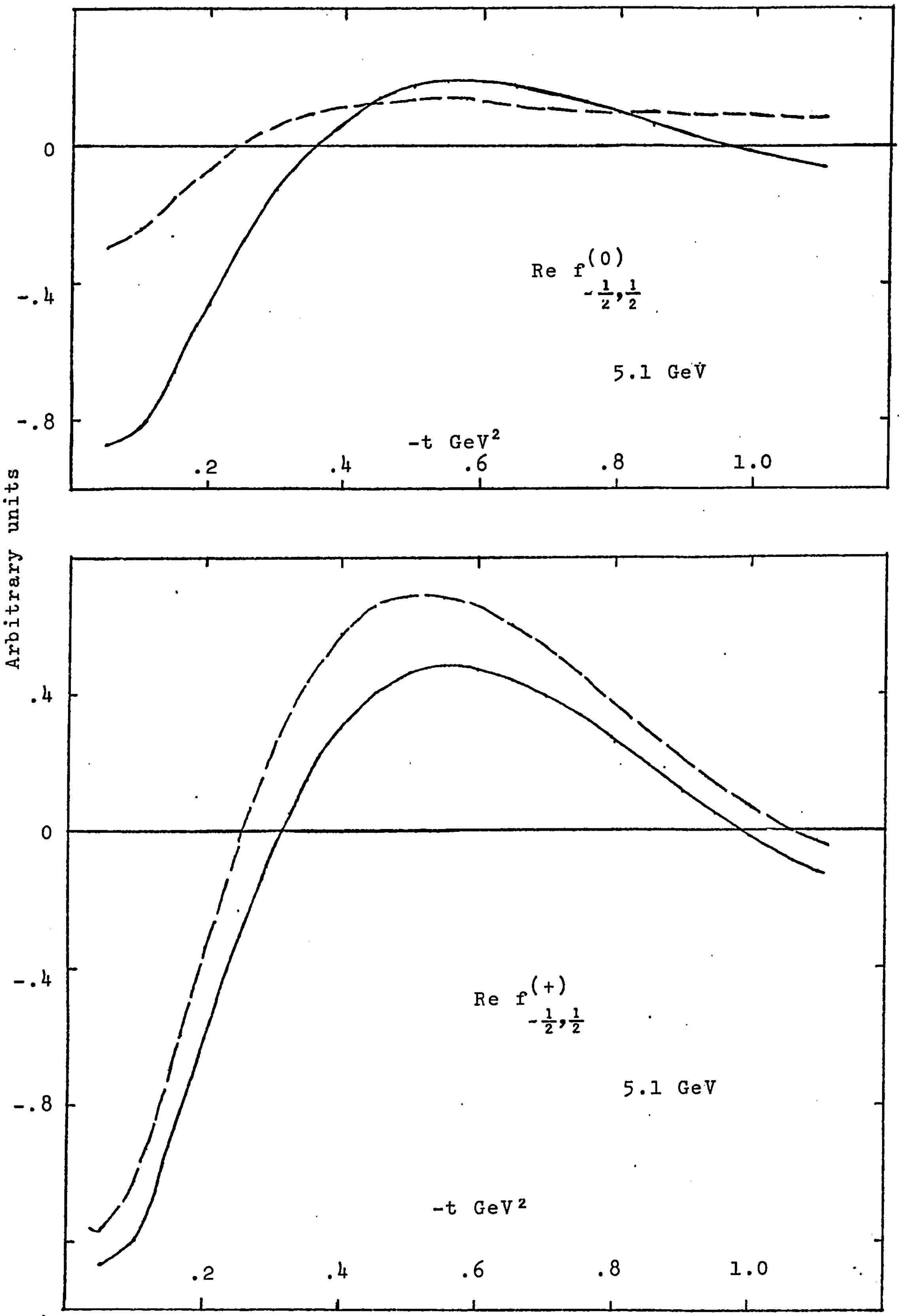
Arbitrary units
Re $f^{(0)}_{-\frac{1}{2},\frac{1}{2}}$
5.1 GeV
$-t$ GeV^2
0
-.4
-.8
.2
.4
.6
.8
1.0
Re $f^{(+)}_{-\frac{1}{2},\frac{1}{2}}$
5.1 GeV
$-t$ GeV^2
.4
0
-.4
-.8
.2
.4
.6
.8
1.0

Fig. 18

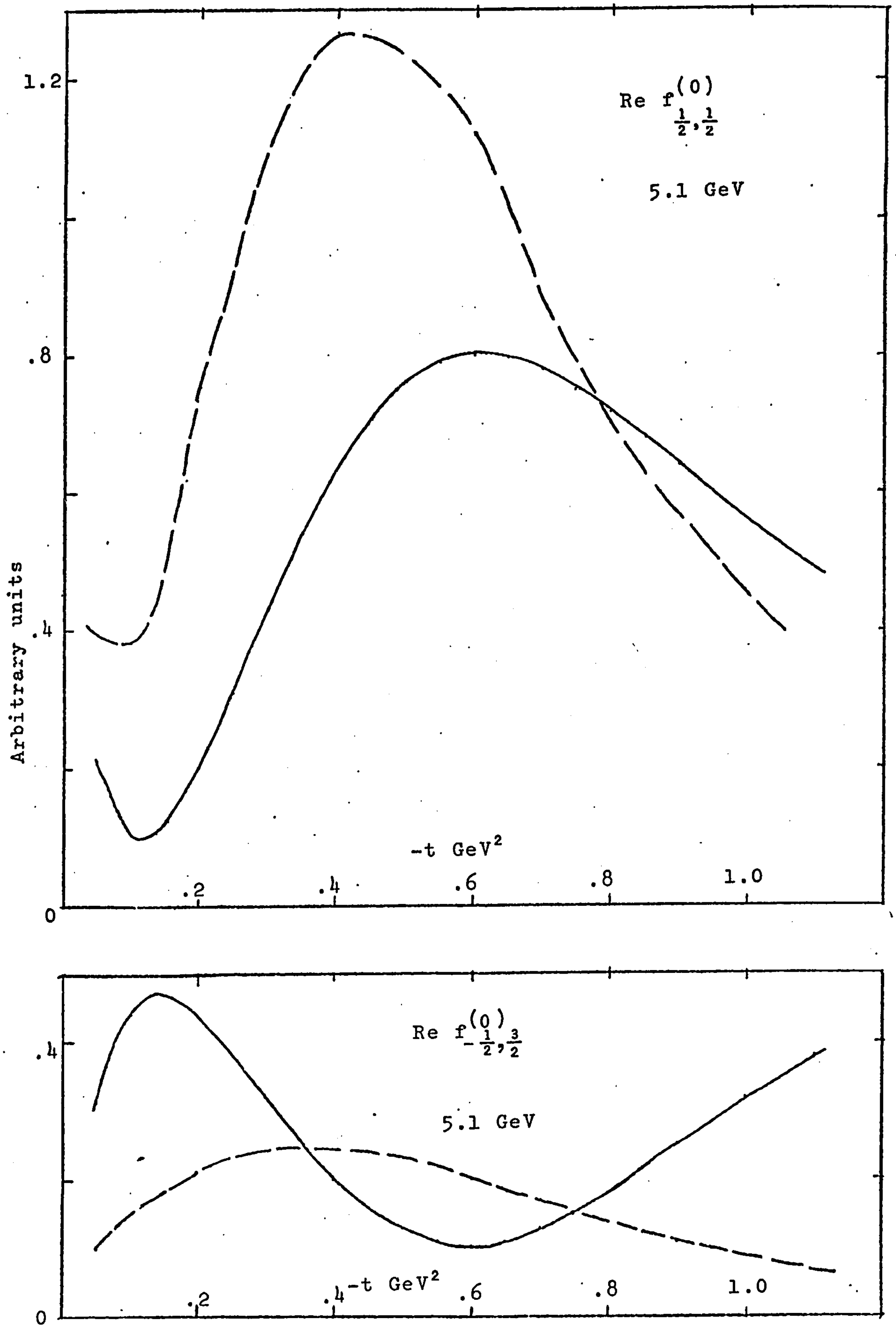

1.2
.8
.4
0
Arbitrary units
Re $f^{(0)}_{\frac{1}{2},\frac{1}{2}}$
5.1 GeV
-t GeV^2
.2
.4
.6
.8
1.0
.4
0
Re $f^{(0)}_{-\frac{1}{2},\frac{3}{2}}$
5.1 GeV
-t GeV^2
.2
.4
.6
.8
1.0

Fig. 19

Fig. 20

$\gamma p \to \eta p$

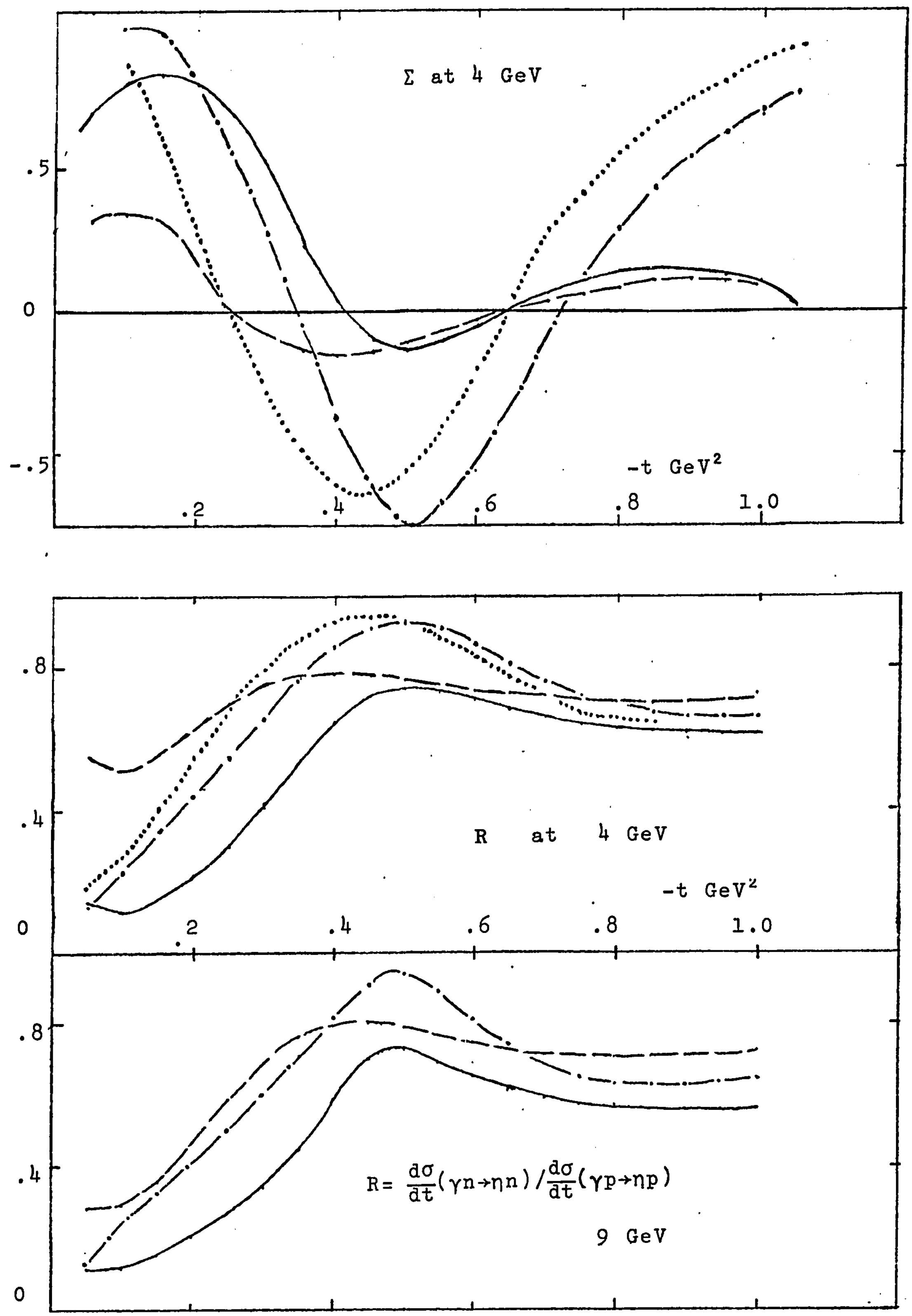

Fig. 21

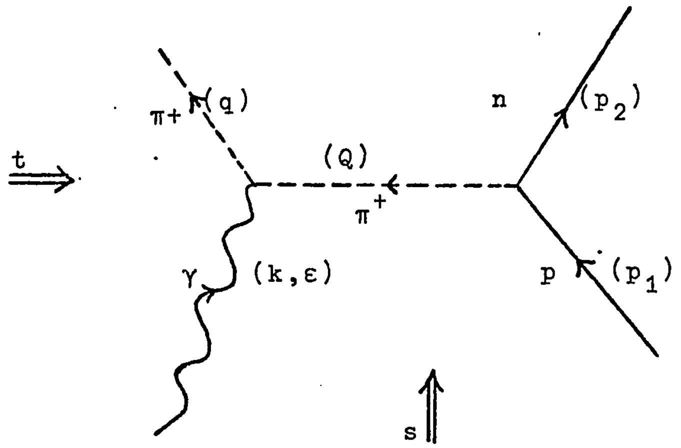

(a)

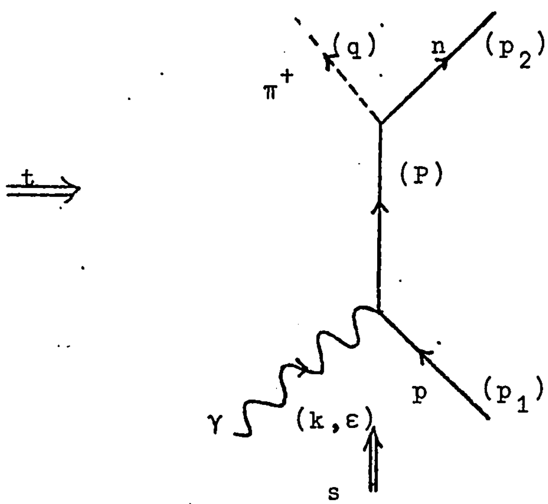

(b)

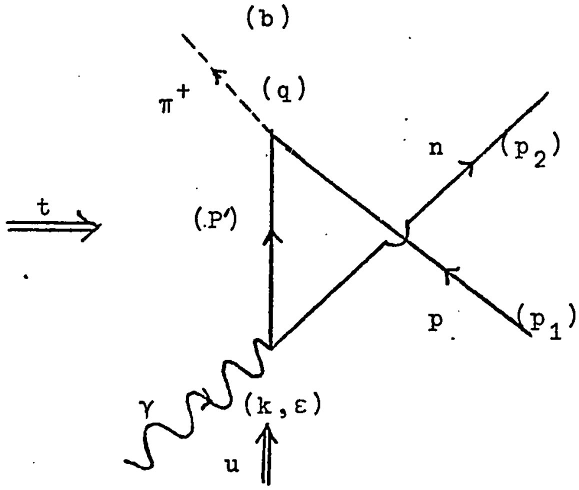

(c)

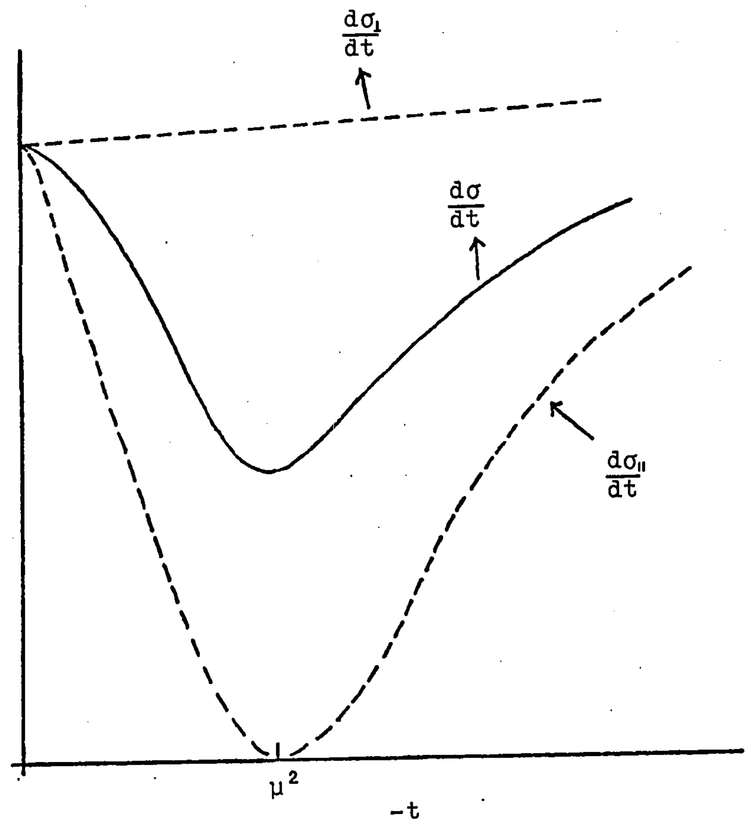
$\frac{d\sigma_\perp}{dt}$
$\frac{d\sigma}{dt}$
$\frac{d\sigma_\parallel}{dt}$
μ^2
$-t$

Fig. 22

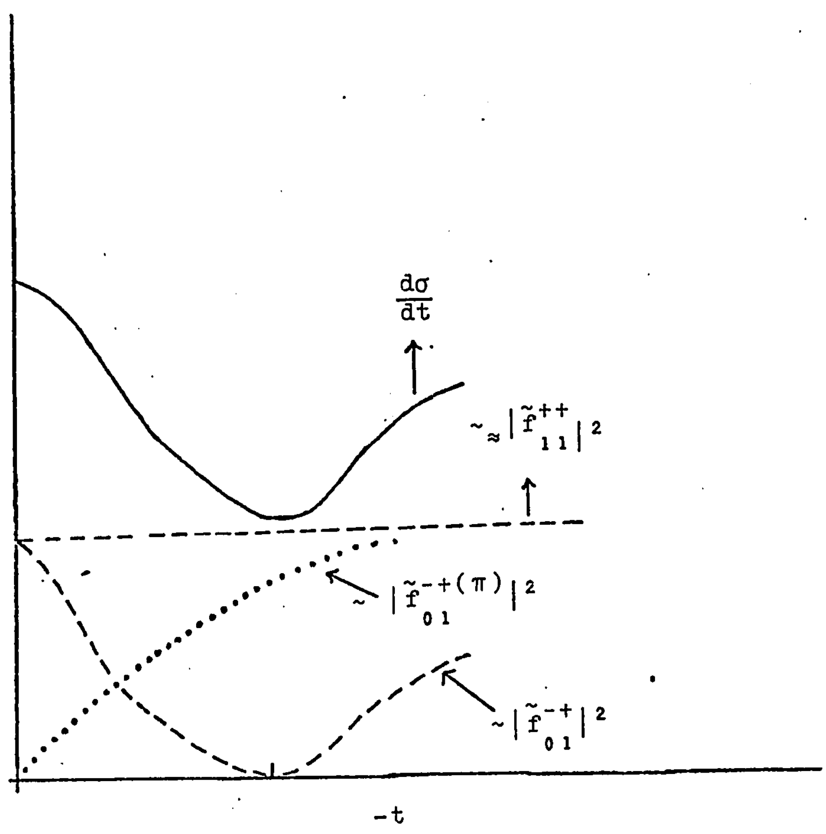
$\frac{d\sigma}{dt}$
$\sim\approx|\tilde{f}_{11}^{++}|^2$
$\sim|\tilde{f}_{01}^{-+(\pi)}|^2$
$\sim|\tilde{f}_{01}^{-+}|^2$
$-t$

Fig. 23

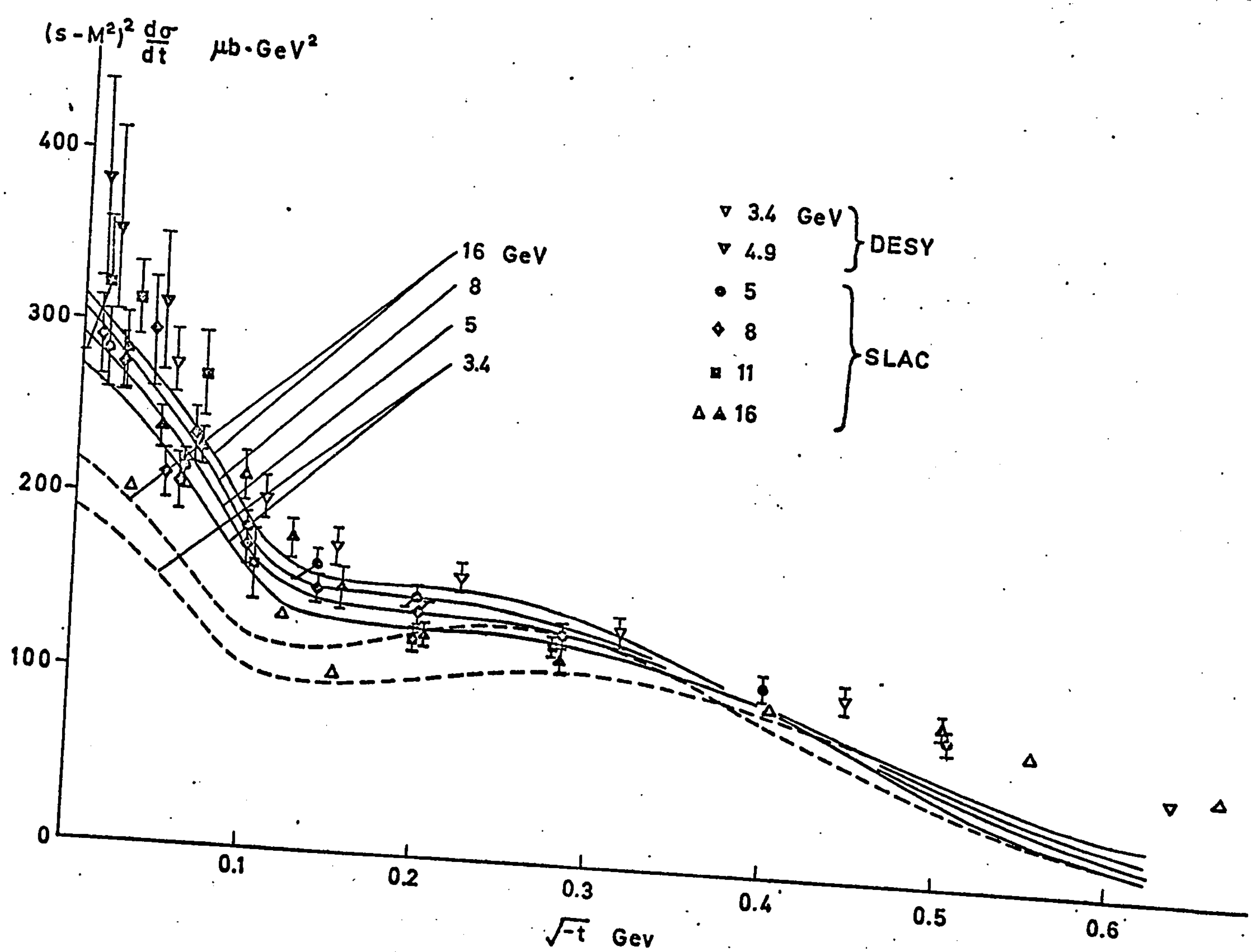

(s - M²)² dσ/dt μb·GeV²
400
300
200
100
0
0.1
0.2
0.3
0.4
0.5
0.6
√-t Gev
16 GeV
8
5
3.4
3.4 GeV
4.9
DESY
5
8
11
16
SLAC

Fig. 24

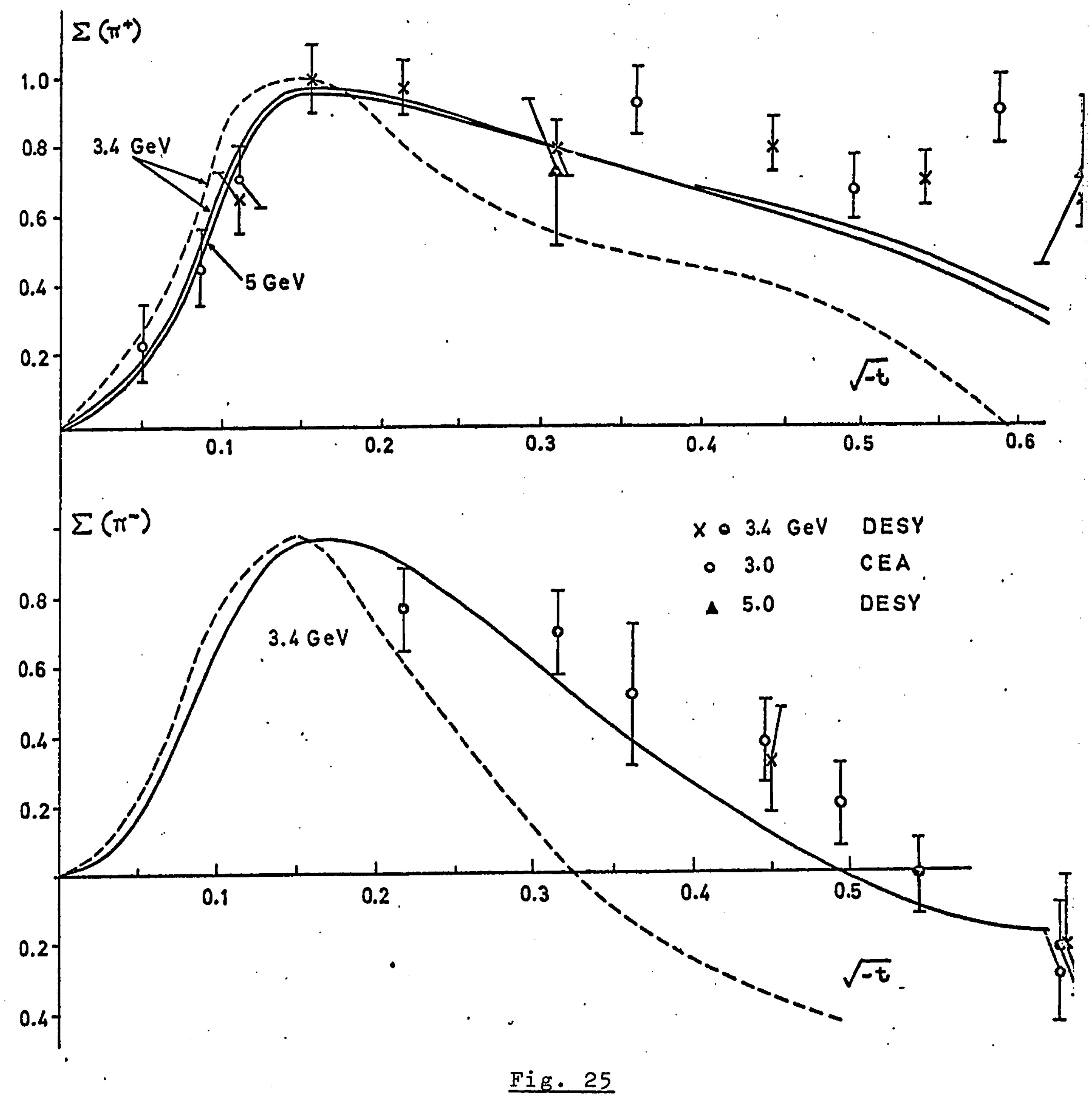

Σ (π⁺)
1.0
0.8
0.6
0.4
0.2
3.4 GeV
5 GeV
√-t
0.1
0.2
0.3
0.4
0.5
0.6
Σ (π⁻)
0.8
0.6
0.4
0.2
3.4 GeV
X o 3.4 GeV DESY
o 3.0 CEA
▲ 5.0 DESY
0.1
0.2
0.3
0.4
0.5
0.2
0.4
√-t

Fig. 25

Fig. 26

$$R = \frac{d\sigma}{dt}(\gamma n \to \pi^- p) / \frac{d\sigma}{dt}(\gamma p \to \pi^+ n)$$

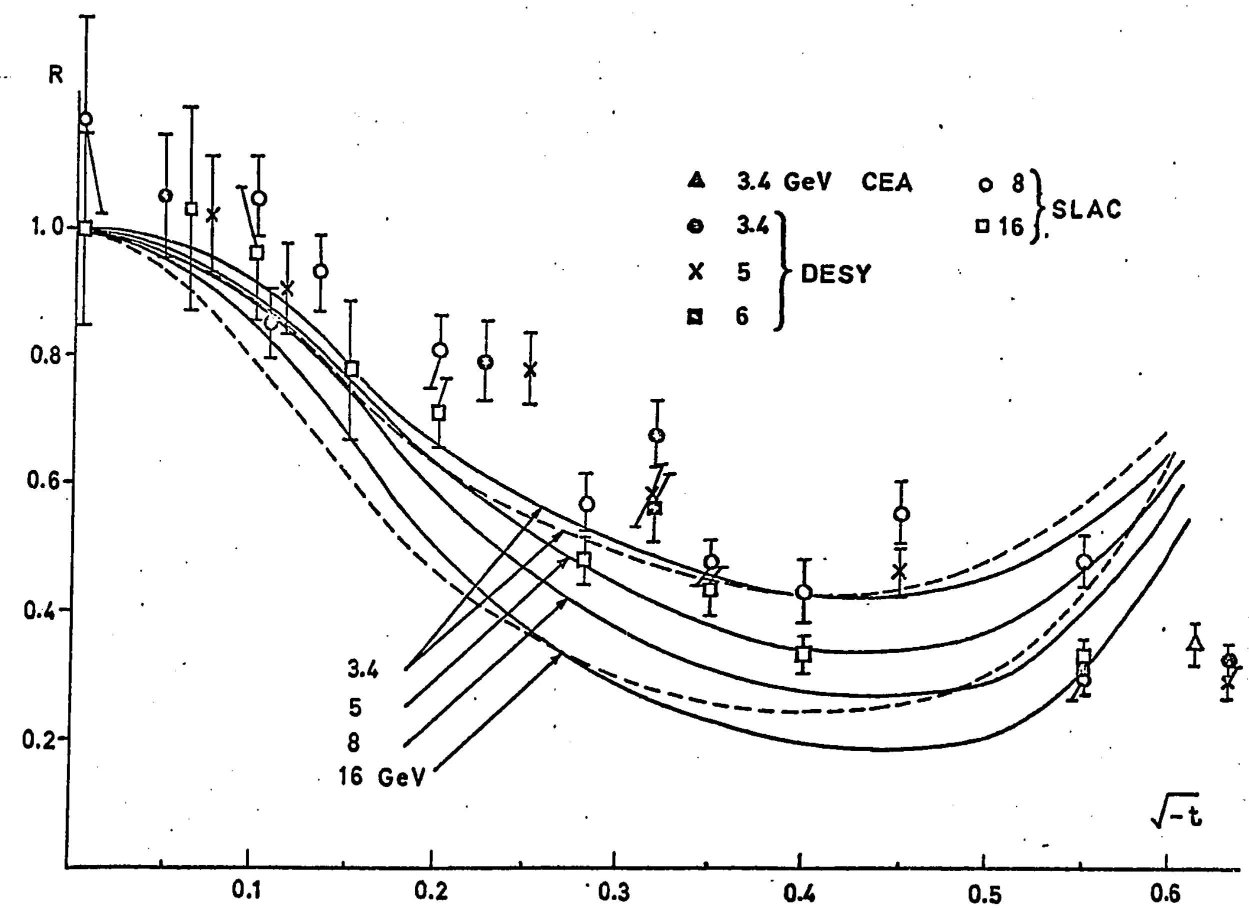

Fig. 27

T for $\gamma p \to \pi^+ n$

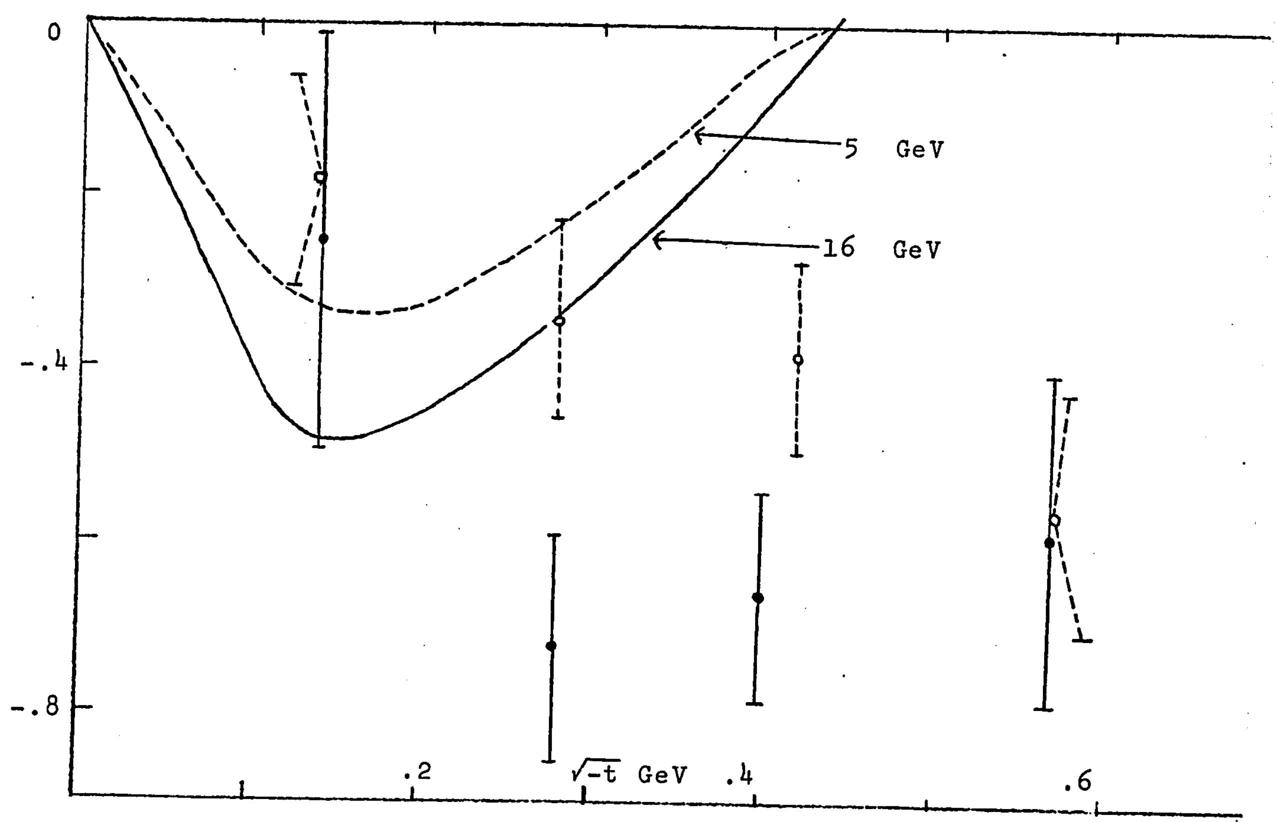

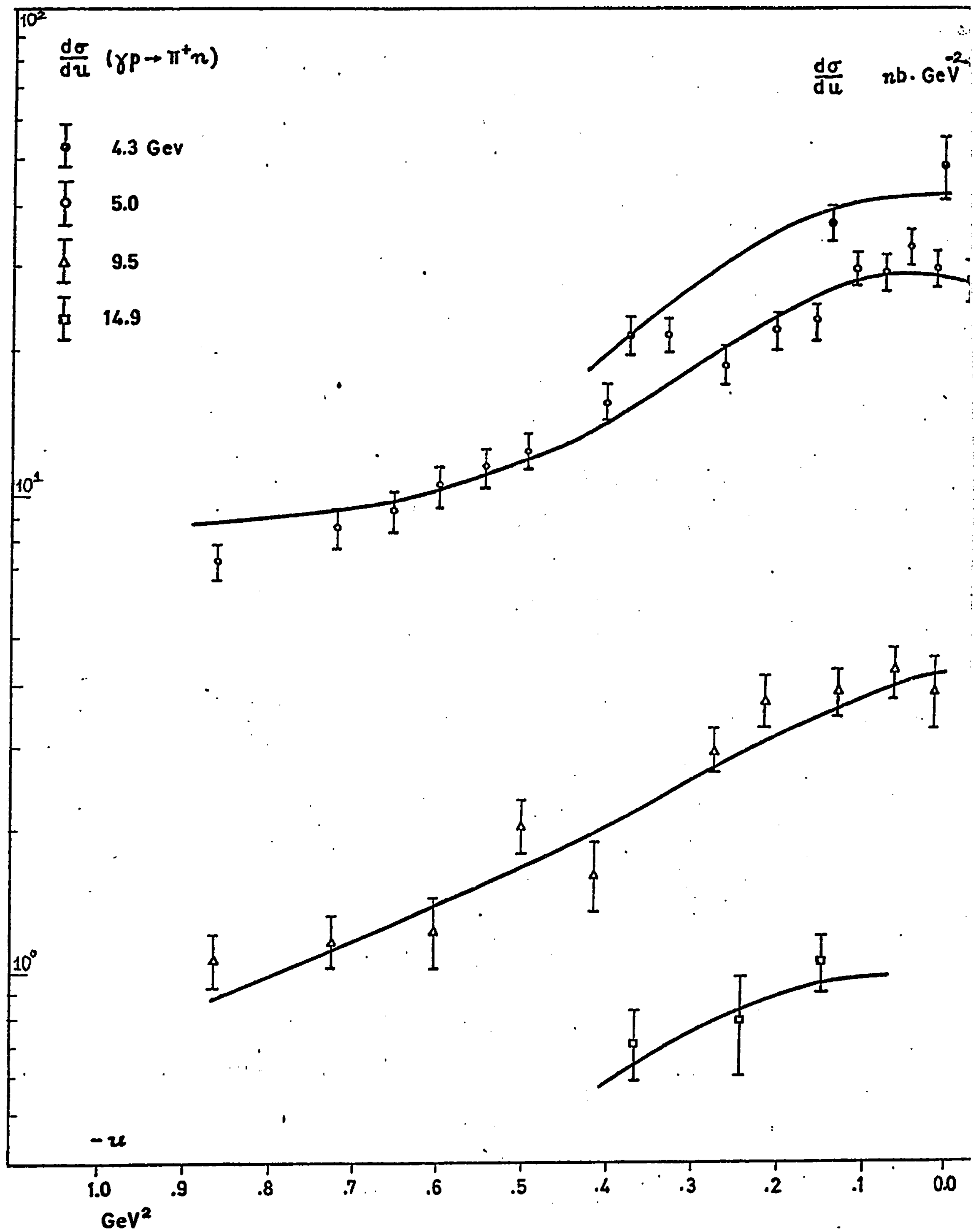

$\frac{d\sigma}{du}$ ($\gamma p \to \pi^+ n$)
$\frac{d\sigma}{du}$ nb·GeV^{-2}
4.3 Gev
5.0
9.5
14.9
10^2
10^1
10^0
$-u$
1.0
.9
.8
.7
.6
.5
.4
.3
.2
.1
0.0
GeV^2

Fig. 28